Quench Simulation of VLHC Transmission Line Magnet

(Final Report)

Nickolay A. Shatil

Abstract

Two thermohydraulic models of transmission line drive conductor with and without the void fraction in the superconductor space were developed and simulated. Quench analysis of 60m transmission line conductor carrying 100kA under self field 0.5T is presented. Conductor models are treated numerically with use of VINCENTA code. All models are described in detail. Results on Normal Zone propagation velocity, hot spot temperature of conductor, maximal helium pressure etc. are given.

St.-Petersburg, Russia

February 1999

Contents

1. INTRODUCTION

Two thermohydraulic models for quench simulation of Transmission Line conductor with and without the void fraction in the cable space between the invar tubes were developed. Quench simulation of 60m transmission line conductor carrying 100kA (average background field 0.5T) under testing conditions is considered. Conductor models are treated numerically with use of VINCENTA code. Detail description of numerical models used are described. Simulation have been performed for central initialized quench. Results on Normal Zone propagation velocity, hot spot temperature of conductor, maximal helium pressure and etc. are given.

2. MATHEMATICAL MODELS

The set of models considered below are proper parts of VINCENTA code[1-3][1]. The followed models of VINCENTA are used for modeling of the transmission line conductor

- helium flow
- conductor
- collector
- valve
- wall

2.1 Helium flow

The model is intended for simulating the transient parameters of compressible helium flow inside the channel. The model described by a set of 1D equations of continuity, momentum and energy conservation laws completed with the transverse mass, momentum and energy transfer terms to take into account the thermal-hydraulic coupling with different flows and solid materials[2]. Final set of equations describing a transient process for helium flow in the *i* channel including interaction with flows in the *k* channels and *m* conductors has a form:

$$\frac{\partial \rho_i}{\partial t} + \frac{\partial \rho_i V_i}{\partial x} = \frac{\sum_k \Gamma^{\rho}_{ki}}{A_i} \quad (1)$$

[1] Code is intended for transient thermal-hydraulic analysis of complicated superconducting and ryogenic systems (including cryogenic plant elements and armature such as pumps, valves and heat exchangers), which are cooled by forced flows of the single and/or two-phase helium.

[2] In common case the helium flow in a channel being considered can simultaneously have a thermal contact with some various solid materials and helium in another channels. Besides, the different helium flows inside channels can be hydraulically coupled between themselves in longitudinal direction (due to the transverse holes). As sample, it take a place in Cable-In-Conduit Conductor (CICC) with a central channel and similar model may be applicable to Transmission Line Conductor, where the helium in void space between the strands of Rutherford type cable is considered as *second* channel.

$$\frac{\partial \rho_i V_i}{\partial t} + \frac{\partial}{\partial x}\left(P_i + \rho_i V_i^2 \right) = \frac{-2 f_i \rho_i V_i |V_i|}{D_{h_i}} + \frac{\sum_k \Gamma_{ki}^{\rho V}}{A_i} \quad (2)$$

$$\frac{\partial}{\partial t}\rho_i \left(H_i + \frac{V_i^2}{2} - \frac{P_i}{\rho_i} \right) + \frac{\partial}{\partial x}\rho_i V_i \left(H_i + \frac{V_i^2}{2} \right) = \frac{\sum_m Q_{mi}^{conv} + \sum_k \Gamma_{ki}^{\rho H}}{A_i} \quad (3)$$

where ρ, P, H, V – helium density, pressure, enthalpy and velocity accordingly; f – friction factor (see item 4.4); A – helium cross sectional area ; D_h – hydraulic diameter; Q_{mi}^{conv} – convective heat transfer from conductor m to helium i per unit of length; $\Gamma_{ki}^{\rho} = -\Gamma_{ik}^{\rho}$, $\Gamma_{ki}^{\rho V} = -\Gamma_{ik}^{\rho V}$, $\Gamma_{ki}^{\rho H} = -\Gamma_{ik}^{\rho H}$ – mass, momentum and enthalpy flux from k to i channel (and vice versa).

The local transverse mass and enthalpy flux from k to i channel can be obtained in the following simple form:

$$\Gamma_{ki}^{\rho} = S_{ki} \cdot \begin{cases} \sqrt{2(P_k - P_i)\rho_k}\,, & P_k > P_i \\ -\sqrt{2(P_i - P_k)\rho_i}\,, & P_k < P_i \end{cases} ,$$

$$\Gamma_{ki}^{\rho H} = \Gamma_{ki}^{\rho} \cdot \begin{cases} H_k + V_k^2/2, & \Gamma_{ki}^{\rho} > 0 \\ H_i + V_i^2/2, & \Gamma_{ki}^{\rho} < 0 \end{cases} .$$

where S_{ki} is a coefficient having dimensionality of cross-section area per unit of length between k and i flows (channels)[3]. Such approach to the transversal transfer processes between flows seems to be relevant for simulating mass and energy exchange if an assumption of a small pressure drop between flows is valid (transverse cross area is large enough). The advantage of this model is a possibility to analyze the influence of transverse coupling on thermal and hydraulic parameters of coupled flows and allows to estimate the transverse mass and energy transport term.

The following boundary conditions are used to close system (1)-(3). The helium pressures at the ends of a *channel* are supposed to be identical to pressures in joined *collectors*. When helium enters the *channel,* the helium enthalpy at an appropriate end of *channel* is assumed to be equal to the enthalpy in joined collector. At the closed end of the tube the helium velocity assumed to be zero.

2.2 Conductor

Transient temperature distribution in conductors is described by 1D equation of heat balance including the transverse conductive and convective heat exchange and Joule heating terms. Temperature distribution across conductor section

---

[3] The transverse mass flux from k flow is suggested to be normal to i flow, the momentum transport term is assumed to be negligible (i.e. $\Gamma_{ki}^{\rho V} = -\Gamma_{ik}^{\rho V} = 0$).

assumed to be uniform[4]. The equation for binary conductor number m including the heat exchange with conductors n and helium flows i[5] has a form:

$$\left(A_m^1 C_m^1 + A_m^2 C_m^2\right)\frac{\partial T_m}{\partial t} = -\cos^2\theta \frac{\partial}{\partial x}\left(\left(A_m^1 k_m^1 + A_m^2 k_m^2\right)\frac{\partial T_m}{\partial x} \right) + \\ + Q_m^{Joule} + \sum_i Q_{im}^{conv} + \sum_n Q_{nm}^{cond} + \sum_k Q_{km}^{wall} \quad (4)$$

$$Q_m^{Joule} = \frac{I_{op}^2}{\left(\sigma_m^1 A_m^1 + \sigma_m^2 A_m^2\right)\cos^2\theta} g(T_m),$$

$$g(T_m) = \begin{cases} 0, T_m < T_{cs} \\ 1 - \dfrac{I_c(T_m)}{I_{op}}, T_{cs} < T_m < T_c \\ 1, T_m > T_c \end{cases} \quad (5)$$

$$Q_{im}^{conv} = h_{im} \cdot \gamma_{im} \cdot (T_i - T_m) \quad (6)$$

$$Q_{nm}^{cond} = h_{nm} \cdot \gamma_{nm} \cdot (T_n - T_m) \quad (7a)$$

$$Q_{km}^{wall} = \gamma_{km} \cdot k_k^{wall} \frac{\partial}{\partial r}\left(T^{wall}(x, r)\right) \quad (7b)$$

where T, C, k, A^1+A^2 – conductor temperature, heat capacity, thermal conductivity and cross section area of components accordingly; h, γ –coefficient and perimeter of heat exchange; Q_{nm}^{cond} –conductive heat transfer from conductors n and m per unit of length; Q_{im}^{conv} -convective heat transfer from helium in channel i to conductor m per unit of length; Q_m^{Joule} - Joule heating of conductor m per unit of length; Q_{km}^{wall}, k^{wall}, T^{wall} - heat flux to wall k, thermal conductivity and temperature of wall k correspondingly; I_{op} - conductor current; σ - conductor electrical conductance; I_c, T_c, T_{cs} - critical current, critical temperature and current sharing temperature accordingly.

In these equations the material cross-section A_m is treated as the cross section in a plane that is normal to the conductor axis ("twisted" cross section). The same notice concerns to the material heat exchange perimeter γ_m. It is taken, that "twisted"

---

[4] Uniform temperature distribution is "natural" assumption of 1D approach and considered as average temperature for the given cross-section. This model being applicable to current carrier based on following approaches:

- uniform current density distribution (and consequently Joule heating distribution) during quench between transposed strands and copper tape
- Bio's number in application to actual current carrier is much less than 1 ($Bi=h\delta/k << 1$, where $h= k_{inv}/ \delta_{inv}$ the heat transfer coefficient which is treated on the boundary of the current carrier as ratio of invar thermal conductivity k_{inv} to the radial thickness of the invar tube δ_{inv}; δ the radial thickness of the current carrier and k its average thermal conductivity.

Real temperature non-uniformity can be estimated as $\delta T=q_v\delta^2/8k$, where q_v is specific Joule power. If take into calculation $q_v=j^2\rho$=2e8 W/m^3, δ^2=3e-6 m^2 and k=60 W/(mK) the following rough estimation can be did as the worst: δT<10K, Bi<0.02.

[5] In common case *conductor* could have simultaneously a contact with different helium flows as well as with another *conductors*.

material cross section and perimeter (for conductors kind of twisted superconducting strands) used in above equations are defined as $A_{tw} = A_{non\ tw}/\cos\theta$ and $\gamma_{tw} = \gamma_{non\ tw}/\cos\theta$, where $\theta>0$ is an average twist angle[6]. For non-twisted materials $\cos\theta = 1$.

The following boundary conditions are used to close equation (4). The temperatures at the ends of the conductor are supposed to be identical to those in joined conductors.

2.3 Collector

The mathematical model of *collector* is intended for 0D simulation of helium parameters in a collector and used as a node element for connecting different *channels* and *valves* in series-parallel to one another. The laws of mass and energy conservation define the helium behavior inside the collector. For collector number *i* equations have view

$$\Omega_i \frac{d\rho_i}{dt} = \sum_k G^{\rho}_{ki} + \sum_n G^{\rho}_{ni}\ , \quad (8)$$

$$\Omega_i \frac{d}{dt}\left(\rho_i H_i - P_i\right) = \sum_k G^{\rho H}_{ki} + \sum_n G^{\rho H}_{ni} + \sum_m Q^{conv}_{mi}\ , \quad (9)$$

where Ω – collector volume; ρ, P, H – helium density, pressure and enthalpy correspondingly; G^{ρ}_{ki}, $G^{\rho H}_{ki}$ – helium mass and enthalpy flow from channel number k; $G^{\rho}_{ki}, G^{\rho}_{ni}$ - mass flow from channel k and valve n to collector i; $G^{\rho H}_{ki}, G^{\rho H}_{ni}$ - enthalpy flow from channel k and valve n to collector i; Q^{conv}_{im} - convective heat exchange between helium in collector i and *mass* m.

The mass flow terms in (8) are assumed to be positive if flow is coming into the collector considered and vice versa. The energy term in (9) is defined as

$$G^{\rho H}_{ki} = G^{\rho}_{ki} \times \begin{cases} H_k + V_k^2/2, & G^{\rho}_{ki} > 0 \\ H_i & G^{\rho}_{ki} < 0 \end{cases},$$

where H_k, U_k are enthalpy and velocity of helium at the end of channel k connected to collector i. The same equation takes a place for energy flow coming from a valve.

2.4 Valve

The model *valve* is intended for simulation of mass flow through cryogenic elements such as valve, hole, chink, etc. In considered model it is assumed that each *valve* is connected to two collectors.

[6] This generalized angle takes into account the twist of Rutherford cable around the inner invar tube too.

To associate the mass flow through the valve with thermodynamic properties of helium in both collectors we use the simplest model. The flow from a valve inlet up to the most narrow section of valve A_k (valve outlet) simulated as isoentropic process (δH-$\delta P/\rho = 0$). It is assumed that if subcritical flow takes a place then the pressure at the valve outlet is equal to pressure in outlet collector. In case of critical flow the outlet pressure is equal to critical one. So, for calculation of helium properties in the valve outlet k the following system of equations is used:

$$H_k + \tfrac{1}{2}U_k^2 = H_\Omega^{in}, S_k = S_\Omega^{in} \text{ , (10)}$$

$$P_k = \begin{cases} P_\Omega^{out}, U_k < C_k \\ P_k^{crit}, U_k = C_k \end{cases} \text{ , (11)}$$

$$G_k = \mu_k A_k \rho_k U_k \text{ , (12)}$$

where H_k, U_k, P_k, ρ_k is enthalpy, velocity, pressure and density of helium at the valve outlet; H_Ω^{in}, S_Ω^{in} is enthalpy and entropy of helium in the inlet collector; P_Ω^{out} is pressure in the outlet collector and P_k^{crit} is critical pressure in the valve outlet. For the real non-isentropic flow the correction factor $\mu_V < 1$ is used.

2.5 Wall

For simulation transient heat diffusion into the cable shell/jacket a 2D model used in axial-symmetrical approach. For given cross section S of wall k a differential equation for the wall temperature is:

$$C_k(T)\frac{\partial T_k}{\partial t} = q_{V_k}(x,r,t) + + \frac{\partial}{\partial x}\left(\kappa_k(T)\frac{\partial T_k}{\partial x}\right) + \frac{1}{r}\frac{\partial}{\partial r}\left(\kappa_k(T)\cdot r\frac{\partial T_k}{\partial r}\right) \quad , for S \times S_t \text{ , (13)}$$

$$T_k(x,r,0) = \psi(y,z), \quad t = 0$$

The following boundary condition of the third kind is formulated for *wall k* having heat exchange with helium flow i (inner surface of inner invar tube)

$$\kappa_k \frac{\partial T_k}{\partial n} + h_i \cdot \left(T_k - T_i^{He}\right) = 0$$

where h_i is the heat transfer coefficient and T_i^{He} is the corresponding temperature of helium inside the *channel i*. At outer surface of the wall (outer surface of outer invar tube) a boundary condition of second kind $\kappa_k \frac{\partial T_k}{\partial n} = \varphi_1(x,t)$ used. At the contact surfaces between *conductor m* and *wall* k boundary condition of first kind $T_k = T_m$ is assumed[7].

A set of another models used to close the above mentioned models by connecting them between themselves. These models are variety insulation elements, perforation etc. Generalized presentation of thermohydraulic model of the transmission line drive conductor is shown in Figure 2.

[7] In present simulations specific heat power q_V assumed to be neglected because in the transmission line conductor heat balance its power less than 1% of total Joule margin.

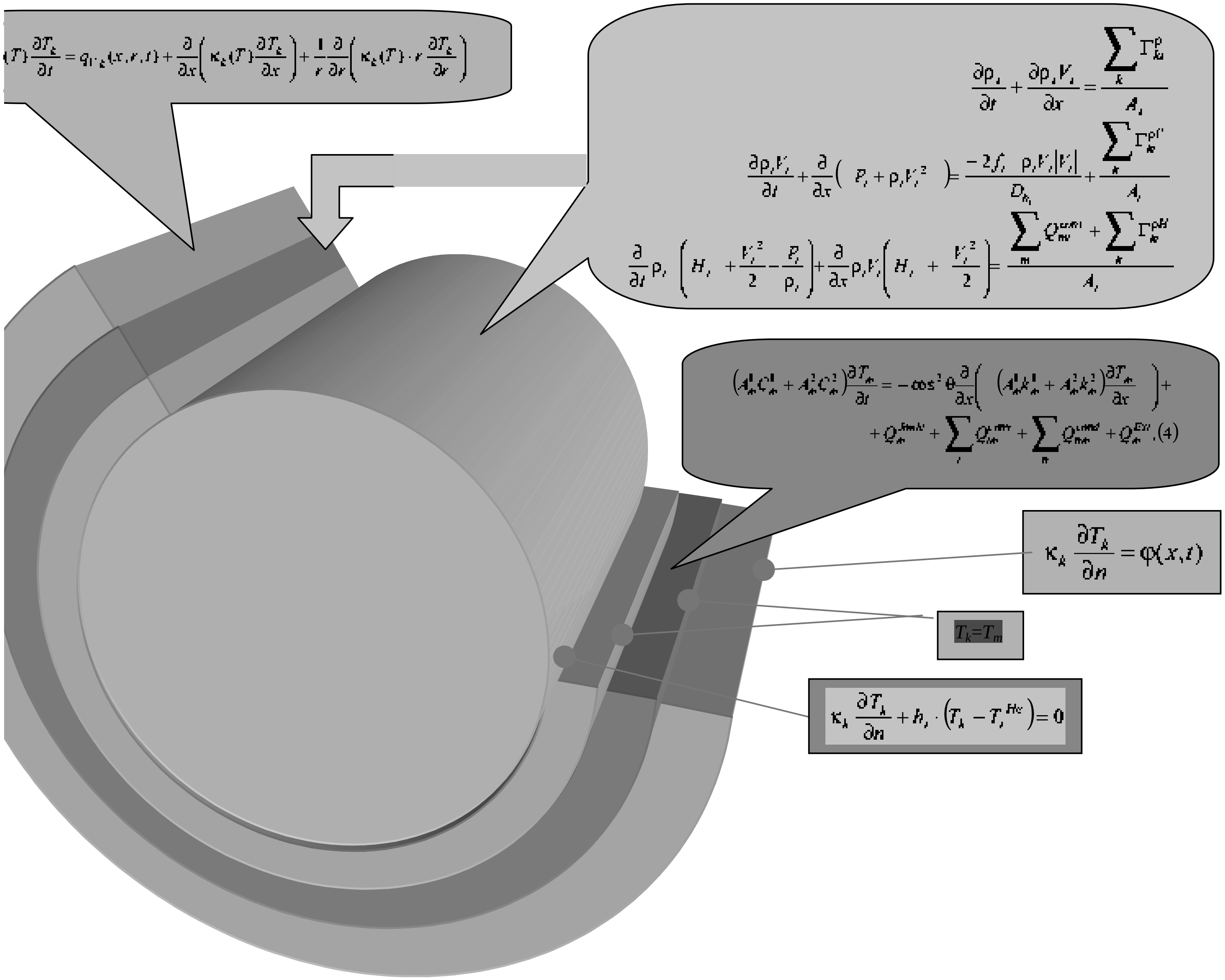

Figure 2 Transmission Line Drive Conductor Heat Model used for Quench Simulation

2.6 Electrical circuit

The simplest LR-circuit used as an electrical model for simulation of current changes during the conductor quench[8]

$$L\frac{dI_{op}}{dt}+\left(R_{NZ}+R_{ext}(t)\right)\cdot I_{op}=U(t)\ ,\ (14)$$

$$R_{NZ}=\frac{P^{Joule}}{I_{op}^{2}}\ ,\ (15)$$

where L – inductance of circuit, H; R_{ext} – external (dump) resistance, Ohm; U – external voltage, V; I_{op} – operating current, A; $P^{Joule}=\int Q_m^{Jole}dx$ - Joule heating over full conductor length, J.

3. NUMERICAL METHOD

For computing the analysis equations (1)-(3), (8), (9) have been written in non-conservative form by using pressure **P** enthalpy **H** and velocity V as flow variables (introducing the Gruneisen parameter ϕ and isentropic speed of sound c) [4]. So, each *channels* is defined by a set of P, H, V variables for helium. All *collectors* are defined individually by P, H variables for helium.

All equations related to *channels* and *conductors* are resulted in finite differences form on the space variable x. The size of space steps is defined by accuracy of solved task. For *channels* connected between themselves by heat and mass transfer in longitudinal direction the number of nodes is identical. The same refers to the conductors that connected between themselves and corresponding channels.

Parabolic partial differential equations (13) is transferred in finite differences form on the space variables x and r.

Thus we have a system of ordinary differential equations on time variable concerning P, H, V and T parameters for all nodes of 1D (*channels* and *conductors*) and 2D (*wall*) meshes. The complete system of ordinary differential equations on time (including equations for *collectors* and *current*) are solved simultaneously by Runge-Kutta method of forth order.

The computer code VINCENTA is compiled by MS Fortran Power Station 1.0 and used for Intel PC compatible computers.

---

[8] In present simulations it is assumed the inductance of circuit L is much greater than actual margin of the magnet considered. The same refers to the dump resistor: $R_{ext} >> R_{NZ}$. So during quench protection the current decay time constant τ defined as $\tau = L/R_{ext}$ (U=0).

4. INITIAL DATA AND APPROACHES

4.1 Cable Geometry and Material utilized

Data on the cable geometry and material utilized are given in Table 1,2.

Table 1

CABLE MATERIALS

Strand	Copper & NbTi
Outer tape	Copper
Inner and Outer tubes (conductor coating)	Invar

Table 2

GEOMETRIES DATA ON TRANSMISSION LINE DRIVE CONDUCTOR:

OD of Outer Invar tube	38.1 mm
ID of Outer Tube	31.8 mm
OD of Copper Tape	35.6 mm
ID of Copper Tape	34.5 mm
OD of superconductor	34.5 mm
ID of superconductor	31.8 mm
Number of strands	8x30
Average $cos(\theta)$[9]	0.86
Cu/NbTi ratio for strand	1.3
Total Cu/NbTi ratio	2.25
Residual Resistivity Ratio (RRR) for Copper	55
Diameter of cooling channel	30.2 mm
Length	60 m

For two channel conductor model (model with the cable void space filled by SHe) it is assumed the void fraction in annulus space between the invar tubes is 10cm^3 per 1m of conductor length (about 7%). Besides transversal cross area punched is supposed to be equal 5mm^2 per 1m of conductor length.

4.2 Helium properties

In a single phase region the helium thermophisical and transport properties are calculated according to [5,6]. Enthalpy H and pressure P are accepted as independent variables. A two-phase helium region is simulated as a homogenous mixture. An equation of state for such mixture has a form

$$1/\rho_{\mathbf{homo}}(P,H) = 1/\rho'(P) + [1/\rho''(P) - 1/\rho'(P)][H - H'(P)]/[H''(P) - H'(P)] \text{ , (17)}$$

where ρ', ρ'', are the liquid and vapor helium densities on a boundary line of helium TS-diagram; H', H'' are the liquid and vapor enthalpies as a function of pressure P.

4.3 Thermal and Electrical Properties of Cable Materials

[9] θ is an average effective twist angle of cable strands and copper tape

Non-linear thermal (copper, invar and NbTi) and electrical (copper only) properties of the cable materials were taken into account in present simulations.

Copper properties

Correlation for thermal and electrical properties of copper is treated through the residual resistivity ratio RRR and field B and based on the Wiedemann-Franz law [8]. Matissen rule used to calculate actual resistivity of copper as $\rho(T)= \rho_{id}(T)+ \rho_{res}$, where $\rho_{res} = \rho(4K)$ is residual resistivity. Residual resistivity ratio RRR = $\rho(273K)/ \rho(4K)$ of copper is taken equal to 55. Ideal resistivity calculated in accordance with the Gruneisen formula $\rho_{id}(T) = C*(T/\Theta)^5 J_5(\Theta/T)$, where C=27.32 $\mu\Omega{\cdot}m$, Θ=333K and $J_5(x) = \int_0^x \frac{x^5 e^x}{(e^x-1)^2} dx$.

Magnetic effect on both the electrical resistivity ρ and thermal conductivity k was taken into account too. The effect of background magnetic field B on the electrical resistivity of the copper was taken as $\rho(T,B)/\rho(T,0)=1+\alpha*B*\rho(273K,0)/ \rho(T,0)$. For transverse effect α is equal to 0.003 (see Fig. 4.3.1a). Accordance to [5] the Wiedemann-Franz law is constant for varying magnetic fields. So, the copper thermal conductivity as function of B calculated assuming the ratio $k(B)\rho(B)/k(0)\rho(0) = 1$. Thermal conductivity of copper for B=0 and B=1T is shown in Fig. 4.3.1b. The Lorentz number $L(T) = k(T)*\rho(T)/T$ for copper with B=0 and B=1T is given in Fig. 4.3.1c. Specific heat of copper shown in Fig.4.3.1d.

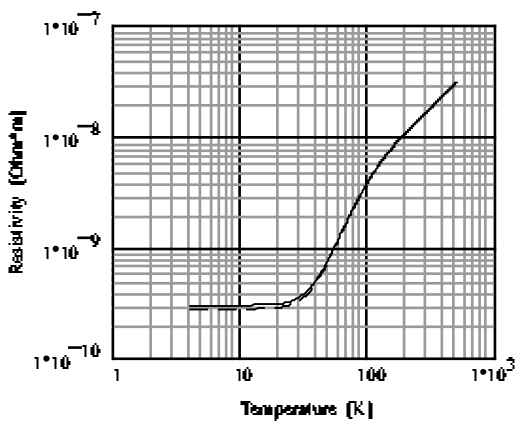

(a)

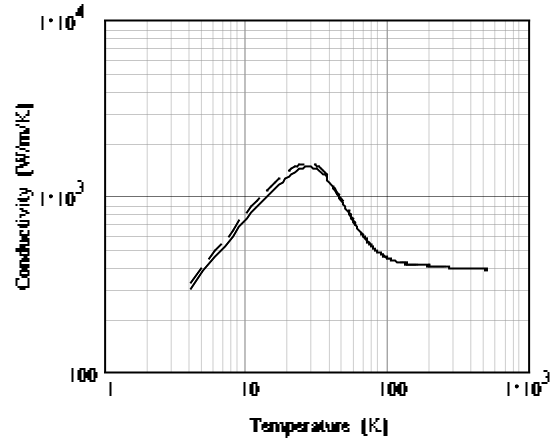

(b)

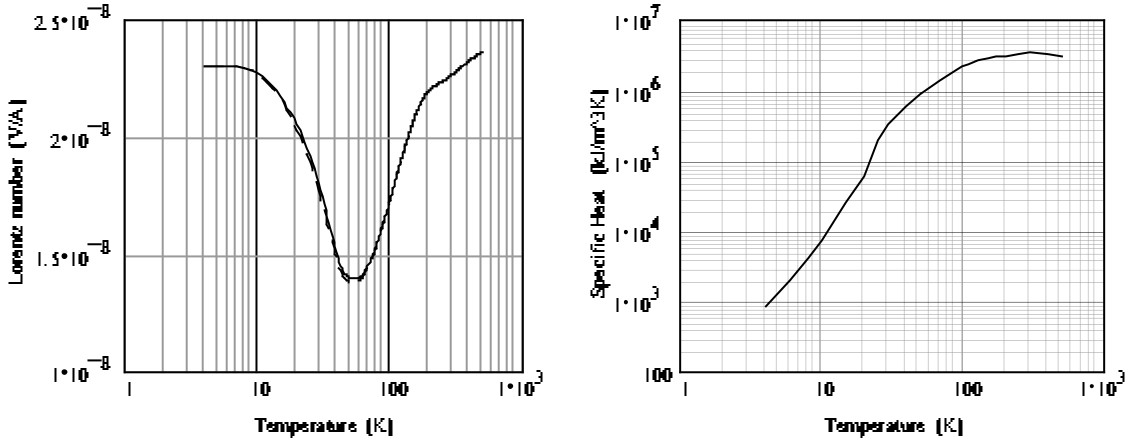

(c) (d)

Figure 4.3.1 Properties of copper RRR=55 as function of temperature for two values of magnetic field B=0 (dash line) and B=1T (solid line)

Invar properties

The data on thermophisical properties of Invar are scant enough and in bad consistency. The data used in present simulation are given in Table

Thermal conductivity and specific heat of Invar

Temperature, K	Conductivity, W/m K	Specific Heat, kJ/m³ K
4	0.22	7.86
6	0.39	12
8	0.57	16.3
10	0.76	20.9
15	1.3	34.3
20	1.9	52.6
25	2.5	77.8
30	3.2	113
40	4.4	221
50	5.6	718
70	7.5	1330
90	8.8	1890
100	9.3	2120
110	9.8	2330
130	10.6	2660
150	11.4	2910
170	12	3110
200	12.9	3330
250	14.2	3600
300	15.2	3810

NbTi properties

A very poor data base is available for NbTi thermal properties at the moment. The data of different references in a bad consistency. The next table shows the specific heat used in present simulation. Thermal conductivity of NbTi was neglected in compare with high conductivity of a copper matrix.

Specific heat of NbTi

Temperature, K	Specific Heat, kJ/m³ K
4	3.66
6	12.1
8	28.4
10	29.4
15	70.9
20	144
25	196
30	329
40	605
50	881
70	1430
90	2010
100	2260
110	2420
130	2690
150	2880
170	3020
200	3170
250	3350
300	3440

Critical properties of NbTi/Cu Strand defined (per a strand) as

$$I_c(B,T)=I_0/\mathrm{sqrt}(B/B_0)*[1-(T-T_0)/(T_c(B)-T_0)],$$

$$T_c(B)=T_{c0}*(1-B/B_{c0})^{0.59},\ B_0=4\mathrm{T},\ T_0=4.2\mathrm{K},\ I_0=725\mathrm{A}$$

4.4 Correlation for heat exchange and friction

For modeling of heat and momentum exchange between the helium flow and wetted surfaces of the central tube and cable strands the following correlation used:

<u>heat transfer coefficient and friction factor in conductor central channel</u>

$$h(\mathrm{Re},T_{He})=\lambda_{He}(T_{He})/D_h\cdot\begin{cases}3.66, & \mathrm{Re}<2300\\ 0.023\,\mathrm{Re}^{0.8}\,\mathrm{Pr}^{0.4}, & \mathrm{Re}>2300\end{cases}$$

$$f(\mathrm{Re}, T_{He}) = \begin{cases} 16/\mathrm{Re}, & \mathrm{Re} < 2300 \\ 0.079/\mathrm{Re}^{0.25}, & \mathrm{Re} > 2300 \end{cases}$$

where $\mathrm{Re} = \dot{m} D_h / \mu A$ is the Reynolds number, $\mathrm{Pr} = C_p \mu / \lambda$ is the Prandtl number.

<u>heat transfer coefficient and friction factor in the cable void space</u>

h_{void} = 2000 W/m^{2}K. This value ensure practically ideal heat exchange of He with cable strands that seems to be relevant

$f_{void} = (19.5/\mathrm{Re}^{0.88}+0.051)/(4.*\mathrm{Void}^{0.72})$. This is ITER reference formula used for calculating of friction factor in momentum equation in the cable void space.

4.5 Hydraulic scheme and initial state

Hydraulic layout used for present simulation of cable quench is shown in Fig. 4.5. Supply and Return Lines are modeled as very large collectors V1 and V6 with following initial parameters of helium: P_{SL}=4.5 bar, T_{SL}=4.52 K and P_{RL}=1.3 bar. The valve hydraulic resistance (cross section area A_k in equation (12)) is balanced in such manner that under steady state mass flow rate 40g/s the pressure in the transmission line inlet equals 3.3Bar. Background heat load on the conductor is 0.2W/m.

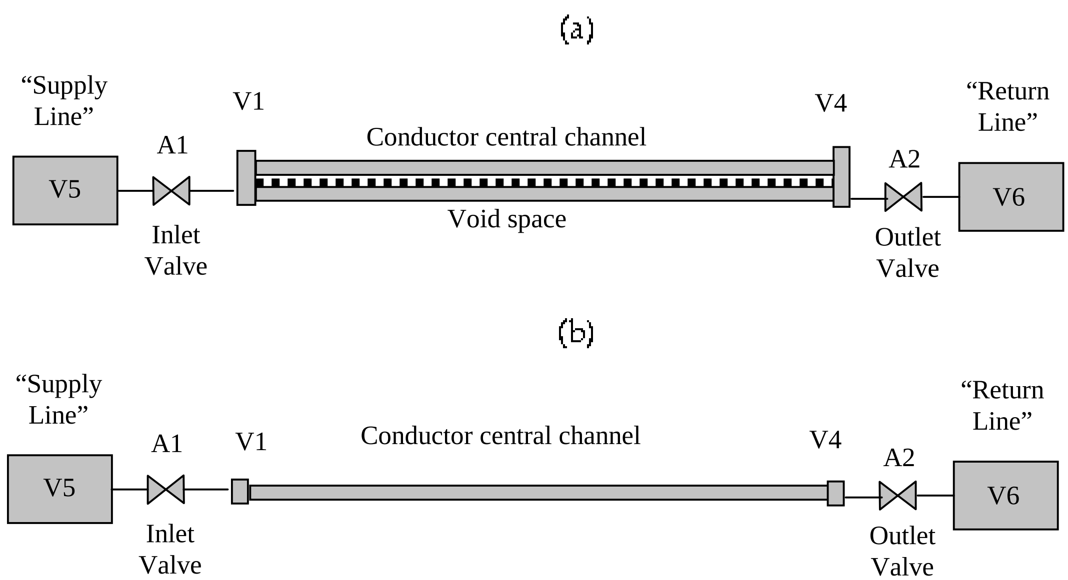

Figure 4.5 Hydraulic layout used for two-channel (a) and single channel (b) models of the transmission line conductor during quench simulation.

4.6 Space and time discretization

Space step Δx along the transmission line conductor (cable and both invar tubes) are chosen in accordance with simulation accuracy and equal to 1cm. Four space steps used in radial direction of both inner and outer invar tubes. Non-uniform radial space steps (four for each tube) are 0.11-0.22mm and 0.18-0.36mm for inner and outer tubes correspondingly. Time step Δt is limited by Currant criteria and equal to 20-40mksec.

5. SIMULATION RESULTS

5.1 Quench scenario

Simulation results are obtained for 5 options when quench is caused by heating pulse located in the middle of the conductor. Rectangular in space and constant in time heating pulse with duration 5ms deposited into 3cm (100cm for Option 2 only) central part of the cable strands. The heating power density for considered options are shown in Table.

Initial disturbance power density

Conductor model	Option	Power density, kW/m
Void fraction 0%	1	2
	2	1.8
	3	2
	4	2.5
Void fraction 7%	5	4

Given values are slightly more than stability margin under operating current I_{op}=100kA and could be considered as stability margin estimation to considered disturbance. Under quench it is assumed that copper tape serves as a current carrier for operation current together with the strand copper. It is assumed in present simulation the twist angle θ is considered as an average common margin both for the cable strands and copper tape.

Protection. When Normal Zone voltage reaches 1V quench detection threshold the operational current starts ramp down with the current decay time constant $\tau = L/R_{ext}$=1 sec.

5.2 Single channel conductor model (zero void fraction)

Four options were considered for this variant of conductor model. Option 1 (RRR=55, L_{dist}=3cm, actual heat exchange) was considered as referenced variant. Option 2 differ from previous one by L_{dist}=100cm. Option 3 differ from Option 1 by zero heat transfer from inner invar tube to conductor SHe. Option 4 differ from Option 3 by copper purity (RRR=100).

5.2.1 Option 1 (Referenced)

Quench detection time delay (1V threshold) is 0.12s from the heat disturbance beginning. Figures 5.2.1.1 through 5.2.1.15 show basic results obtained for Option1. Typical view of the strand temperature for different times is shown in Fig. 5.2.1.1. Transient thermal diffusion in depth of the inner and outer invar tubes leads to temperature difference between the tube surfaces having contact with the cable strands and external ones. These differences are given in Fig. 5.2.1.6, 5.2.1.7. Evolution of Normal Zone voltage, length, resistance and velocity are shown in Fig. 5.2.1.11 through 5.2.1.14. NZ velocity is obtained by numerical differentiation of NZ length curve divided by 2. Because the finite velocity of heat diffusion in depth of the invar tube the SHe temperature in channel begin change with time delay about 0.05s. Small heat transfer coefficient in the center of conductor (zero SHe velocity) is the reason why the SHe temperature in the middle of conductor has a local minimum The features of normal zone spreading in transmission line is its wave form in time because of preheating of conductor by the channel helium. Evolution of SHe mass flow rate at the ends of cable (inlet & outlet valves) and its center is shown in Fig.5.2.1.9. Because the size of inlet valve hole is more than outlet one (the state of valve is fixed during quench)) the average blow up of SHe through it in the inlet collector is higher.

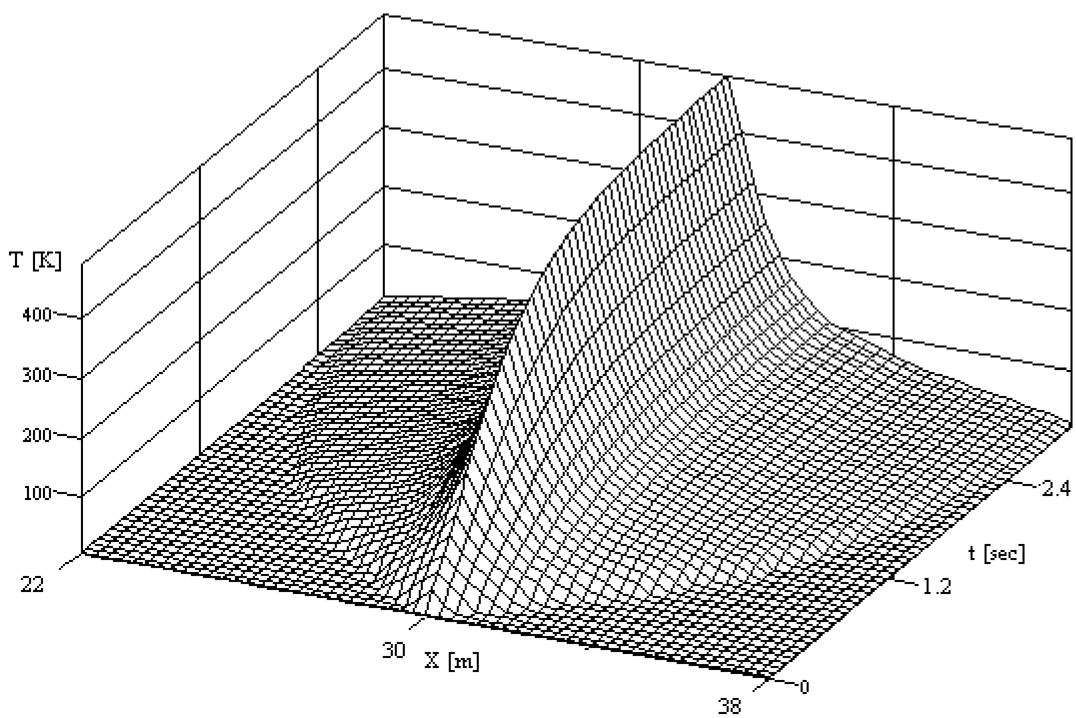

Figure 5.2.1.1a Evolution of the cable strand temperature during quench protection (current decay constant τ=1s, voltage threshold 1V.

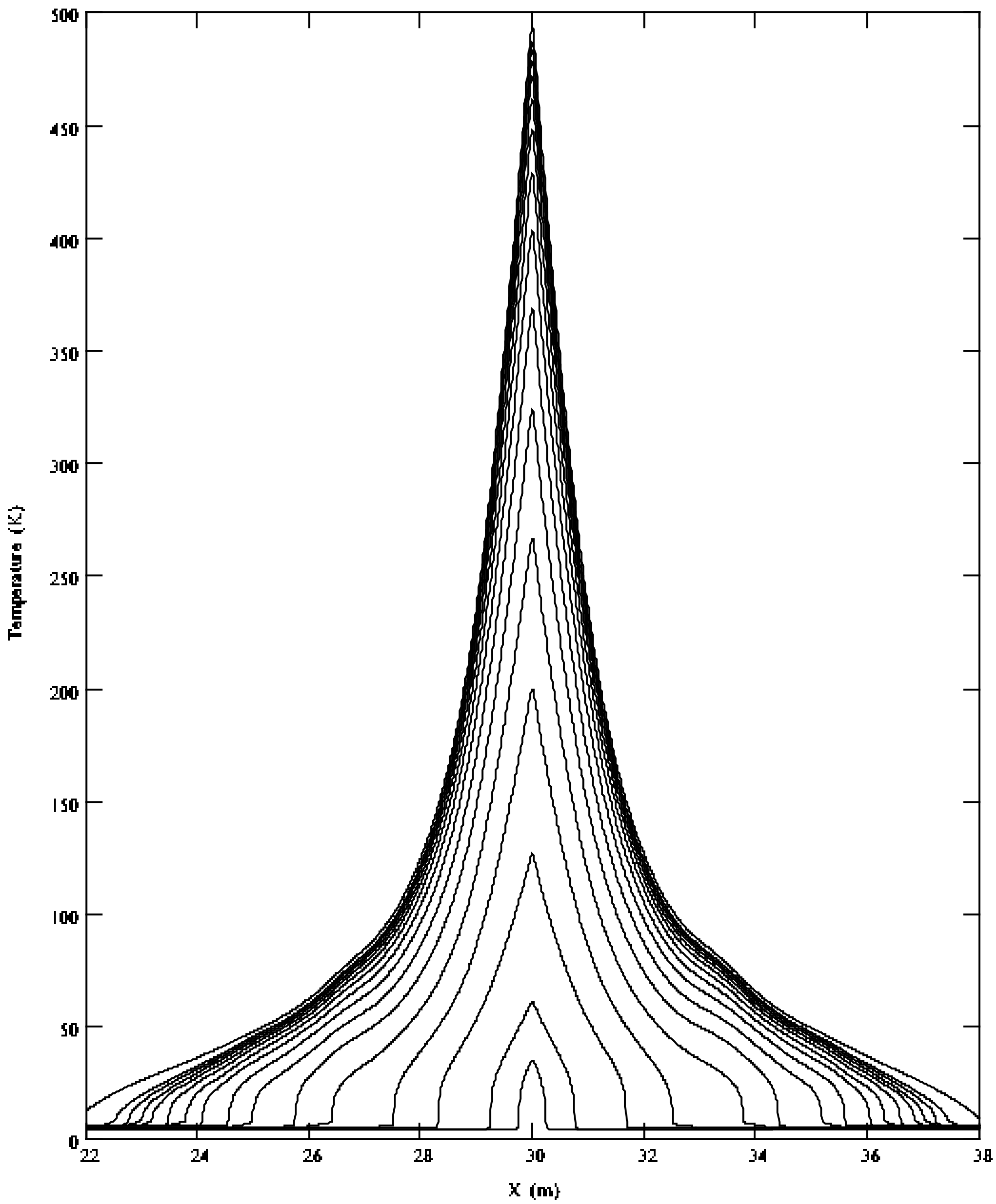

Figure 5.2.1.1b Evolution of the cable strand temperature during quench protection (current decay constant τ=1s, voltage threshold 1V, times: 0.04, 0.12, 0.28, 0.44, 0.60, 0.76, 0.92, 1.08, 1.24, 1.40, 1.56, 1.72, 1.88 2.04, 2.20, 3.00s).

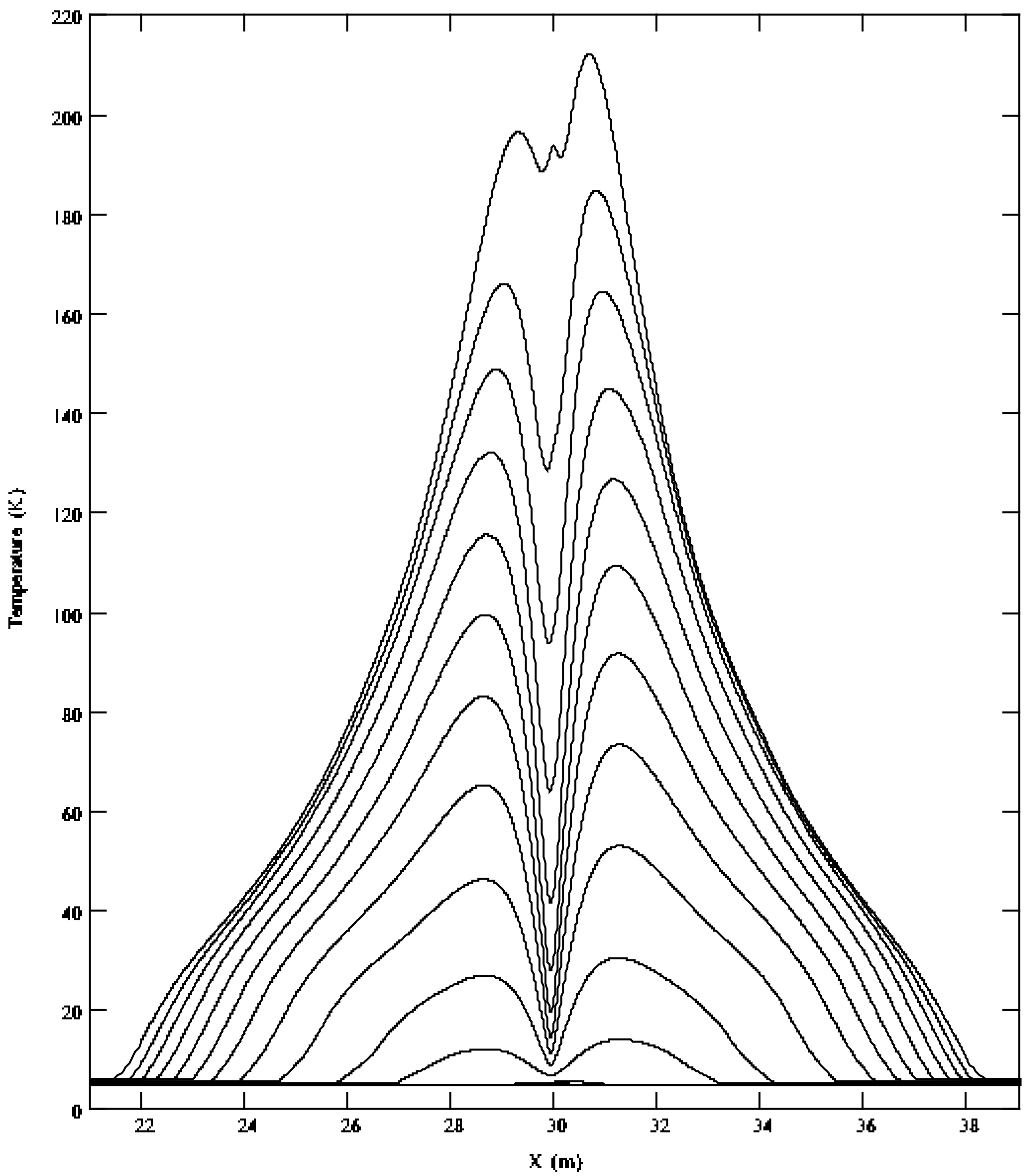

Figure 5.2.1.2 Evolution of the helium temperature during quench protection (current decay constant τ=1s, voltage threshold 1V, times: 0.12, 0.2, 0.44, 0.68, 0.92, 1.16, 1.4, 1.64, 1.88, 2.12, 2.36, 2.6, 3s).

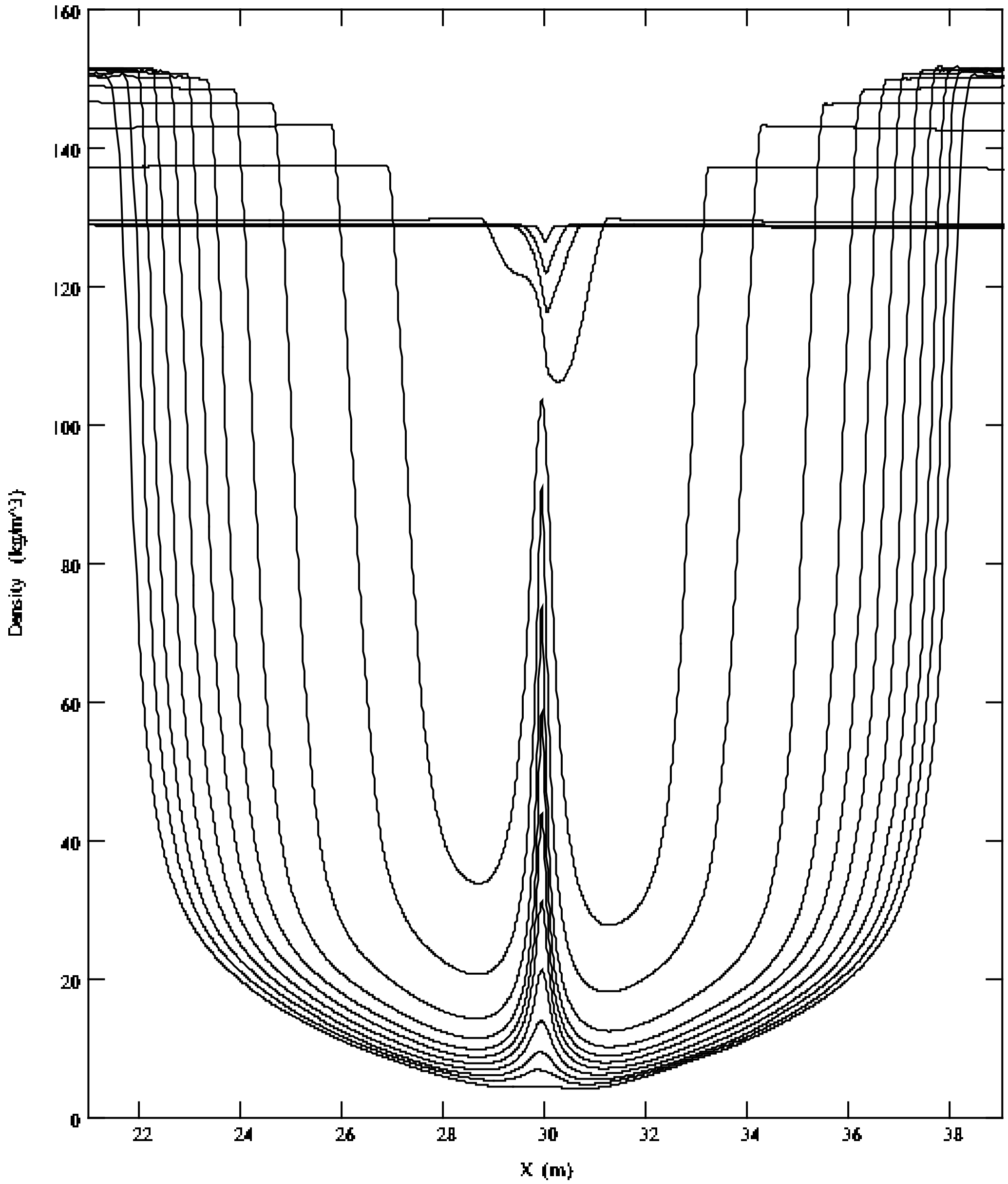

Figure 5.2.1.3 Evolution of the helium density during quench protection (current decay constant τ=1s, voltage threshold 1V, times: 0.04, 0.08, 0.12, 0.2, 0.44, 0.68, 0.92, 1.16, 1.4, 1.64, 1.88, 2.12, 2.36, 2.6, 3s).

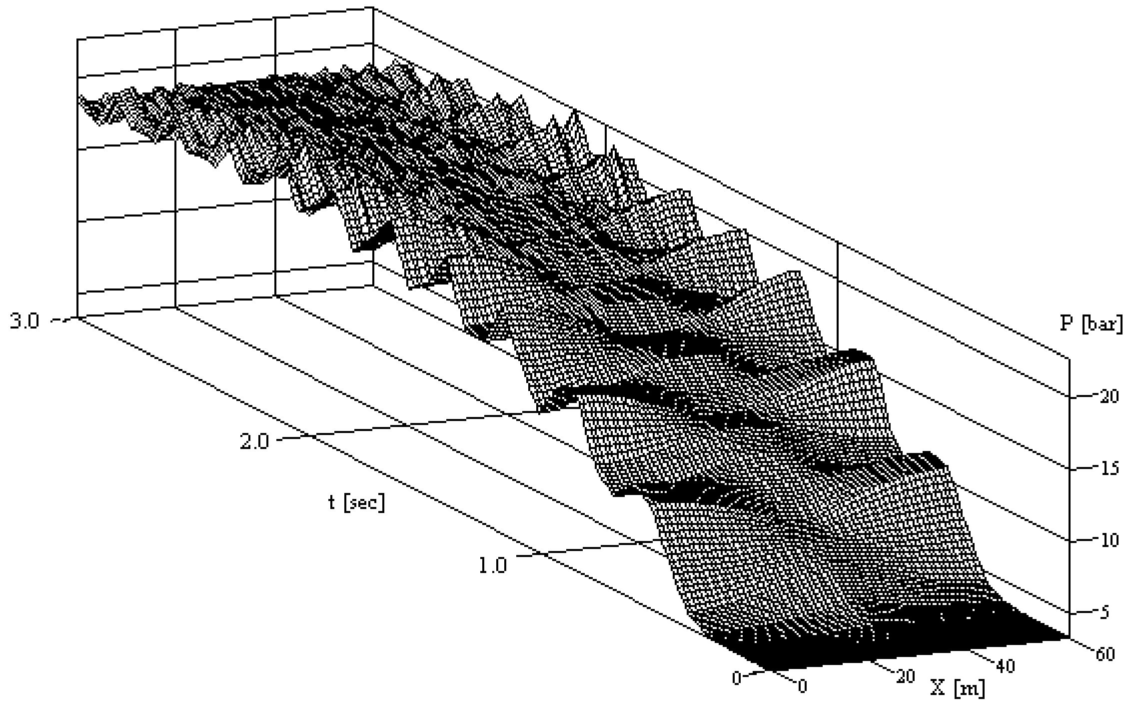

Figure 5.2.1.4 Evolution of SHe pressure (0-3s) inside the cable channel.

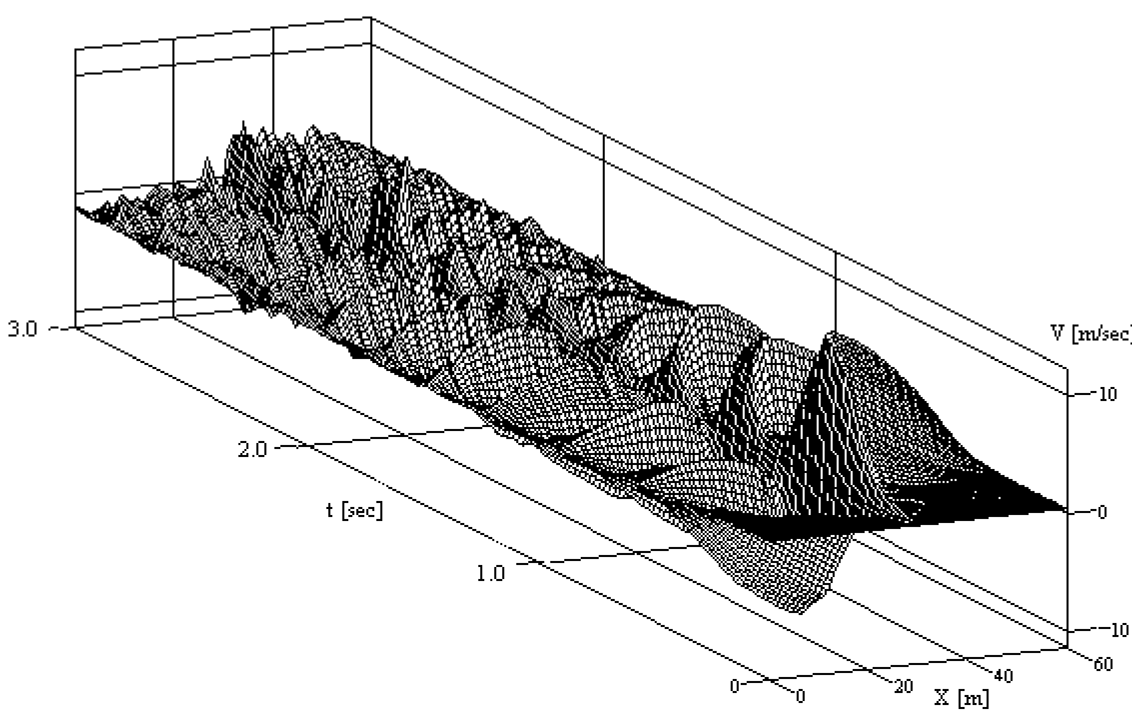

Figure 5.2.1.5 Evolution of helium velocity (0-3s) inside the cable channel.

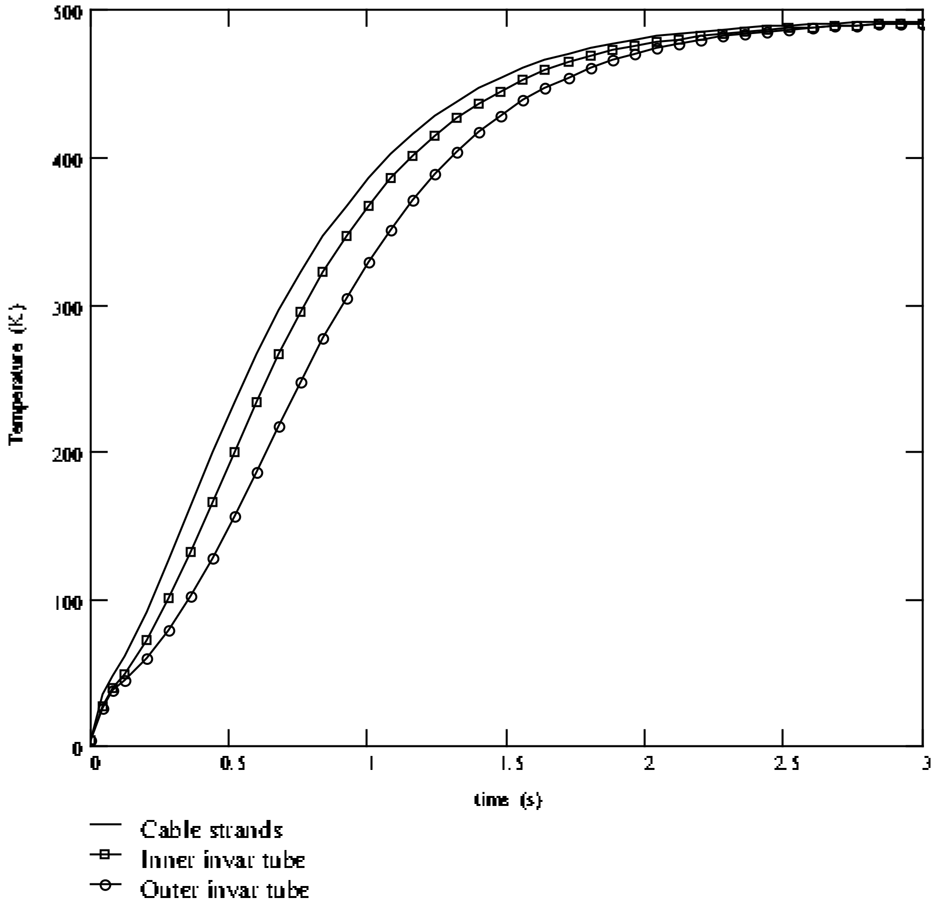

Figure 5.2.1.6 Evolution of maximal temperature (the middle of cable) for the Cable strands and external surfaces of Inner and Outer invar tubes.

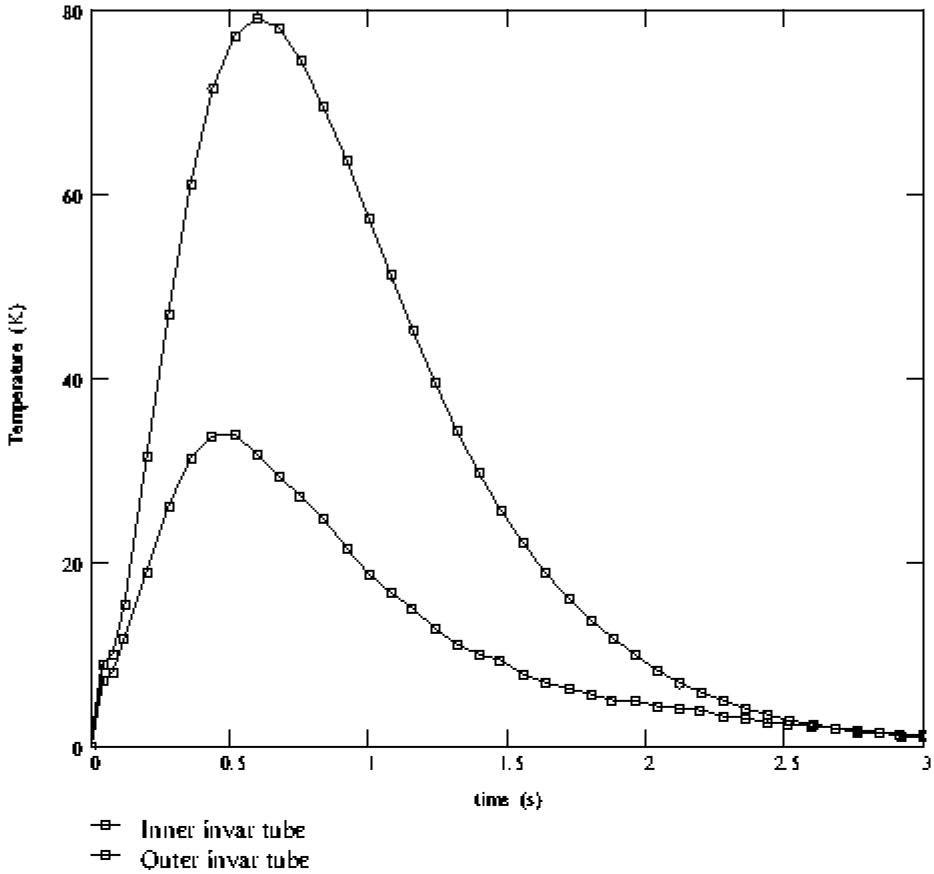

Figure 5.2.1.7 Evolution of the temperature differences across the thickness of Inner and Outer invar tubes.

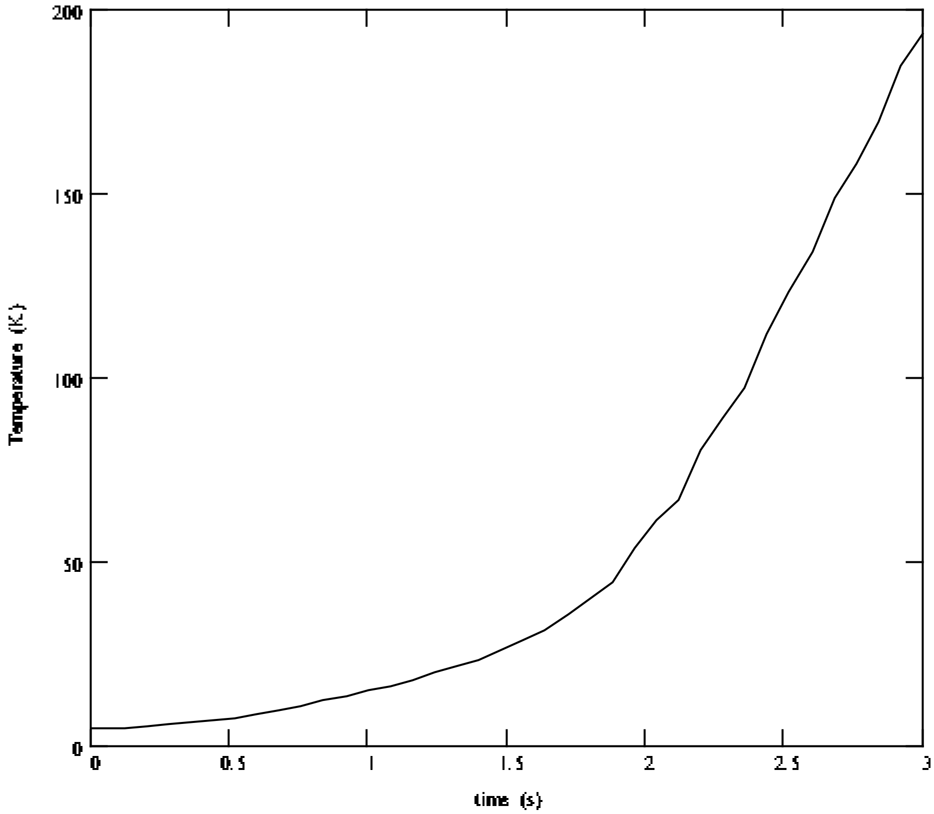

Figure 5.2.1.8 Evolution of the SHe temperature in the middle of the cable channel during quench protection.

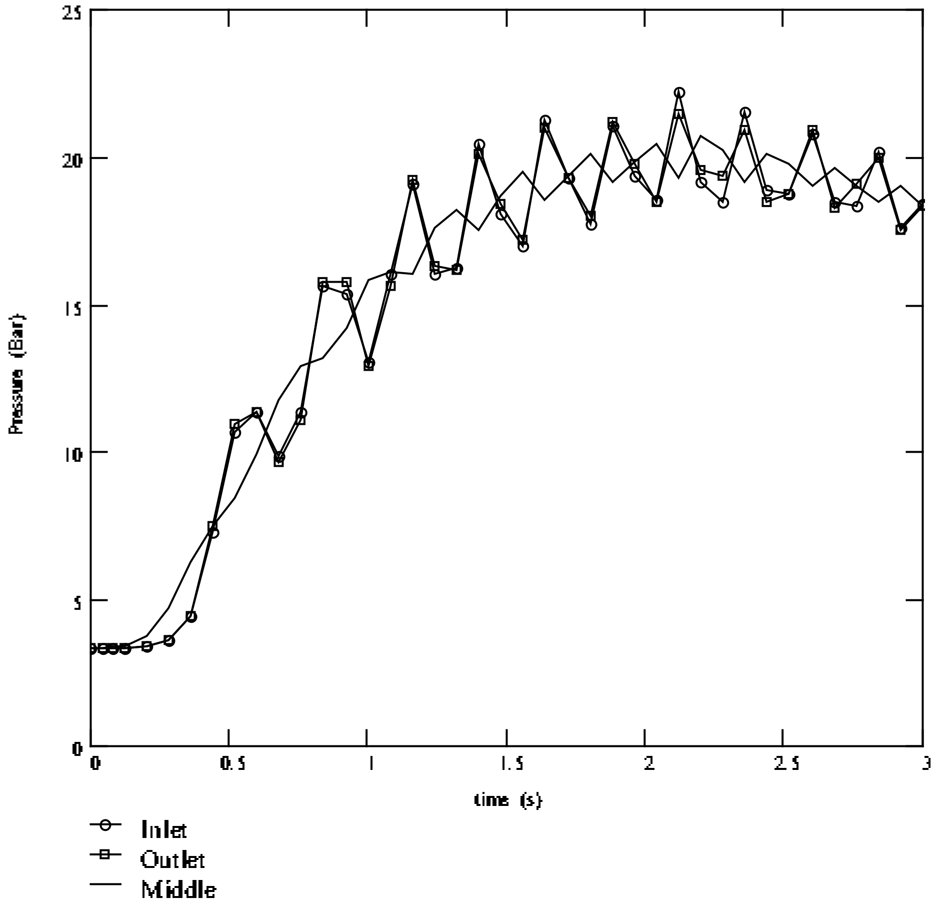

Figure 5.2.1.9 Evolution of the SHe pressure at the cable ends and its center during quench protection.

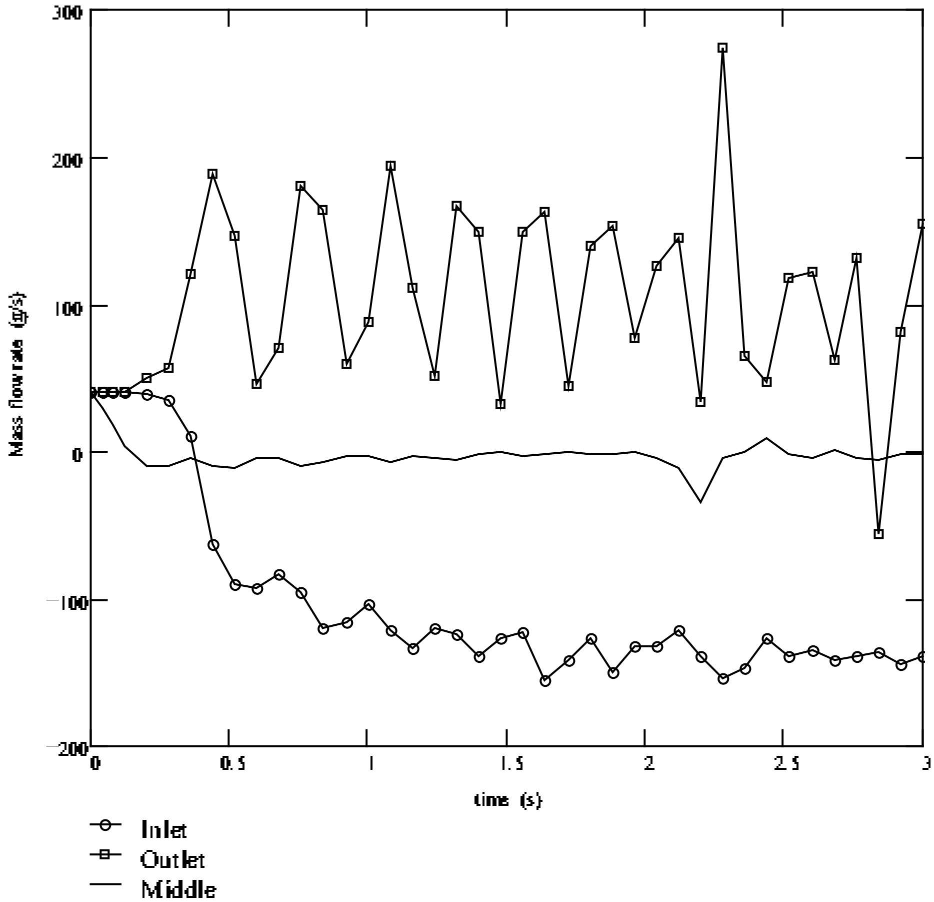

Figure 5.2.1.10 **Evolution of the SHe** mass **flow** rate at the cable ends (inlet & outlet valves) and its center during quench protection.

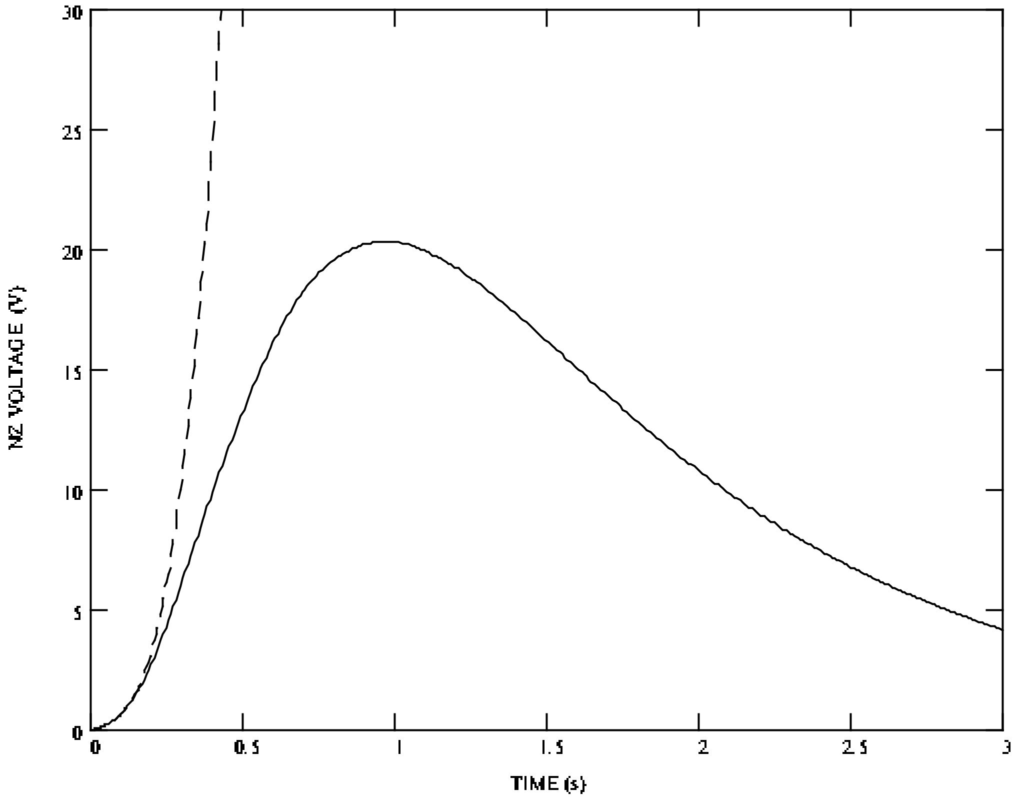

Figure 5.2.1.11 Evolution of Normal Zone voltage during quench protection (solid line) and without protection (dashed line).

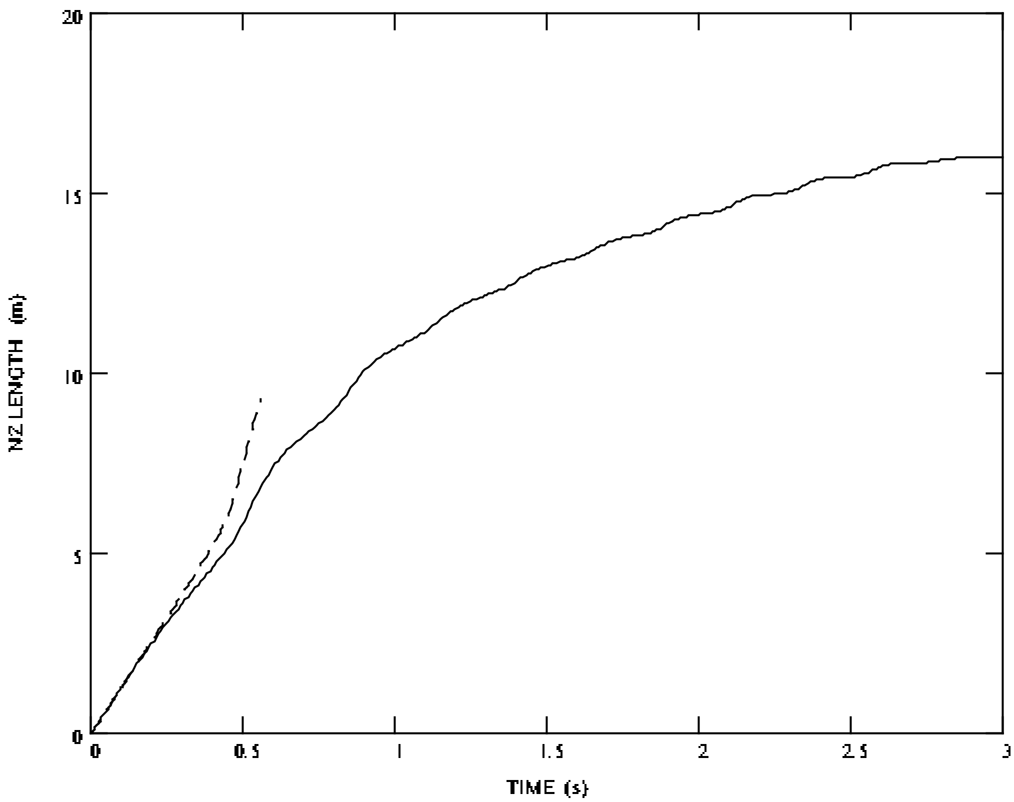

Figure 5.2.1.12 Evolution of Normal Zone length during quench protection (solid line) and without protection (dashed line).

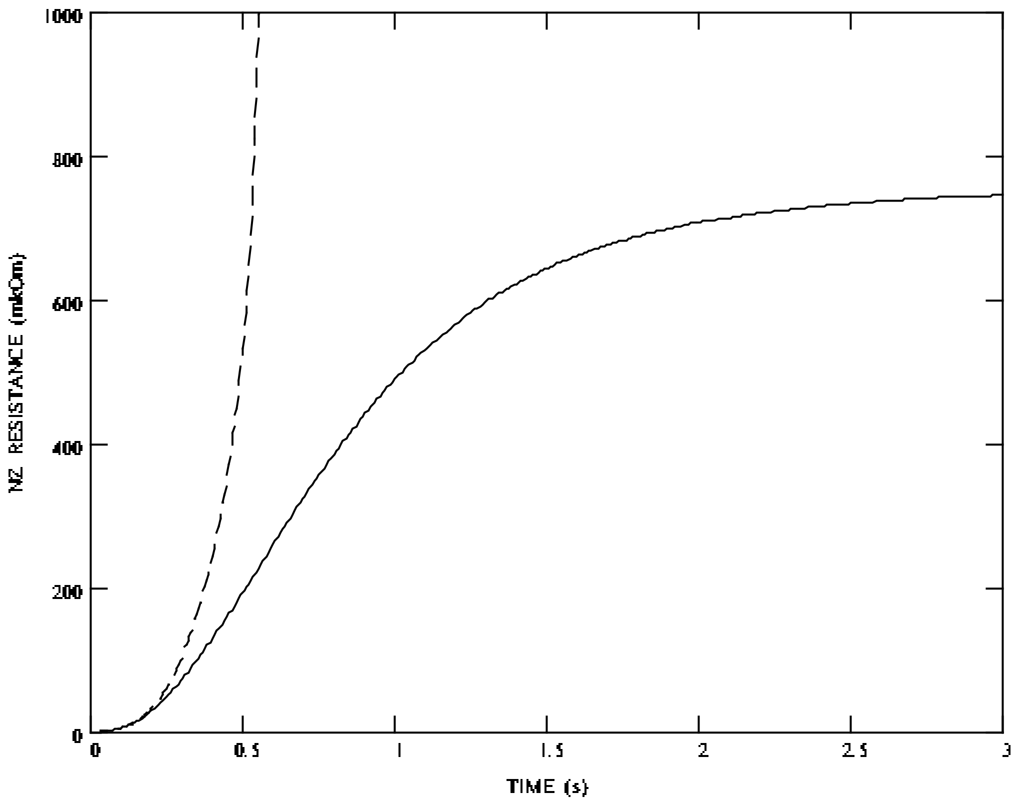

Figure 5.2.1.13 Evolution of Normal Zone resistance during quench protection (solid line) and without protection (dashed line).

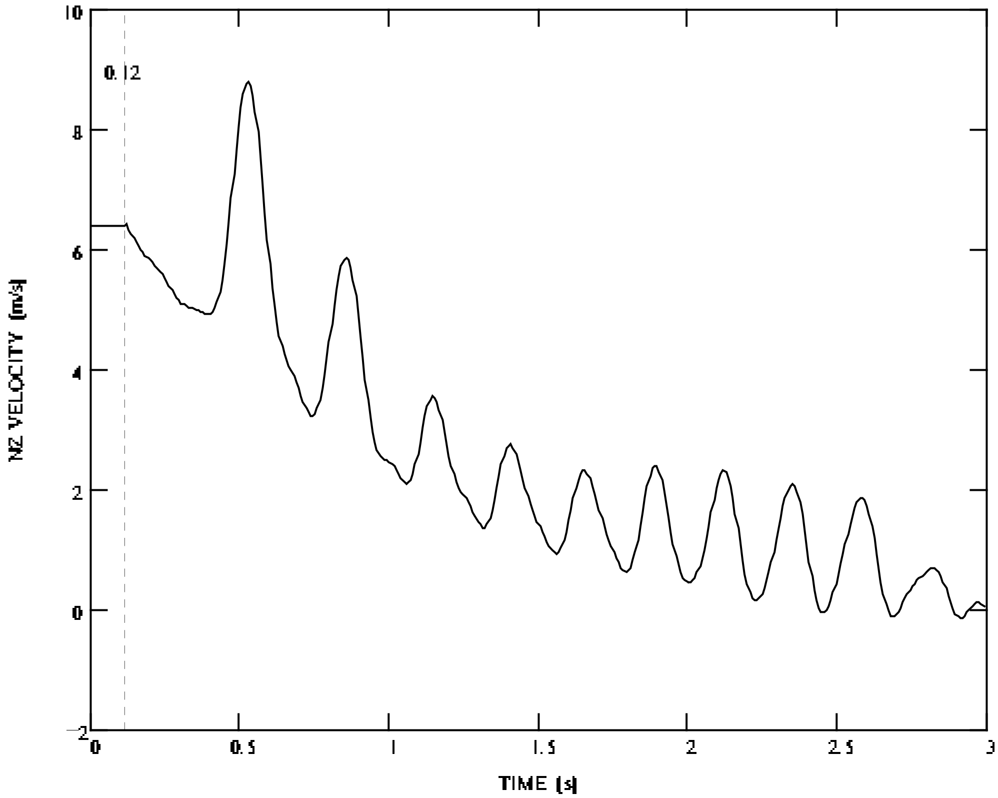

Figure 5.2.1.14 Evolution of Normal Zone velocity during the quench protection.

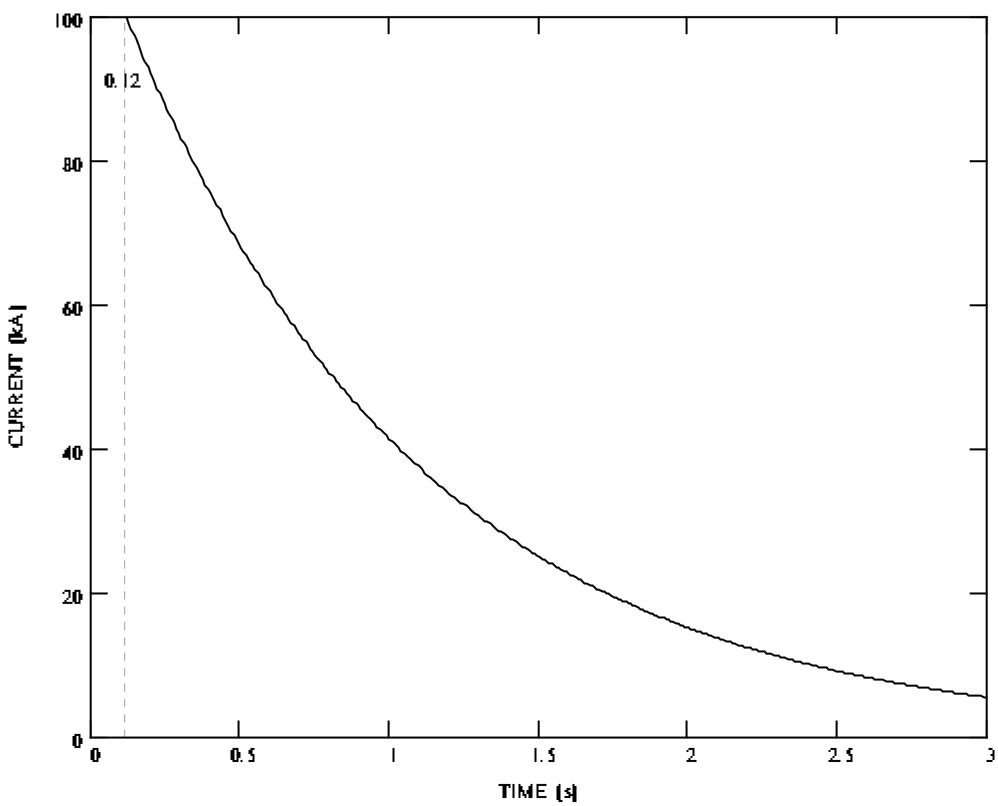

Figure 5.2.1.15 Current decay during protection (t_{delay}=0.12s, τ=1s).

5.2.2 Option 2 (Effect of initial heat disturbance size)

Figures 5.2.2.1 through 5.2.2.15 show basic results obtained for variant with cooling and in compare with the previous similar variant the only difference is another length of the initial heat disturbance zone $L_{disturb.}$=1m instead of 3cm. However this change significantly decreases the quench detection time delay (down to 0.08s for 1.1V quench detection threshold) and hot spot temperature for the same magnitude of the copper residual resistivity ratio RRR=55.

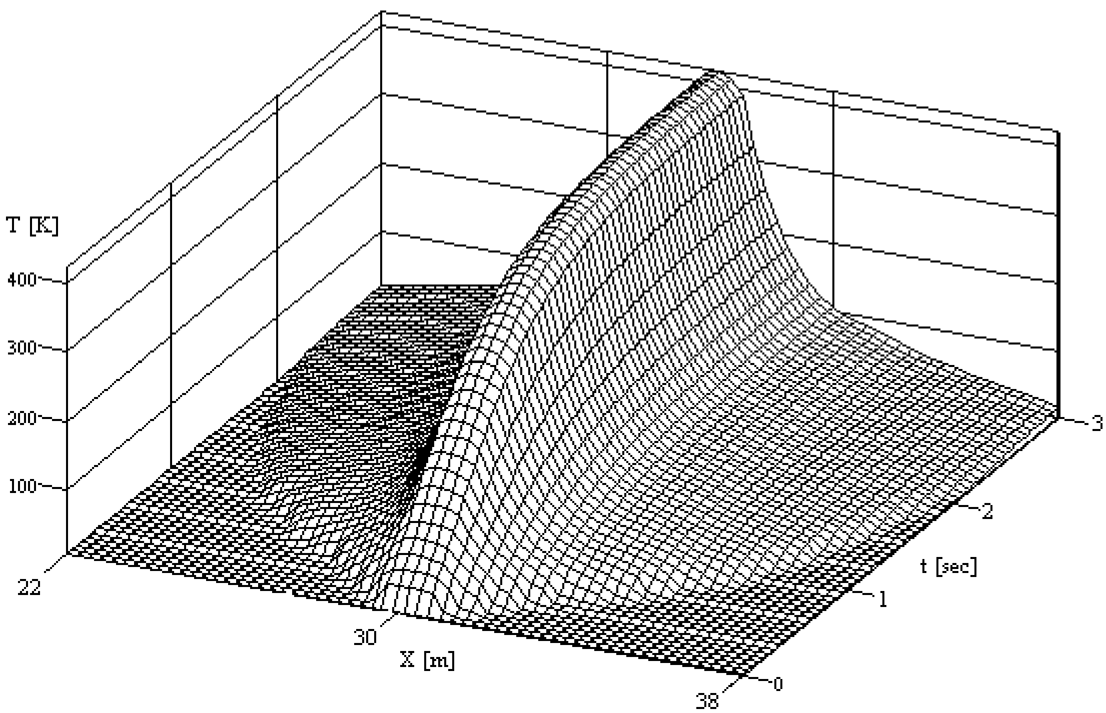

Figure 5.2.2.1a Evolution of the cable strand temperature during quench protection (current decay constant τ=1s, quench detection time delay t_{det}=0.08s).

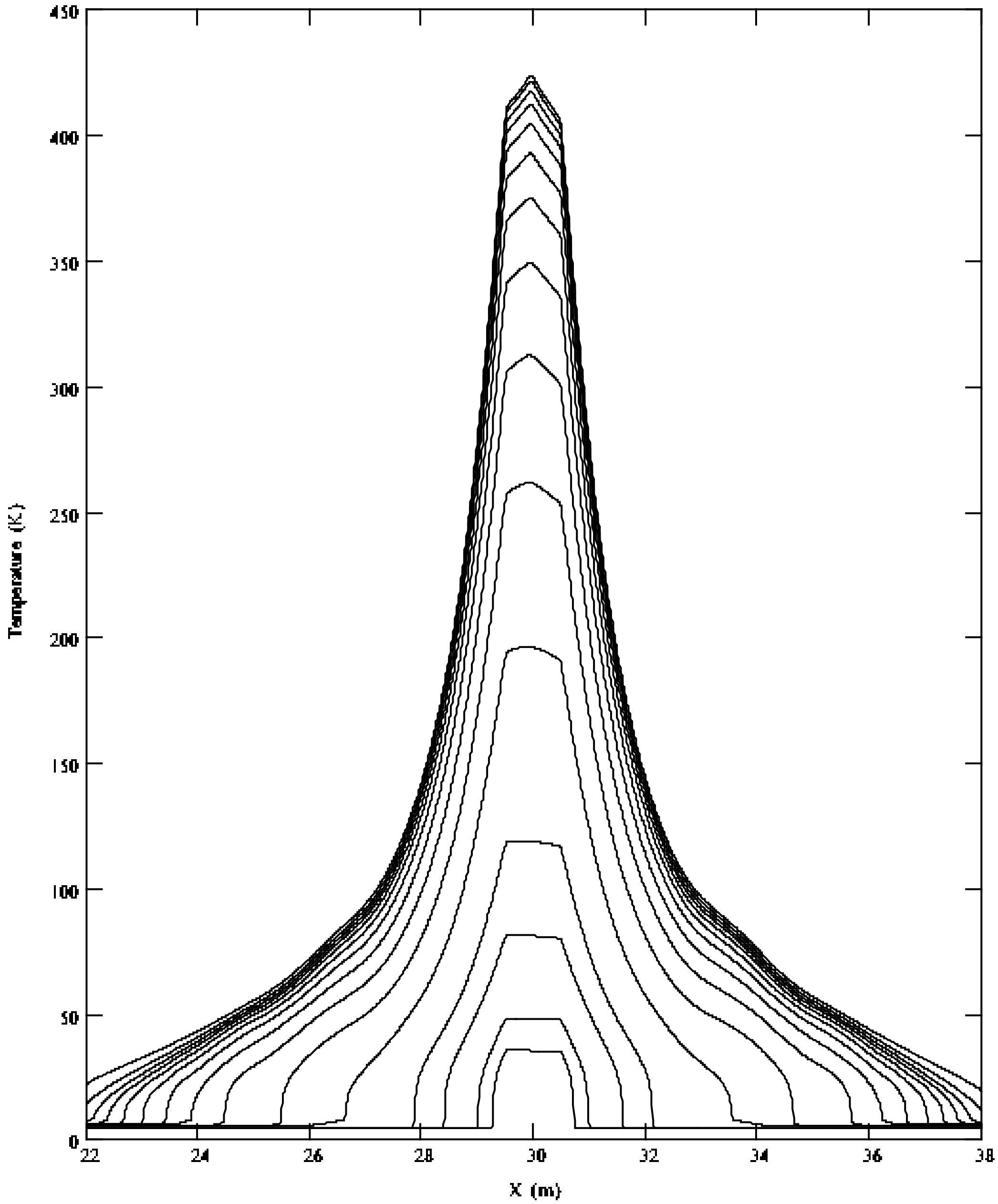

Figure 5.2.2.1b Evolution of the cable strand temperature during quench protection (current decay time constant τ=1s, quench detection time delay t_{det}=0.08s, times: 0.04, 0.08, 0.18, 0.28, 0.48, 0.68, 0.88, 1.08, 1.28, 1.48, 1.68, 1.88, 2.08, 2.38, 2.98s).

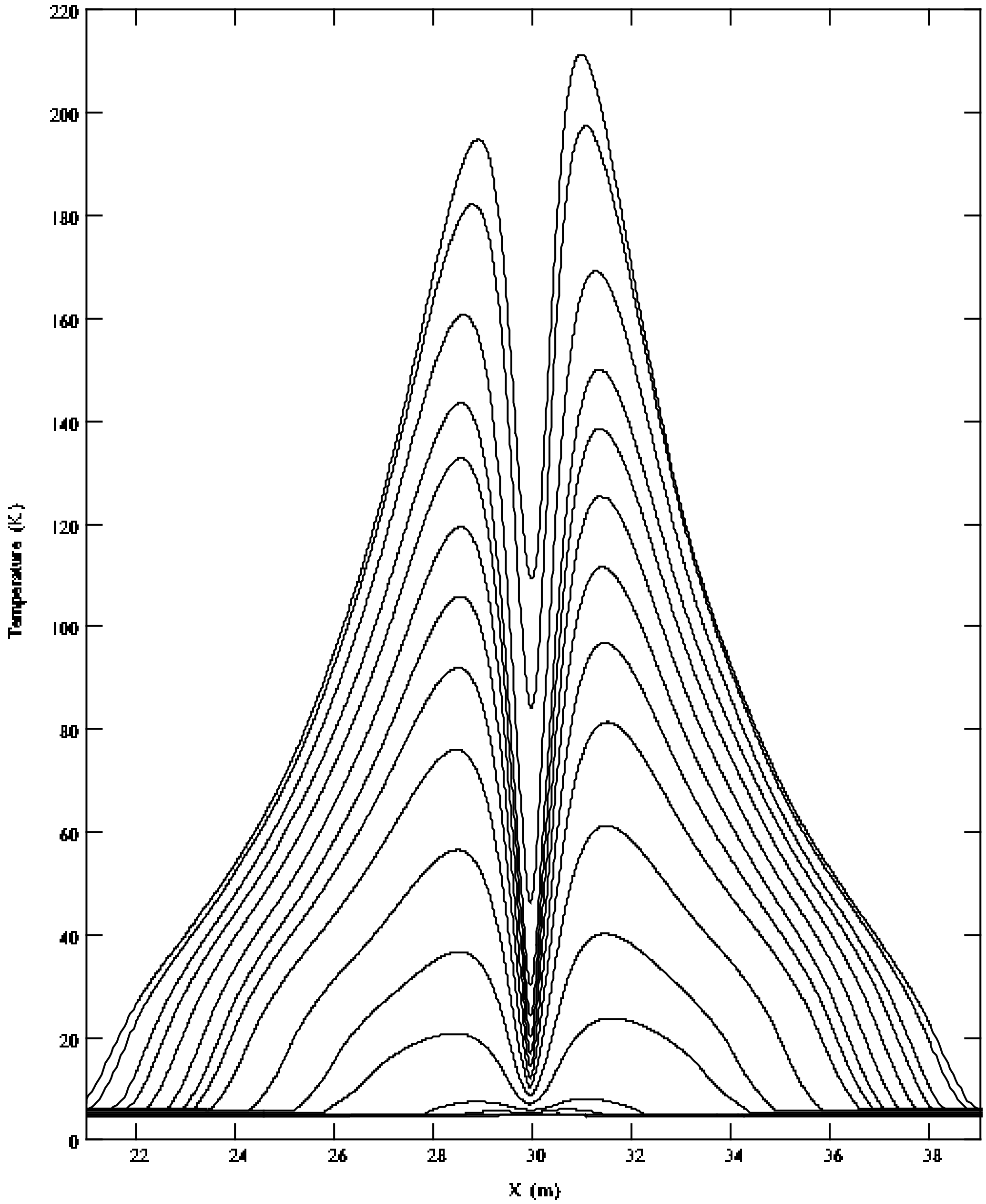

Figure 5.2.2.2 Evolution of the helium temperature during quench protection (current decay time constant τ=1s, quench detection time delay t_{det}=0.08s, times: 0.04, 0.08, 0.18, 0.28, 0.48, 0.68, 0.88, 1.08, 1.28, 1.48, 1.68, 1.88, 2.08, 2.38, 2.78, 2.98s).

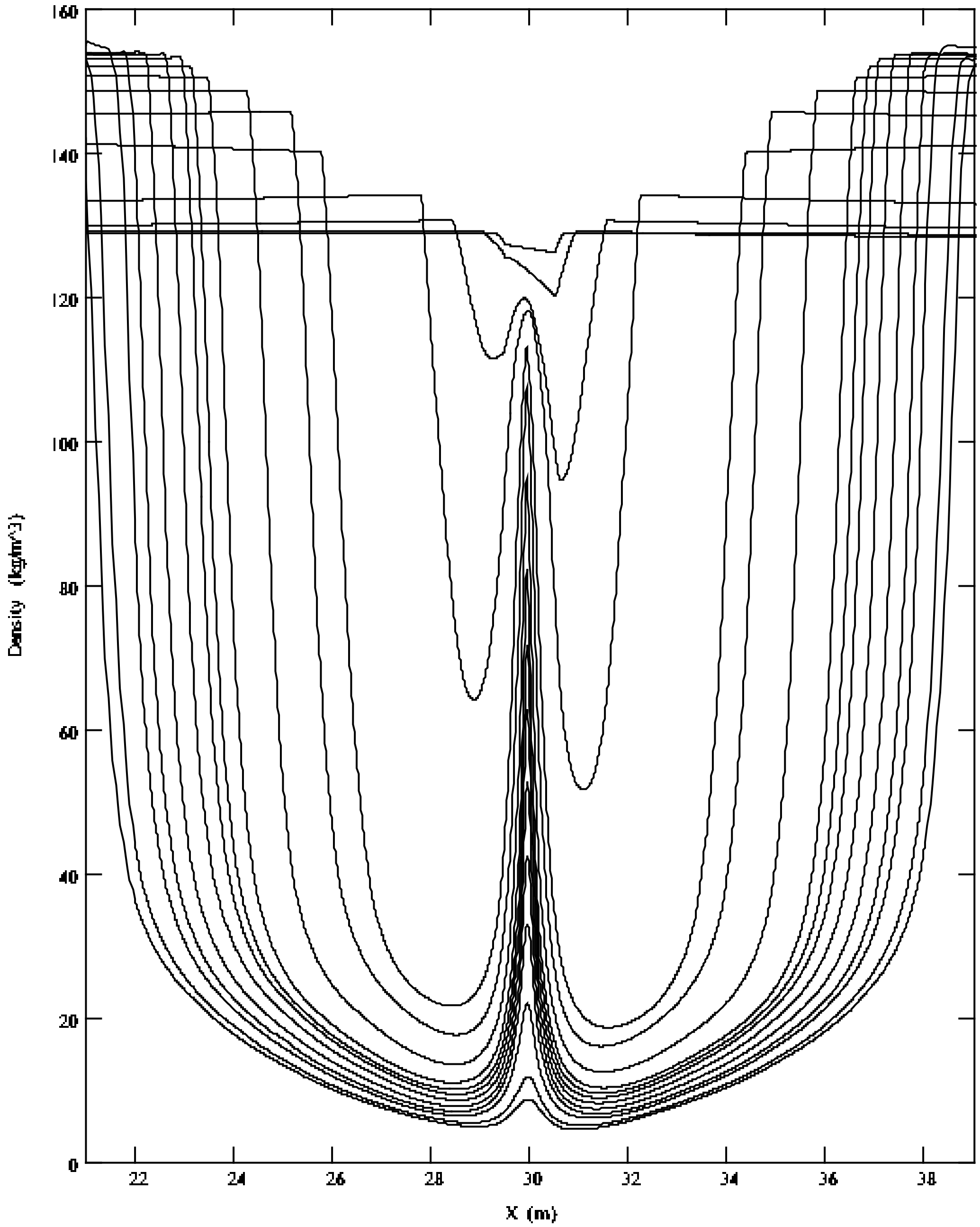

Figure 5.2.2.3 Evolution of the helium density during quench protection (current decay constant τ=1s, quench detection time delay t_{det}=0.08s, times: 0.04, 0.08, 0.18, 0.28, 0.48, 0.68, 0.88, 1.08, 1.28, 1.48, 1.68, 1.88, 2.08, 2.38, 2.78, 2.98s).

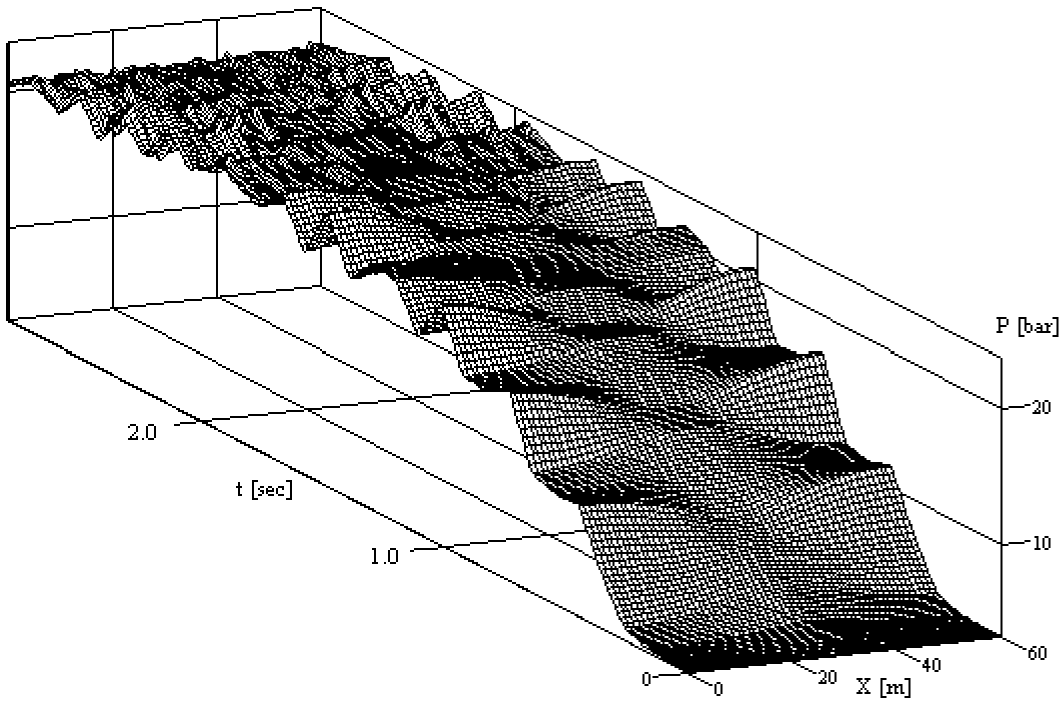

Figure 5.2.2.4 Evolution of SHe pressure (0-3s) inside the cable channel.

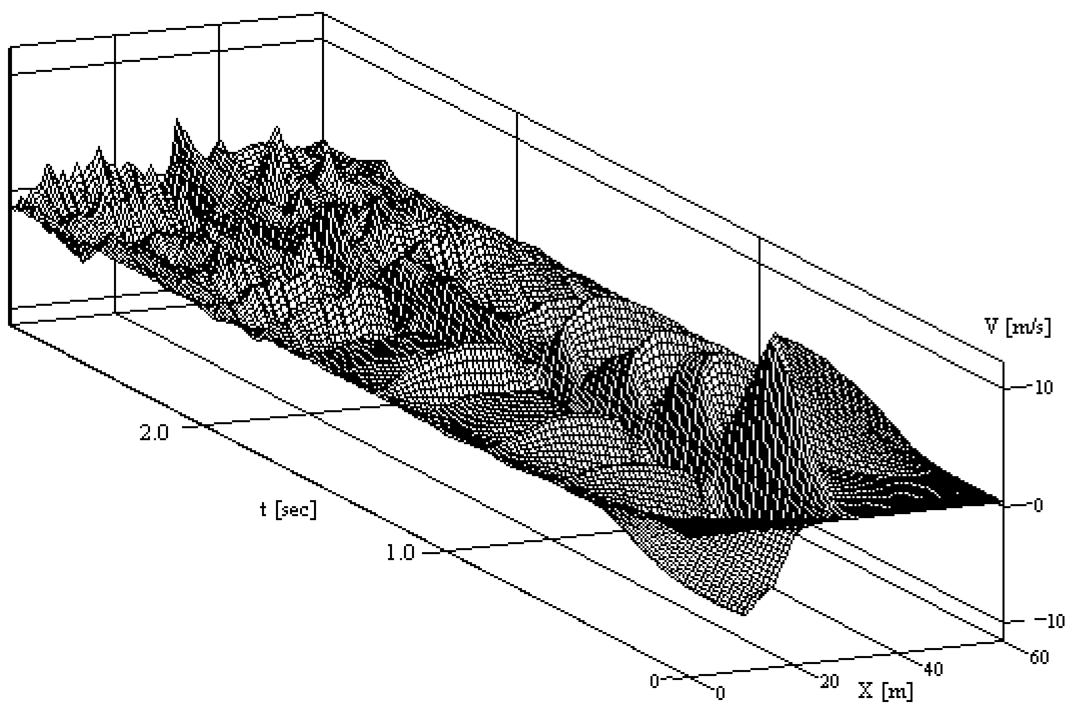

Figure 5.2.2.5 Evolution of helium velocity (0-3s) inside the cable channel.

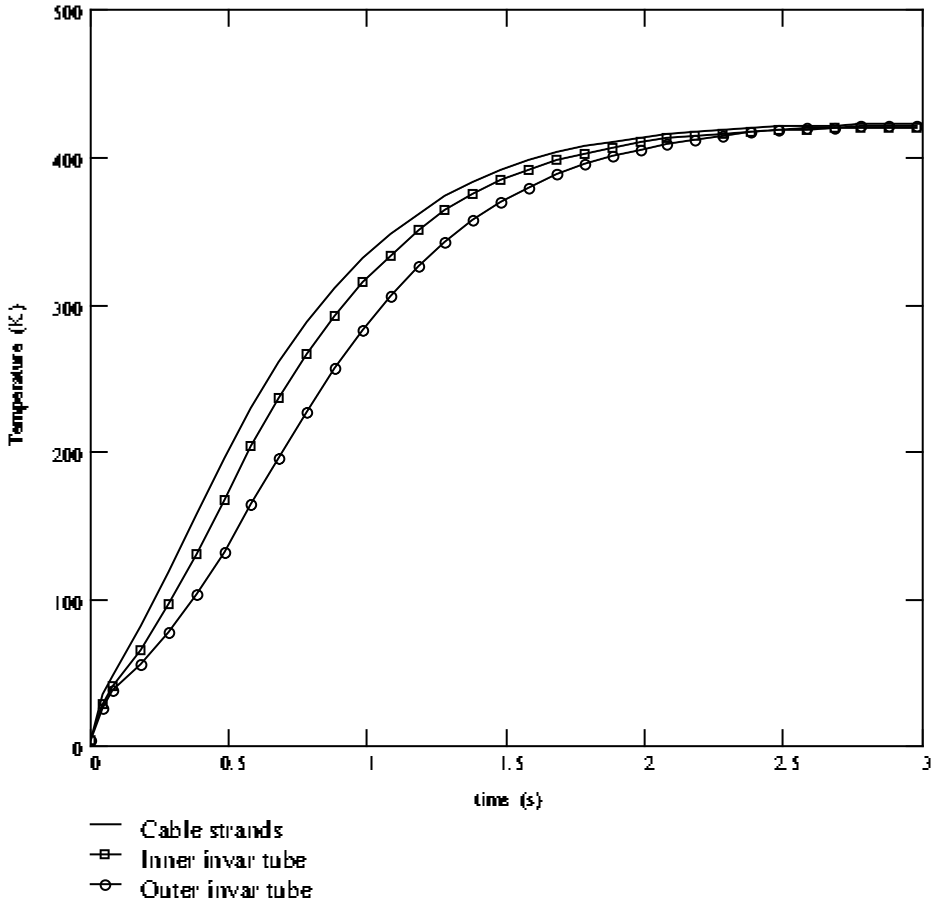

Figure 5.2.2.6 Evolution of maximal temperature (the middle of cable) for the Cable strands and external surfaces of Inner and Outer invar tubes.

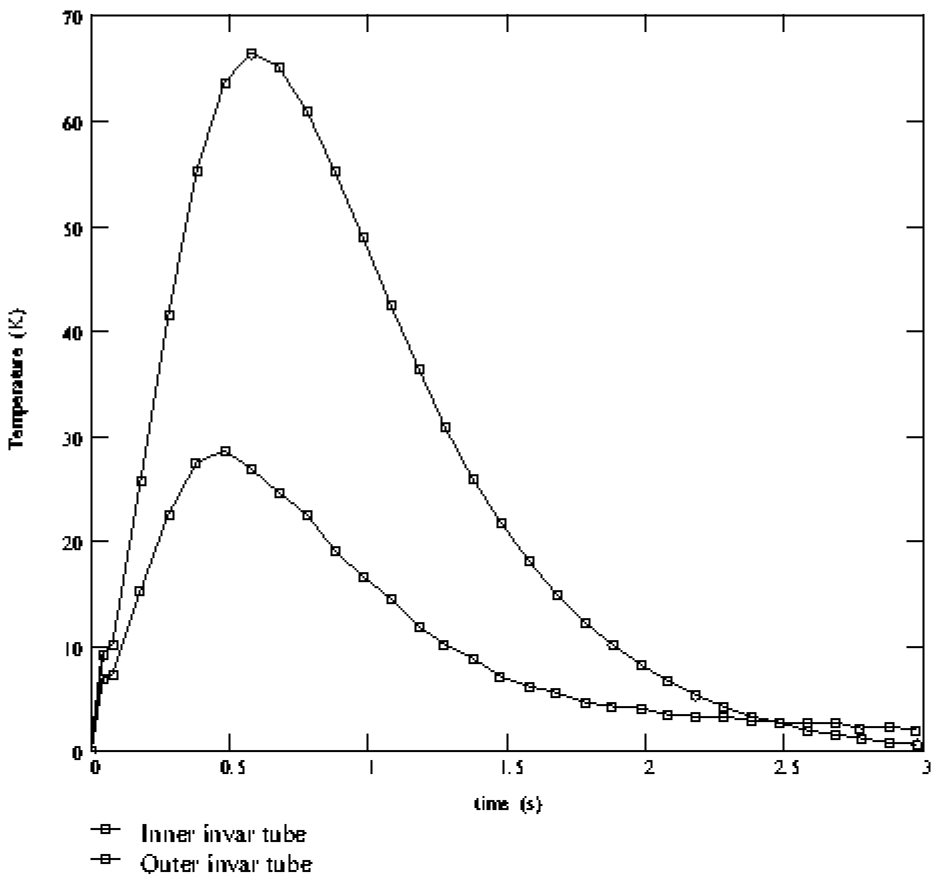

Figure 5.2.2.7 Evolution of the temperature differences across the thickness of Inner and Outer invar tubes.

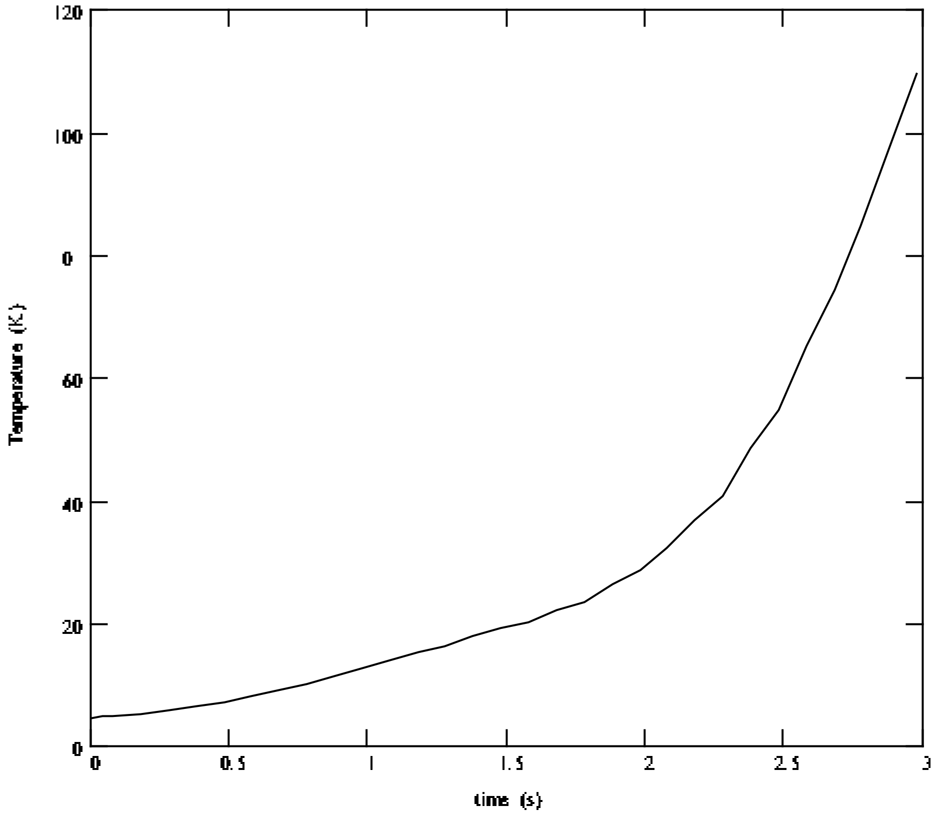

Figure 5.2.2.8 Evolution of the SHe temperature in the middle of the cable channel during quench protection.

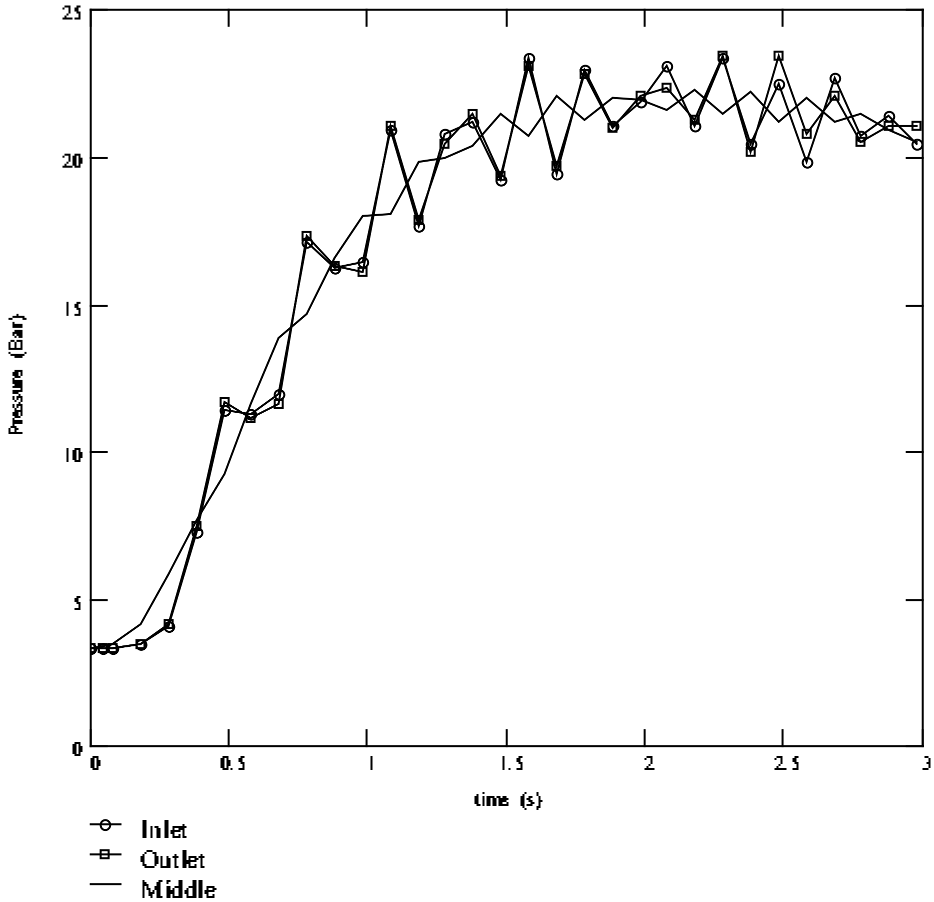

Figure 5.2.2.9 Evolution of the SHe pressure at the cable ends and its center during quench protection.

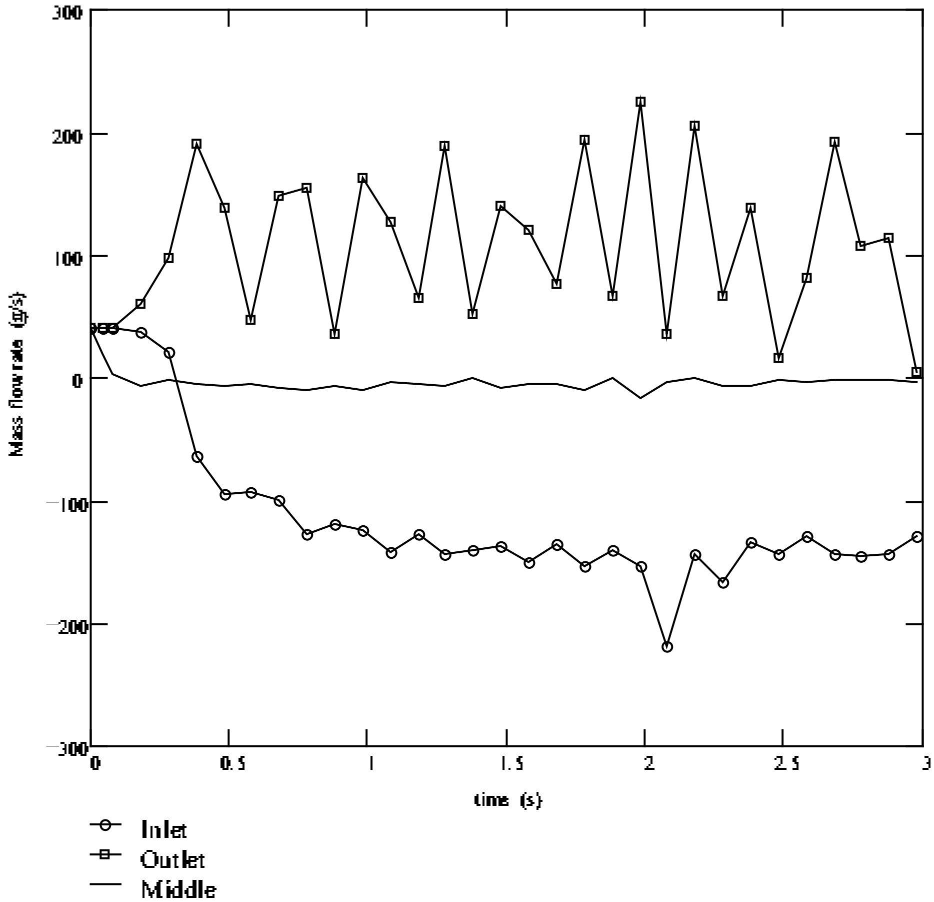

Figure 5.2.2.10 Evolution of the SHe mass flow rate at the cable ends (inlet & outlet valves) and its center during quench protection.

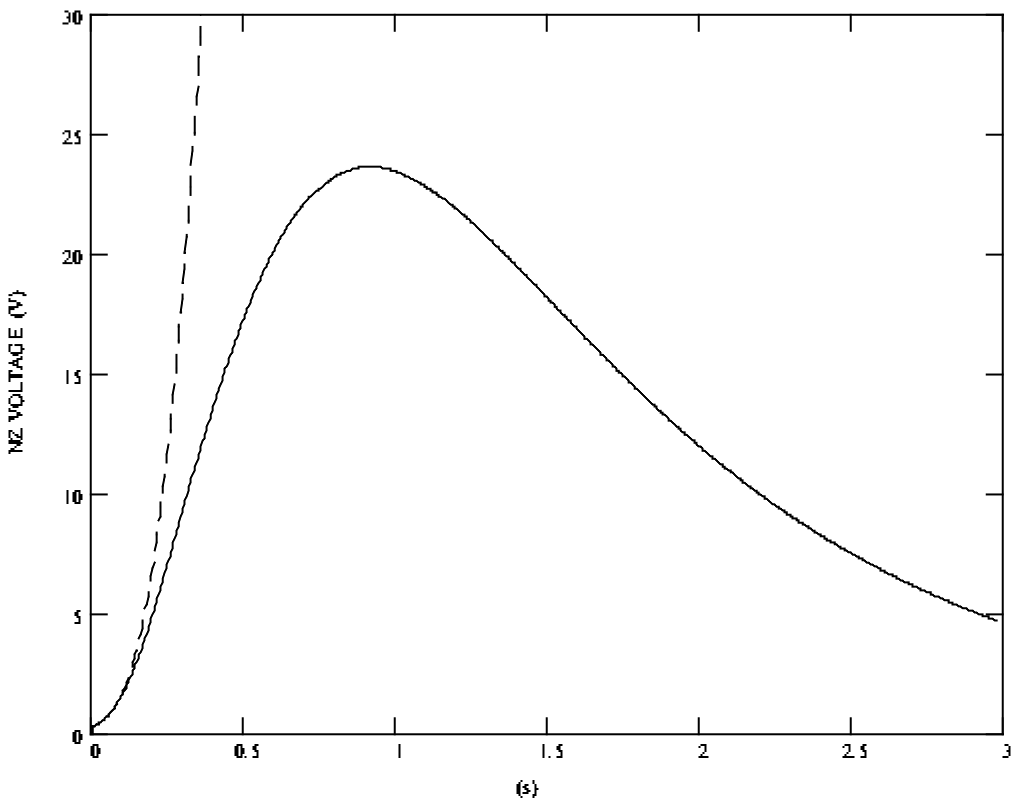

Figure 5.2.2.11 Evolution of Normal Zone voltage during quench protection (solid line) and without protection (dashed line).

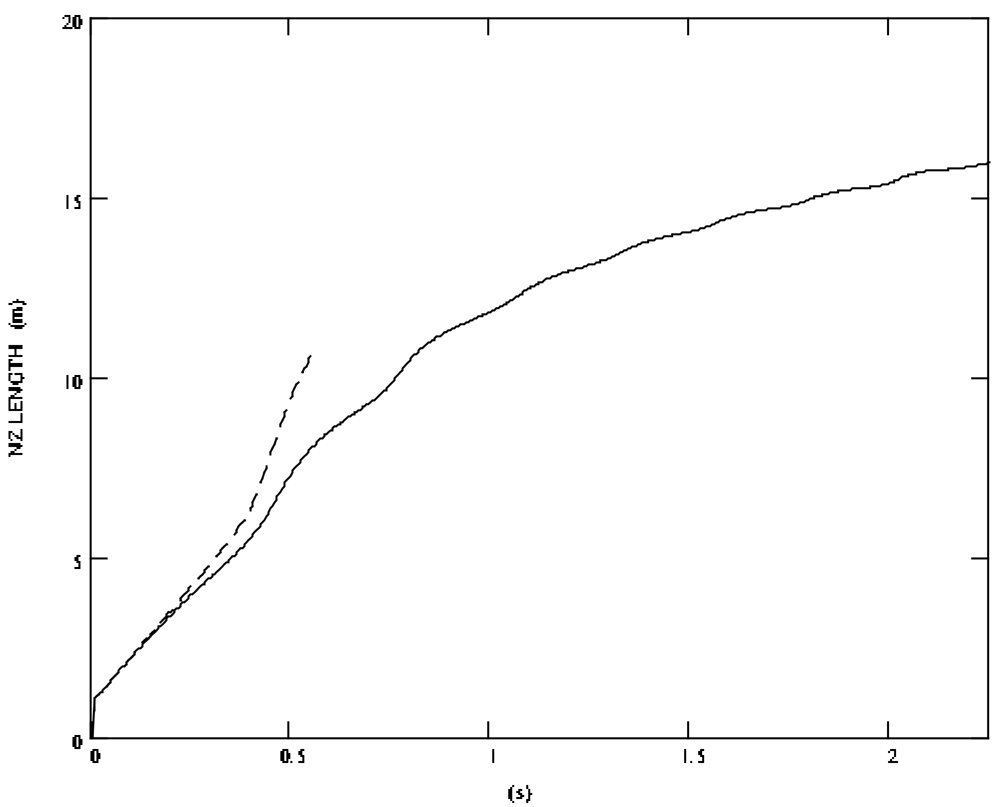

Figure 5.2.2.12 Evolution of Normal Zone length during quench protection (solid line) and without protection (dashed line).

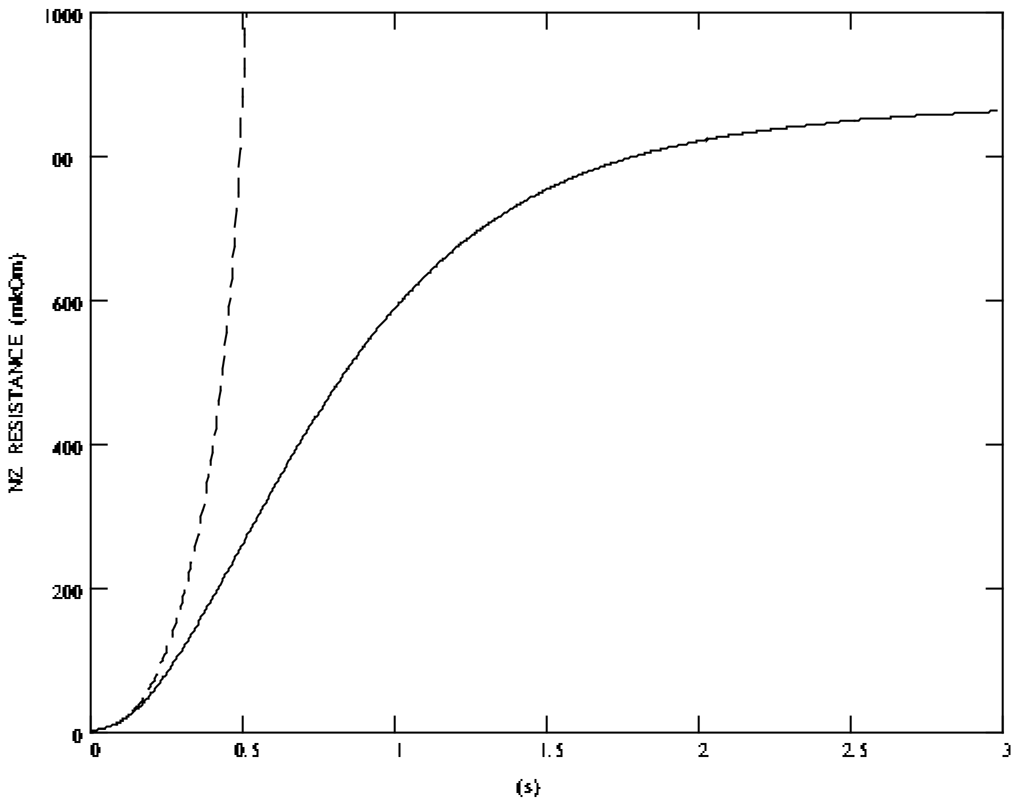

Figure 5.2.2.13 Evolution of Normal Zone resistance during quench protection (solid line) and without protection (dashed line).

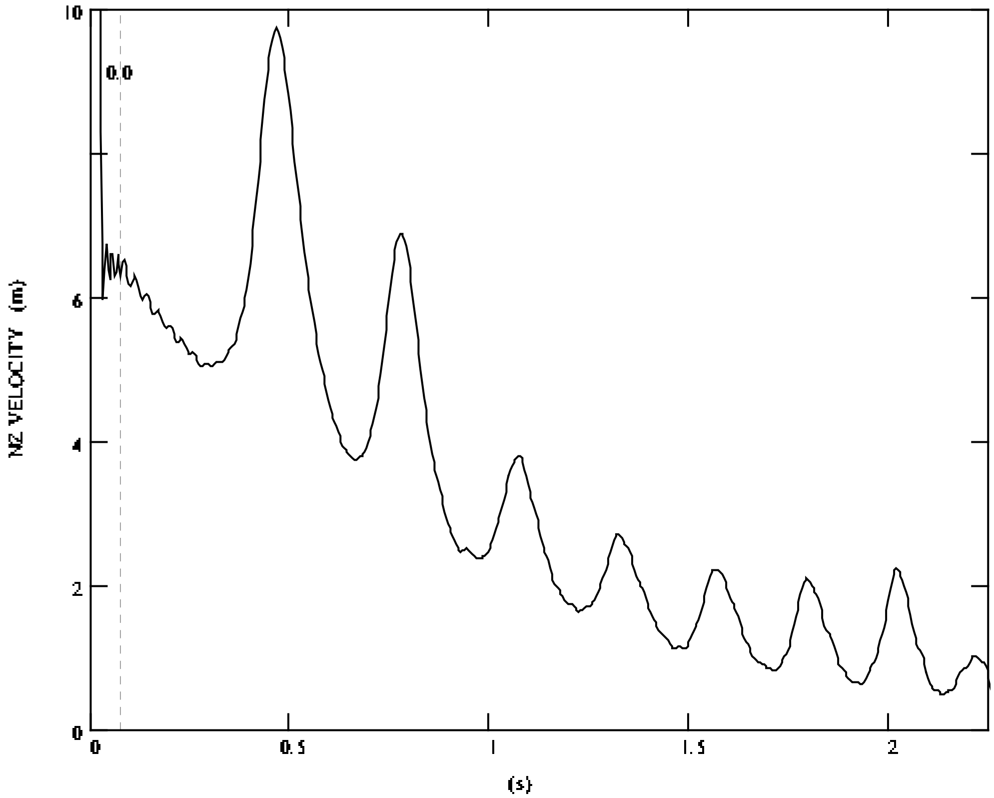

Figure 5.2.2.14 Evolution of Normal Zone velocity during quench protection.

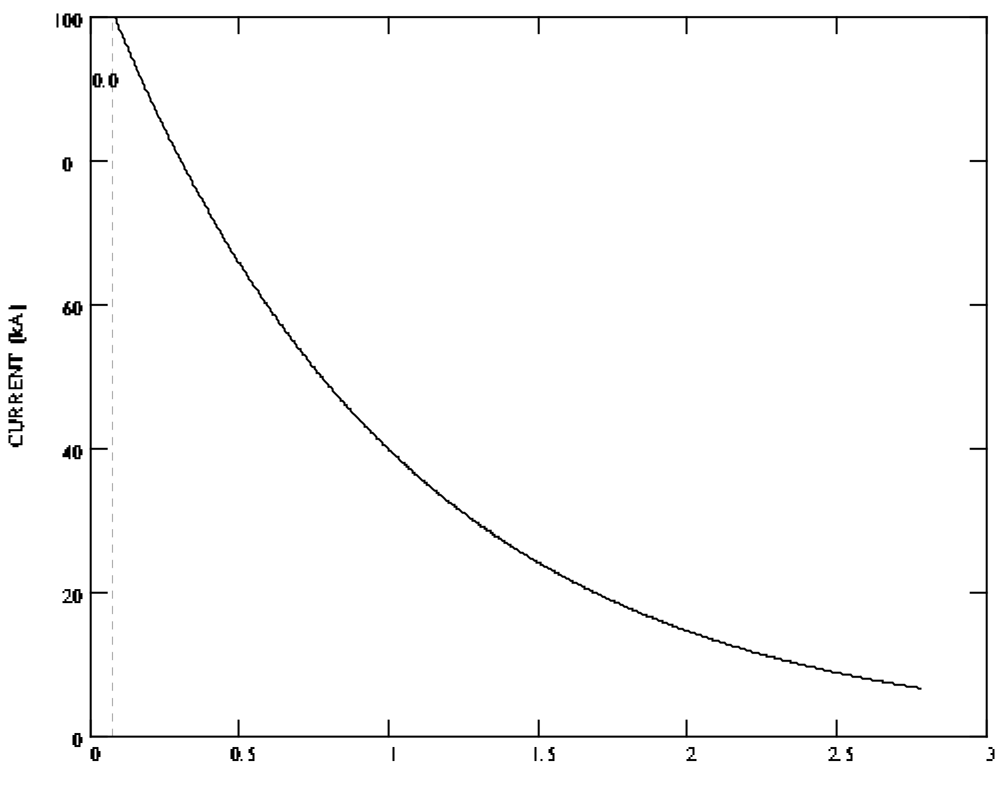

Figure 5.2.2.15 Current decay during protection (t_{delay}=0.08s, τ=1s).

5.2.3 Option 3 (Effect of no cooling)

It is assumed no heat exchange between the transmission line helium and wall of invar tube. We name this variant almost "adiabatic" having in view the heat exchange between the cable strands and invar tubes only. Quench detection time delay (1V threshold) from the heat disturbance beginning is 0.12s.

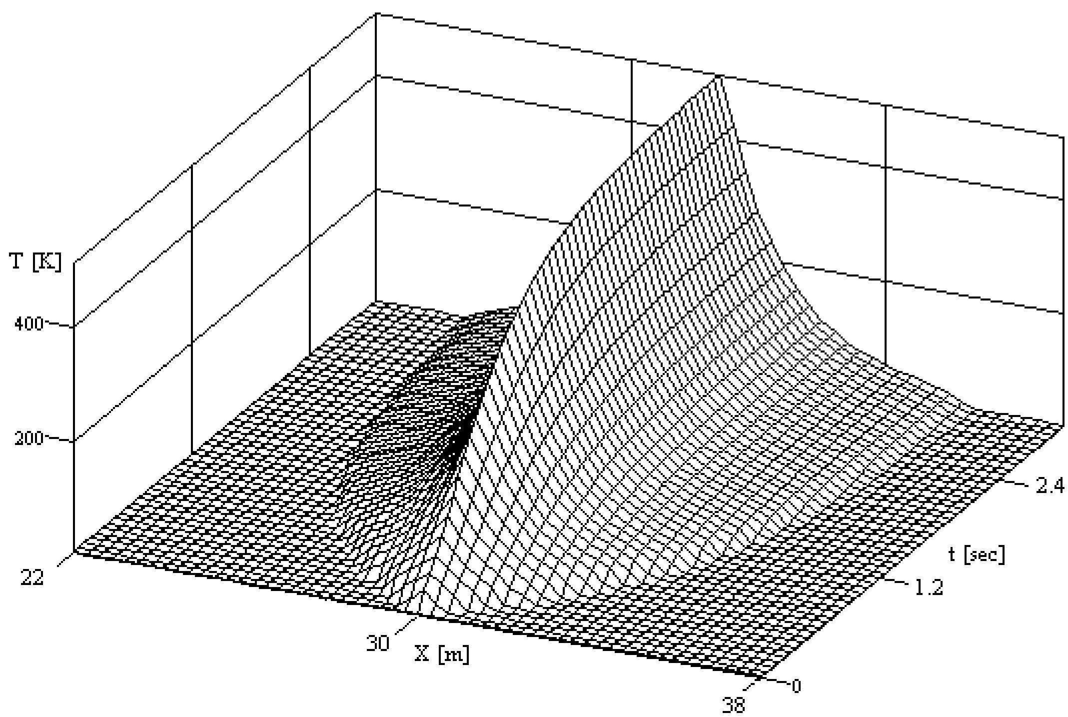

Figure 5.2.3.1a Temperature evolution of the cable strands during quench protection (current decay constant τ=1s, voltage threshold 1V).

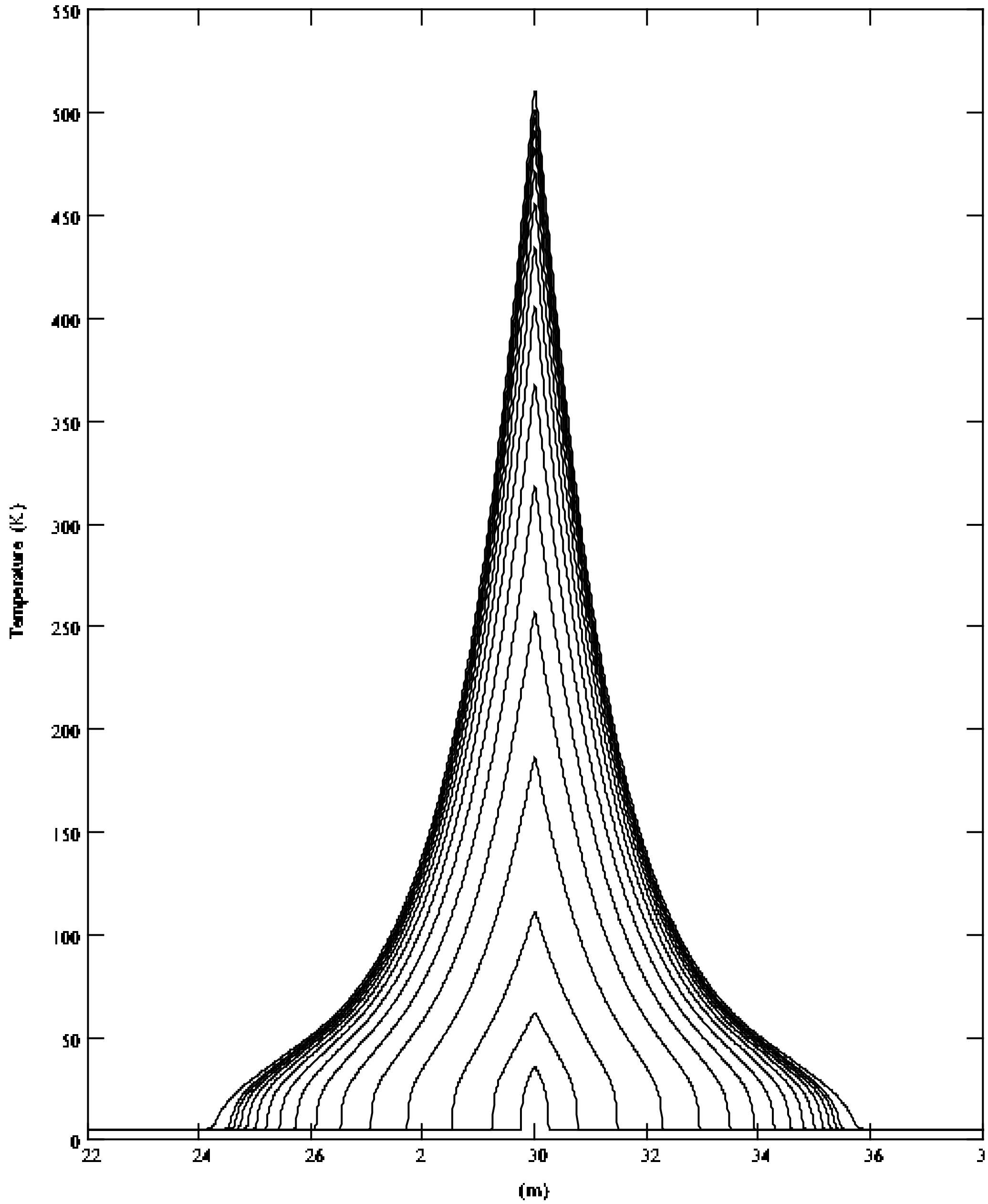

Figure 5.2.3.1b Temperature evolution of the cable strands during quench protection (current decay constant τ=1s, voltage threshold 1V). Time: 0.04, 0.12, 0.24, 0.40, 0.56, 0.62, 0.88, 1.04, 1.20, 1.36, 1.52, 1.68, 1.84, 2.00, 2.16, 2.96s

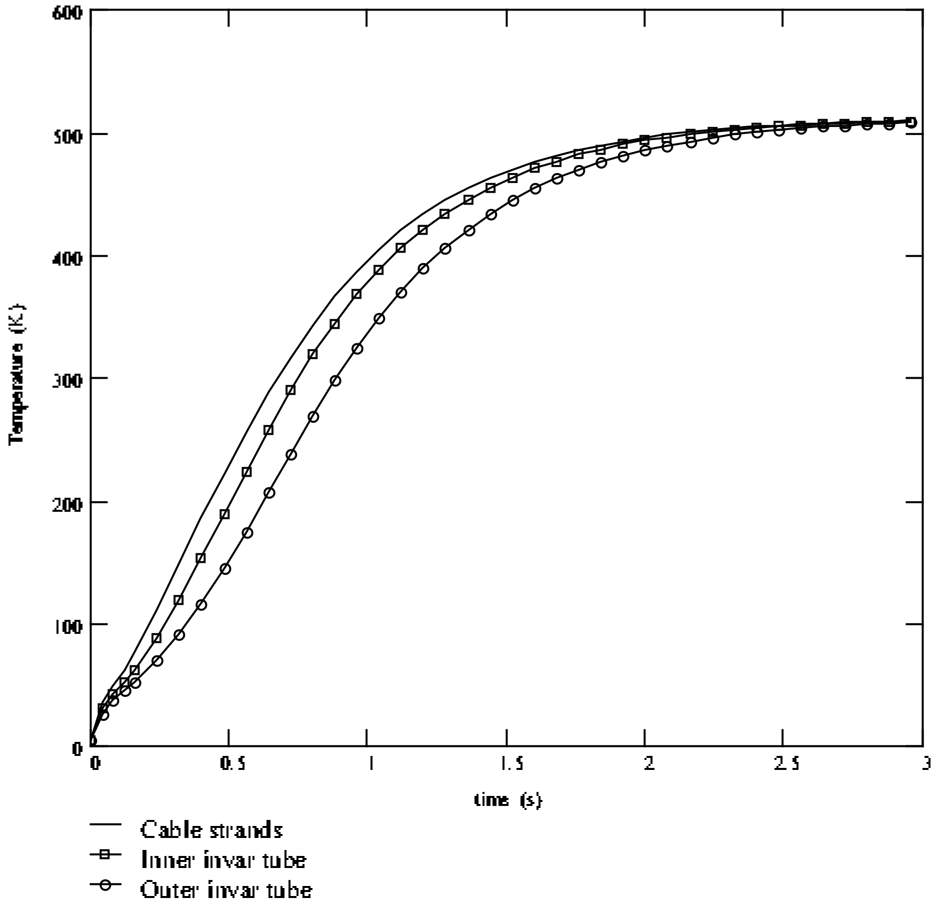

Figure 5.2.3.2 Evolution of maximal temperature (the middle of cable) for the Cable strands and external surfaces of Inner and Outer invar tubes.

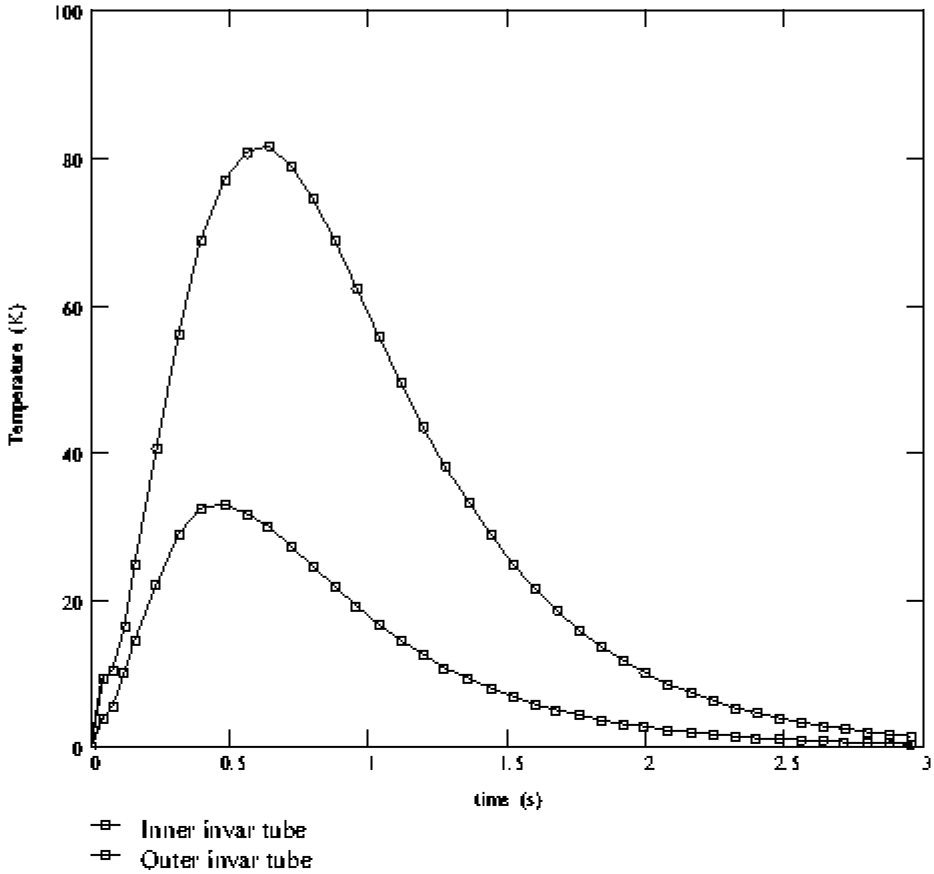

Figure 5.2.3.3 Evolution of temperature differences across the thickness of Inner and Outer invar tubes.

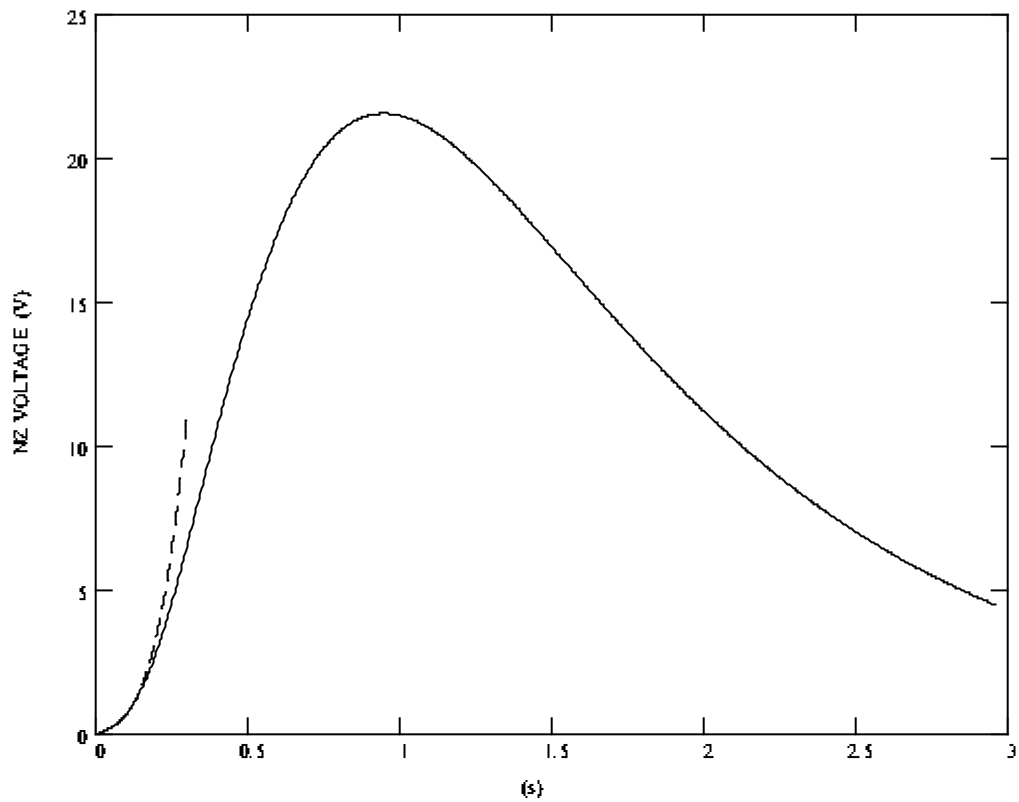

Figure 5.2.3.4 Evolution of Normal Zone voltage during quench protection (solid line) and without protection (dashed line).

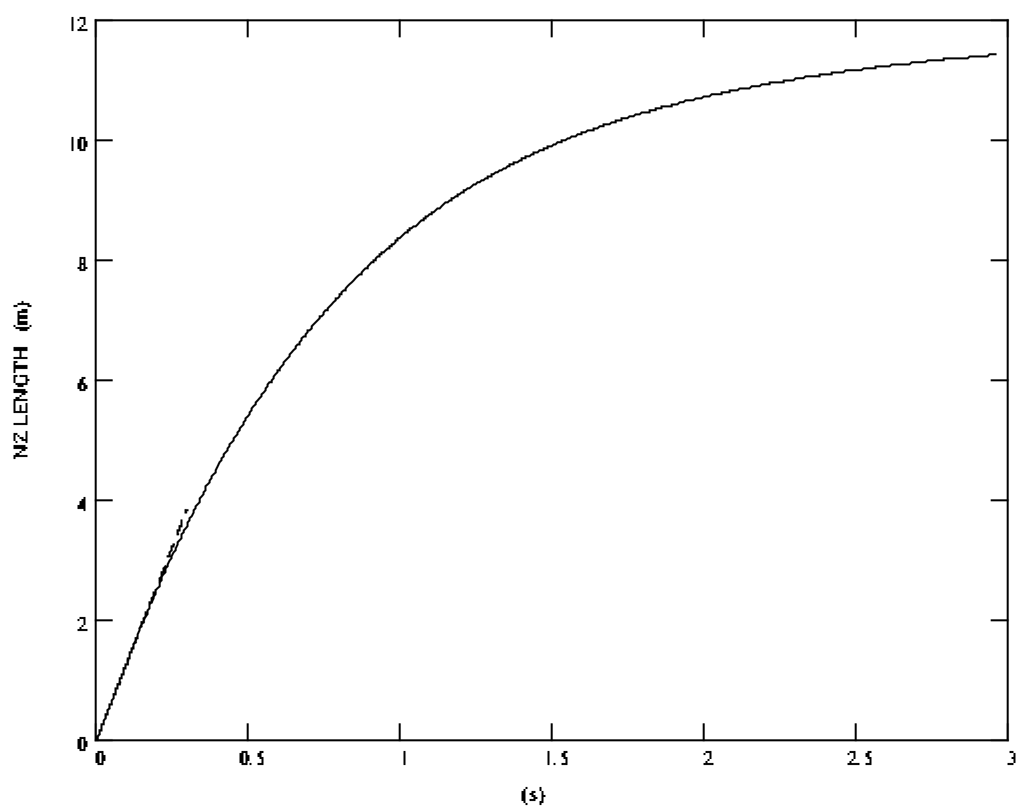

Figure 5.2.3.5 Evolution of Normal Zone length during quench protection (solid line) and without protection (dashed line).

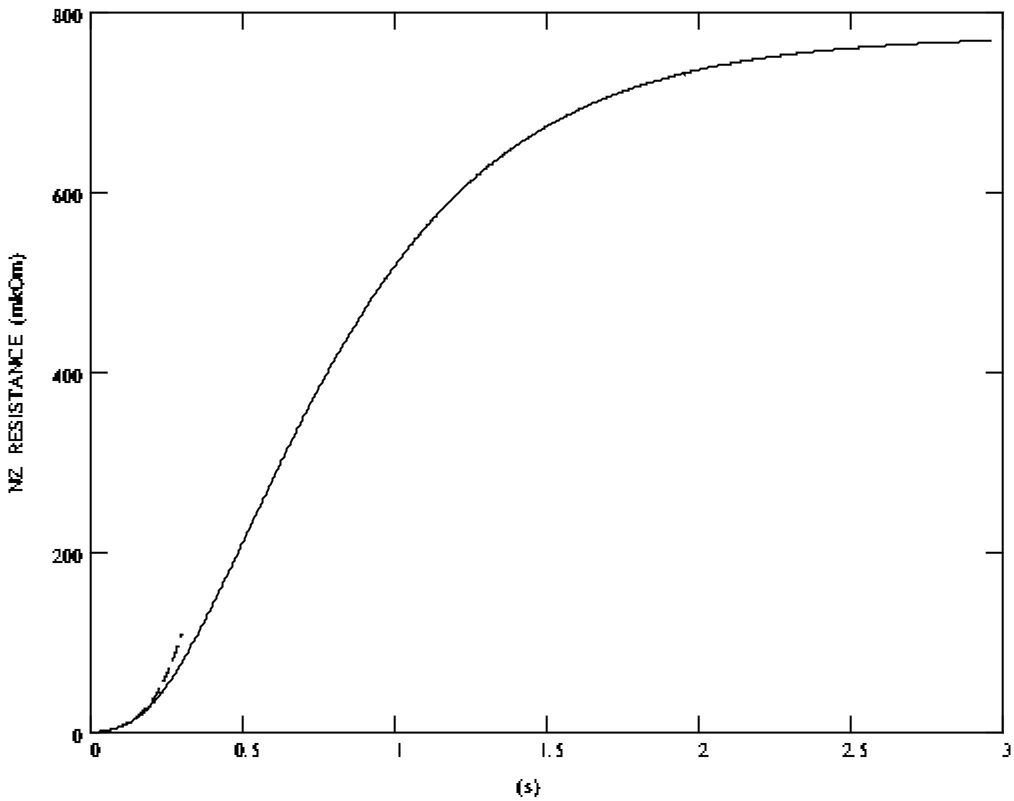

Figure 5.2.3.6 Evolution of Normal Zone resistance during quench protection (solid line) and without protection (dashed line).

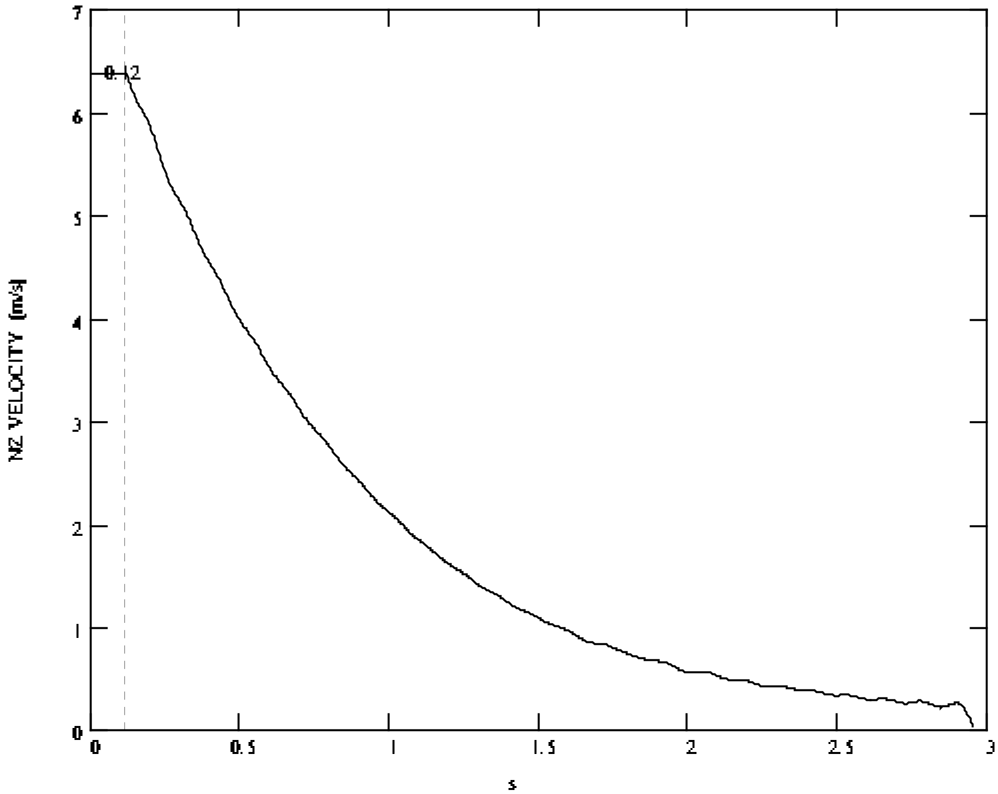

Figure 5.2.3.7 Evolution of Normal Zone velocity during quench protection.

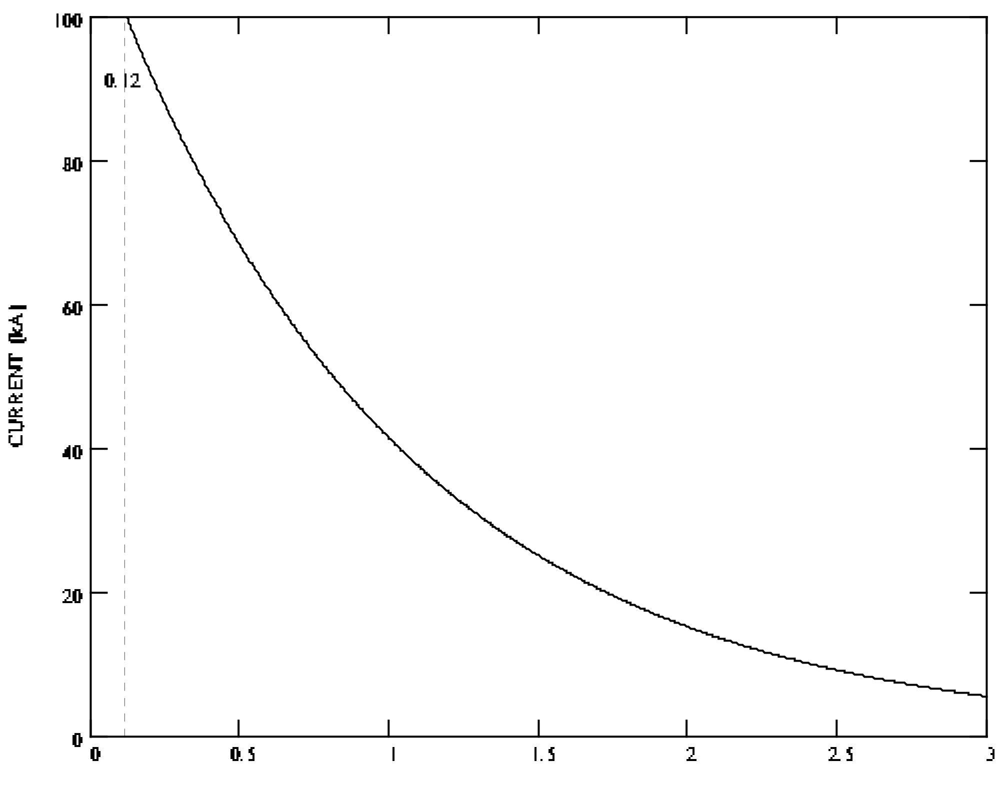

Figure 5.2.3.8 Current decay during protection (t_{delay}=0.12s, τ=1s).

5.2.4 Option 4 (Effect of copper purity)

In compare with the previous similar option the only difference is **RRR**=100 instead of 55. However it significantly increases the quench detection time delay up to 0.16s for 1V threshold. Typical view of the strand temperature for different times during quench protection is shown in Fig. 5.2.4.1. Transient thermal diffusion in depth of the inner and outer invar tubes leads to temperature difference between the tube surfaces. This difference is given in Fig. 5.2.4.2, 5.2.4.3. Evolution of Normal Zone voltage, length, resistance and velocity are shown in Fig. 5.2.4.4 through 5.2.4.7. NZ velocity is obtained by numerical differentiation of NZ length curve divided by 2. Without protection conductor burns out in about 0.6sec.

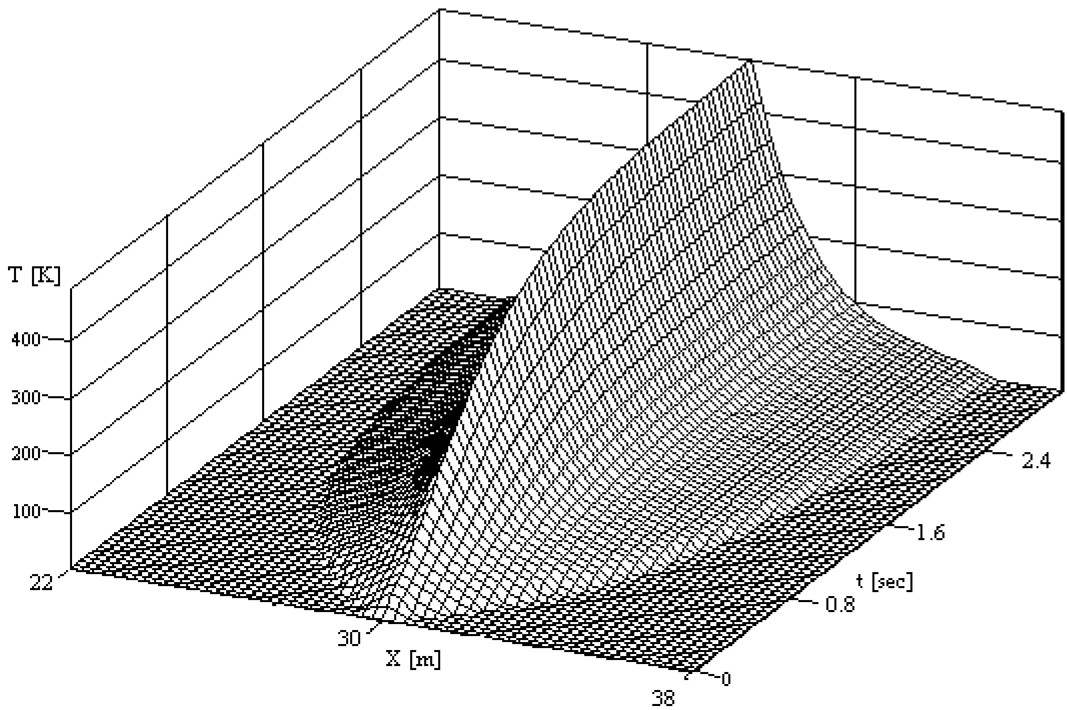

Figure 5.2.4.1a Temperature evolution of the cable strands during quench protection (current decay time constant τ=1s, quench detection time delay t_{det}=0.16s).

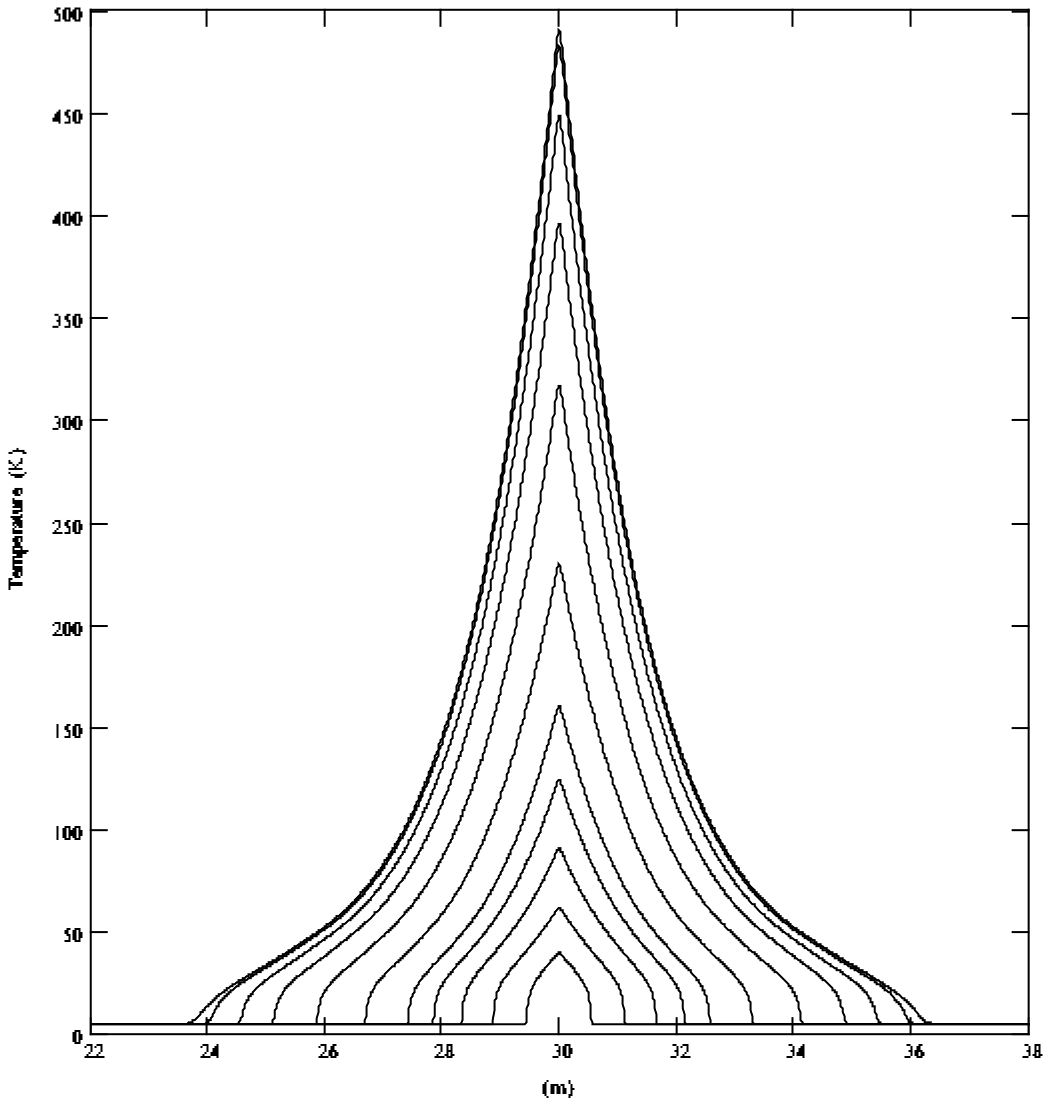

Figure 5.2.4.1b Temperature evolution of the cable strands during quench protection (current decay time constant τ=1s, quench detection time delay t_{det}=0.16s). No cooling. Time: 0.08, 0.16, 0.24, 0.32, 0.4, 0.56, 0.8, 1.12, 1.52, 2.24, 2.96s

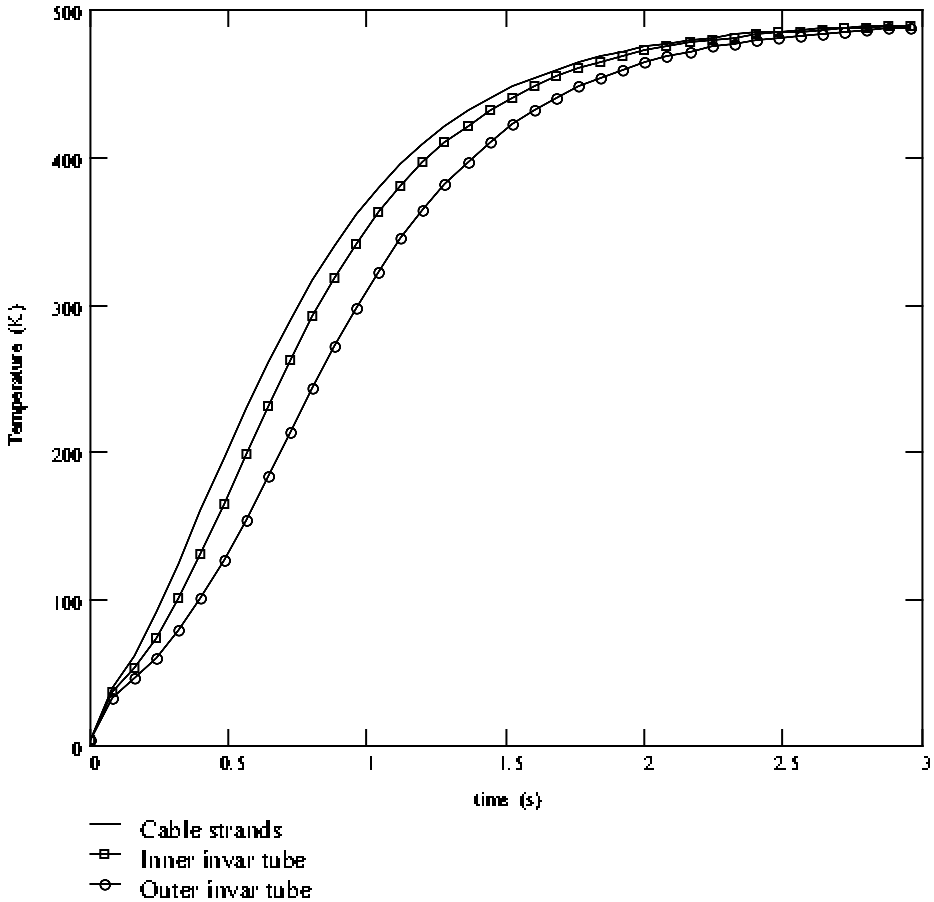

Figure 5.2.4.2 Evolution of maximal temperature (the middle of cable) for the Cable strands and external surfaces of Inner and Outer invar tubes.

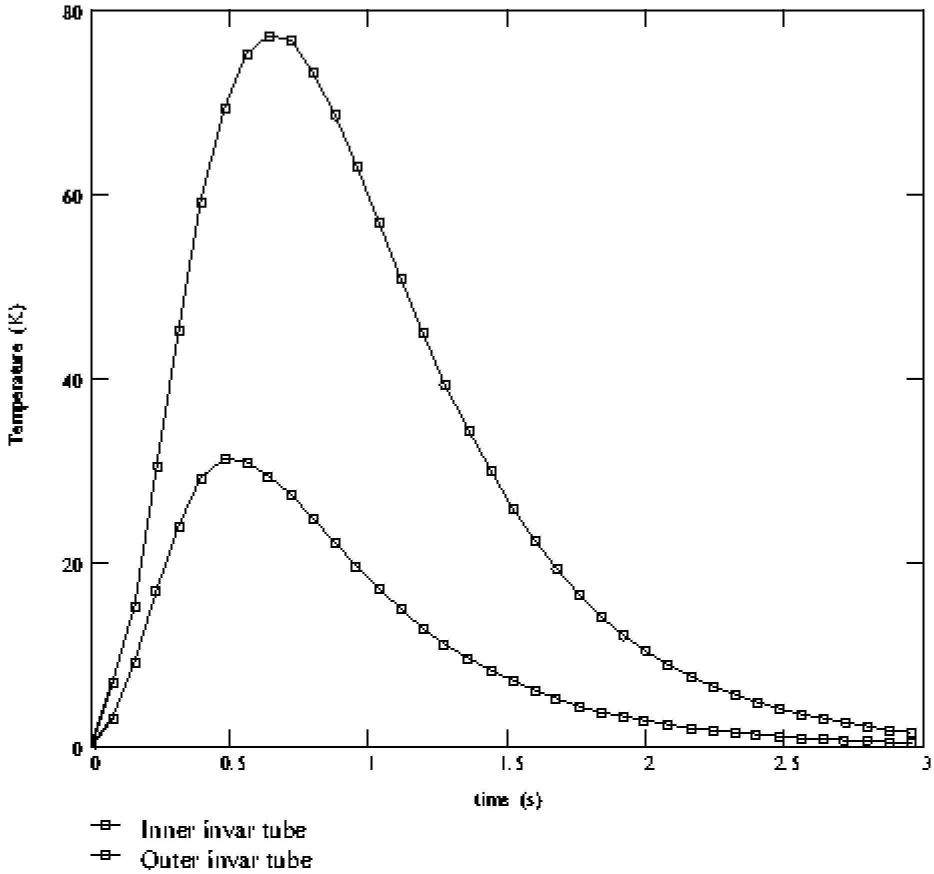

Figure 5.2.4.3 Evolution of temperature differences across the thickness of Inner and Outer invar tubes.

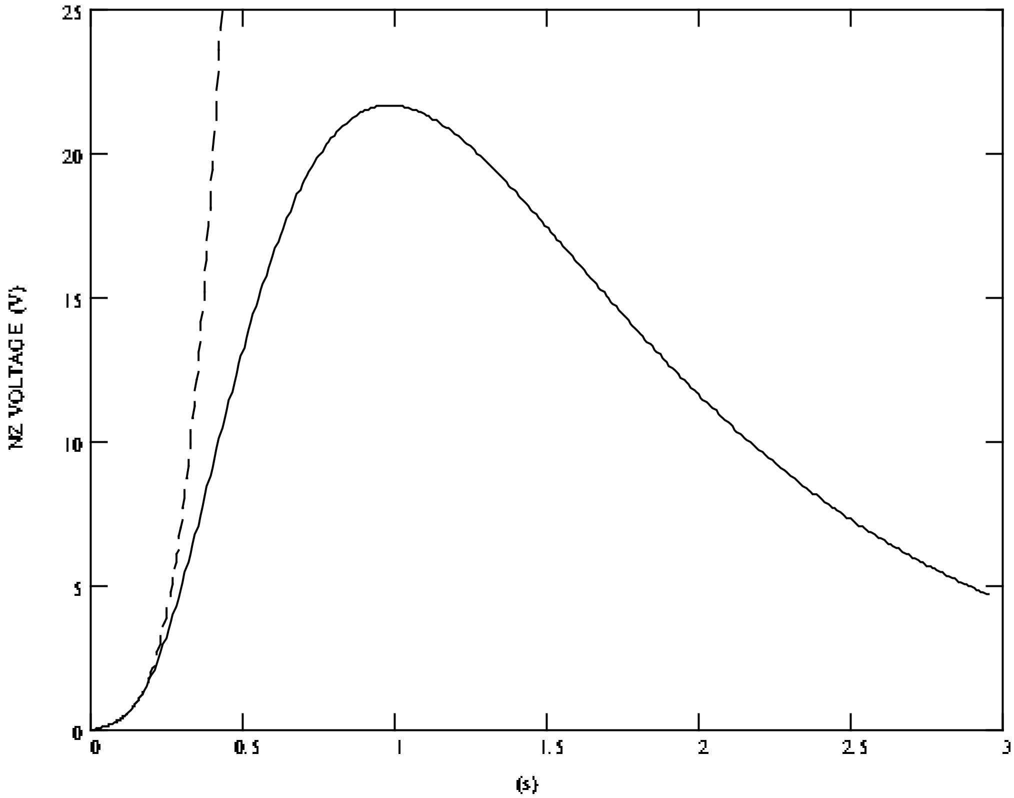

Figure 5.2.4.4 Evolution of Normal Zone voltage during quench protection (solid line) and without protection (dashed line).

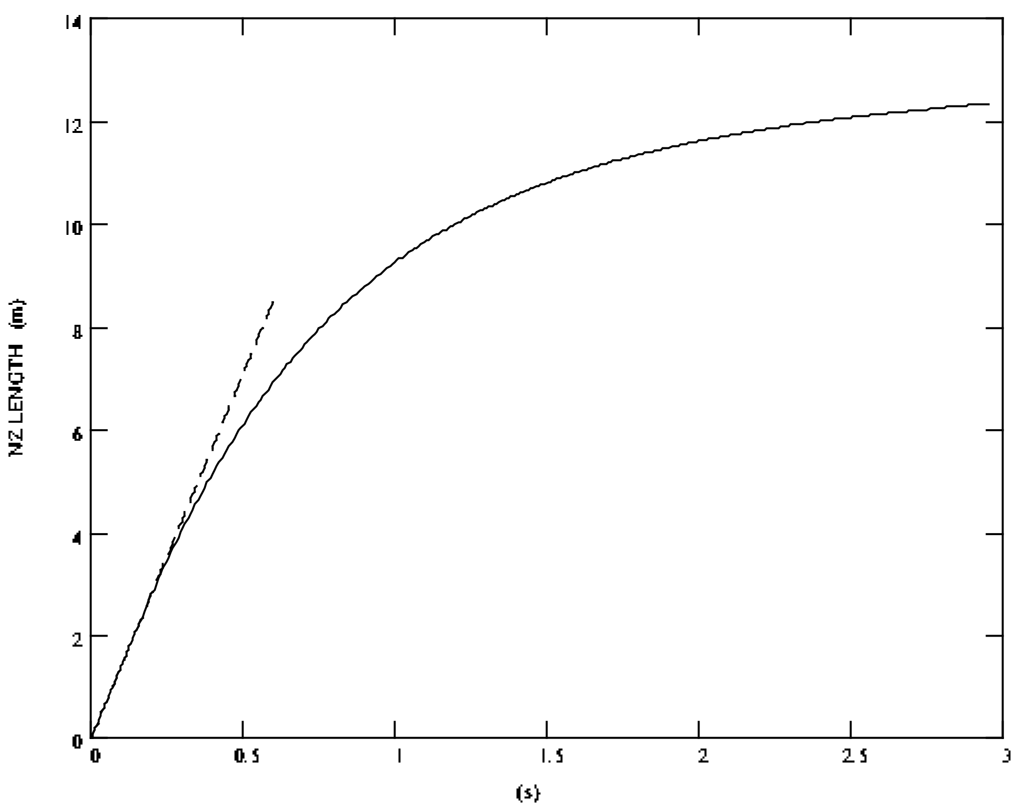

Figure 5.2.4.5 Evolution of Normal Zone length during quench protection (solid line) and without protection (dashed line).

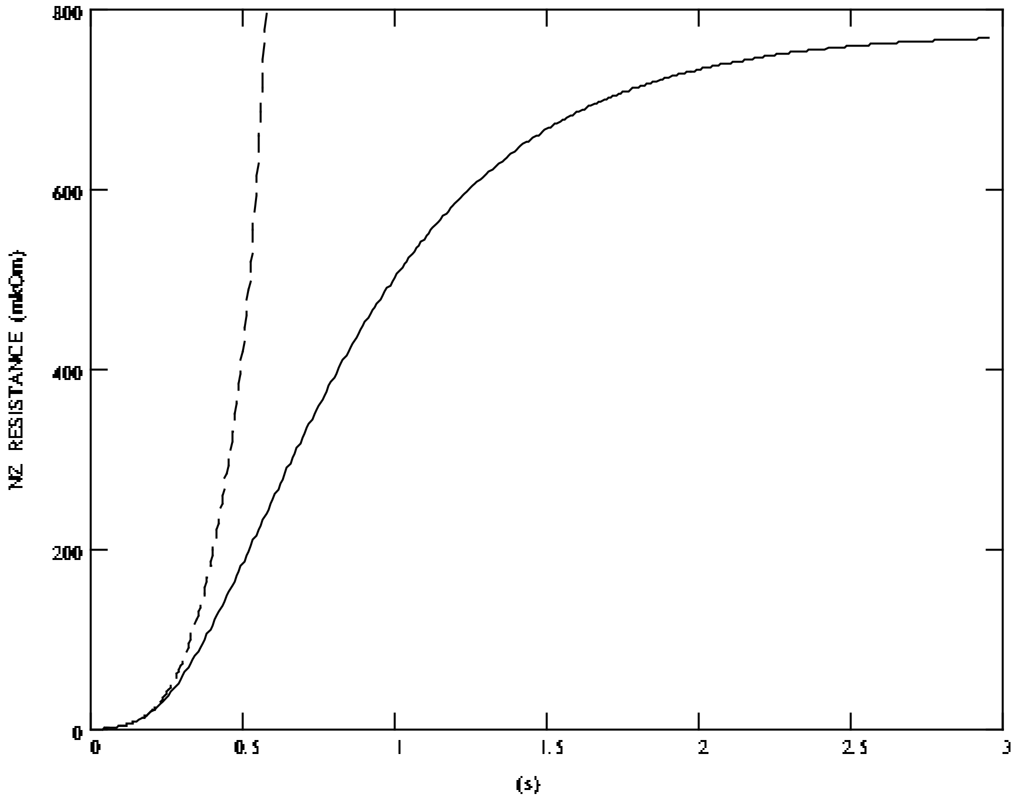

Figure 5.2.4.6 Evolution of Normal Zone resistance during quench protection (solid line) and without protection (dashed line).

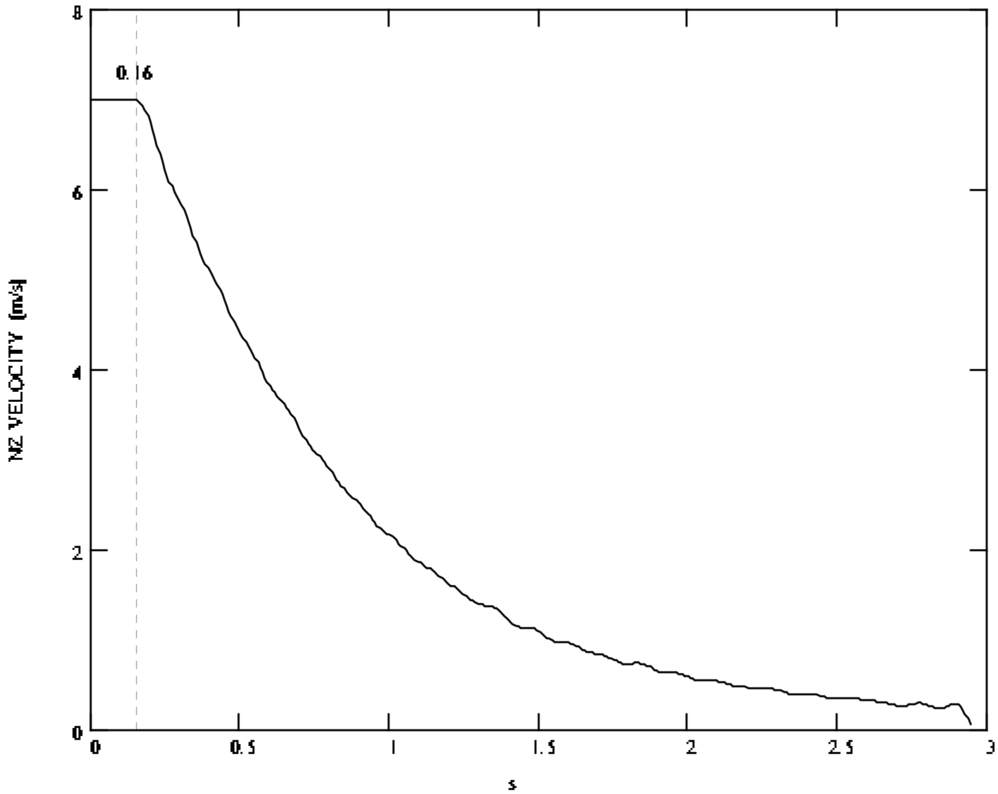

Figure 5.2.4.7 Evolution of Normal Zone velocity during quench protection.

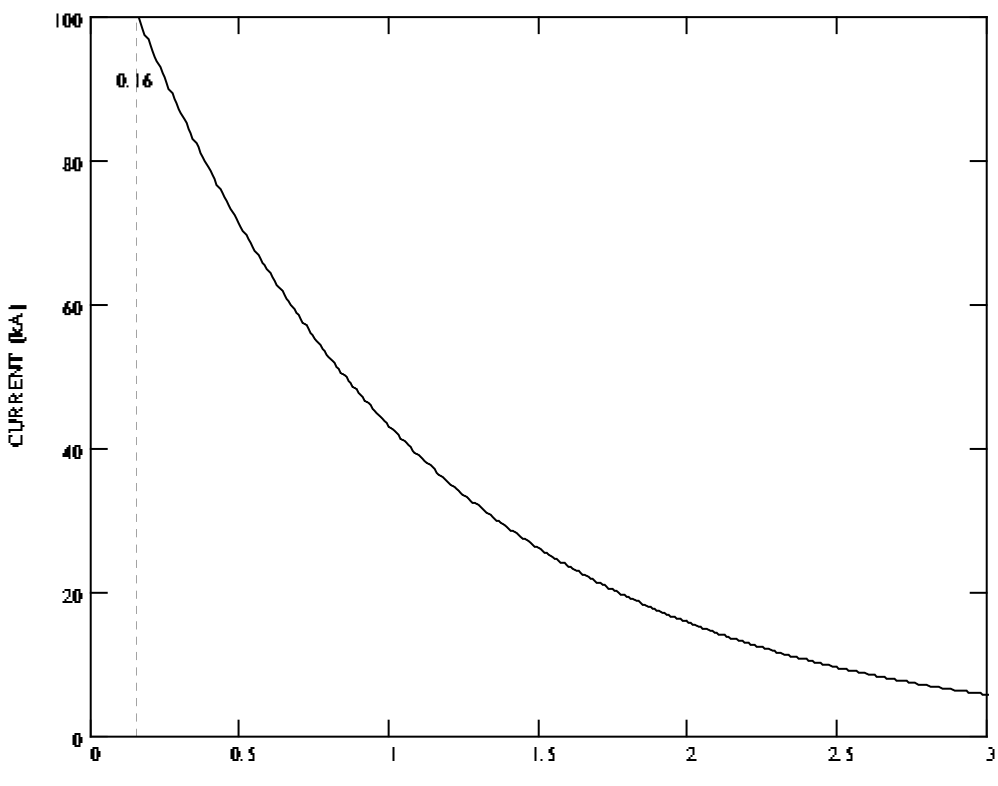

Figure 5.2.4.8 Current decay during protection (t_{delay}=0.16s, τ=1s).

5.3 Two-channel conductor model (7% void fraction).

5.3.1 Option 5

This option differ from Option1 only by non-zero void fraction in cable space filled by SHe. Quench detection time delay for this model (1V threshold) equals to 0.125s that is slightly more (initial normal zone velocity is slightly less) compared with referenced Option 1 of previous model. The reason is small SHe percentage in void space and significant thermal non-equilibrium between the helium and cable strands on the moving boundary of Normal Zone, i.e. Steckly parameter is small. At the boundary of NZ there is a pressure drop between the SHe in the void space and central channel. Magnitude of pressure drop is defined by punched transversal cross area. For considered case (with A=5mm^2 per 1m of cable length) its initial value is about 1 bar and should be decreased proportionally to A^{-2}.

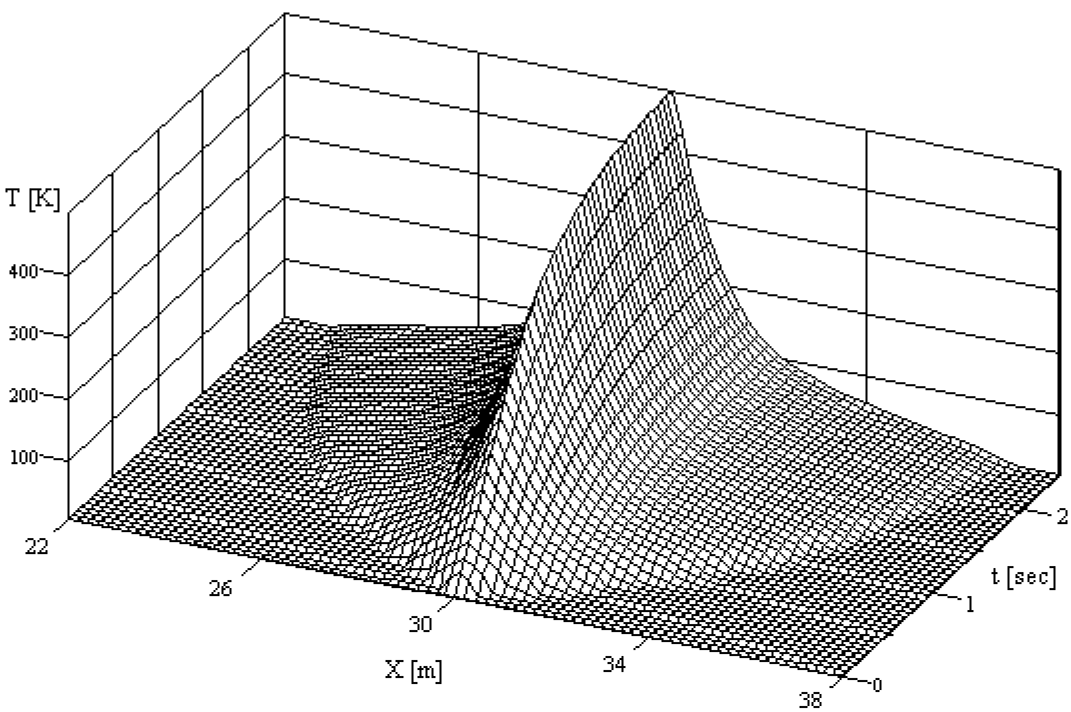

Figure 5.3.1.1a Evolution of the cable strand temperature during quench protection (current decay constant τ=1s, quench detection time delay t_{det}=0.125s).

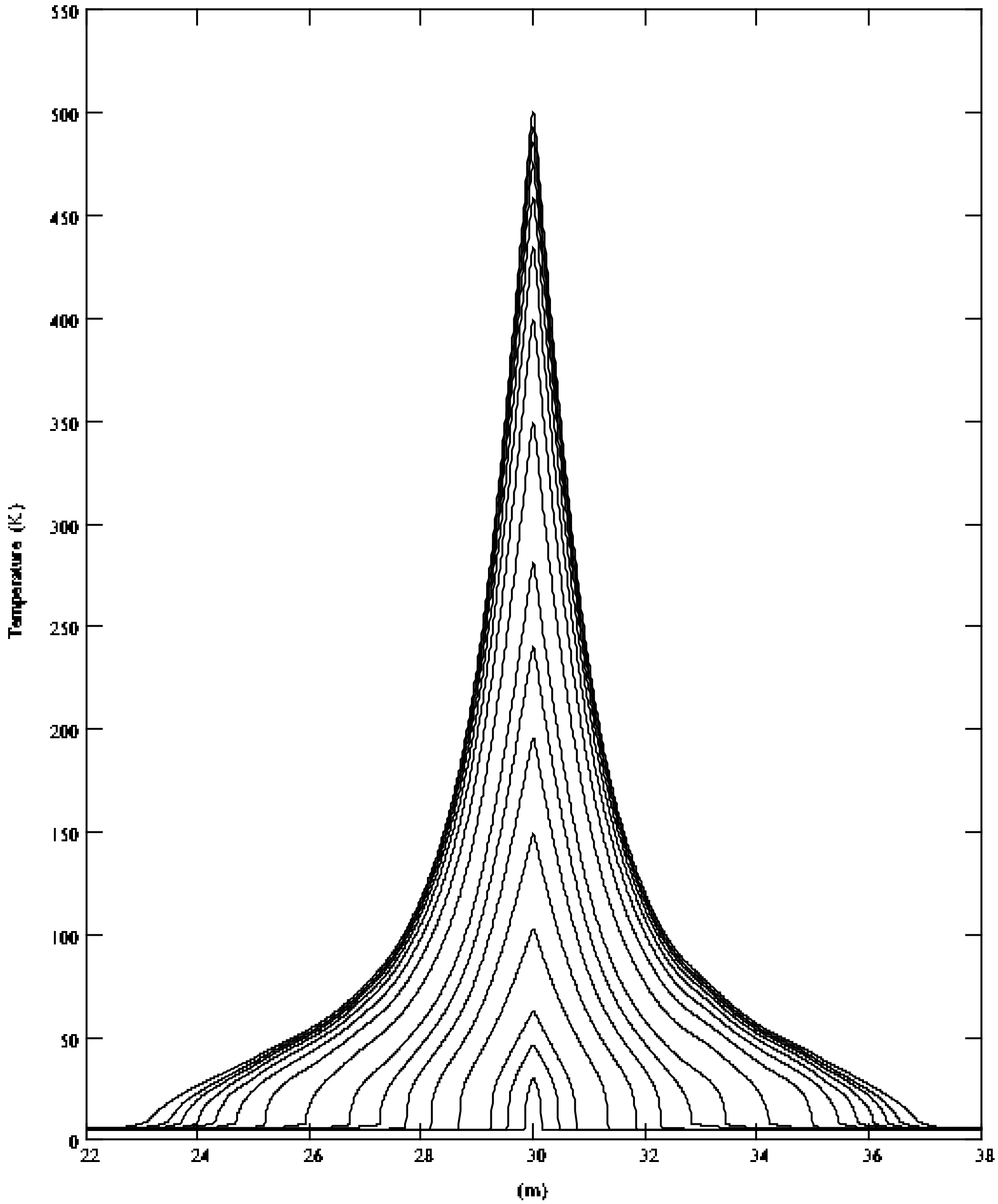

Figure 5.3.1.1b Evolution of the cable strand temperature during quench protection (current decay constant τ=1s, quench detection time delay t_{det}=0.125s, times: 0.025, 0.075, 0.125, 0.225, 0.325, 0.425, 0.525, 0.625, 0.825, 1.025, 1.225, 1.425, 1.625, 1.825, 2.025, 2.425s).

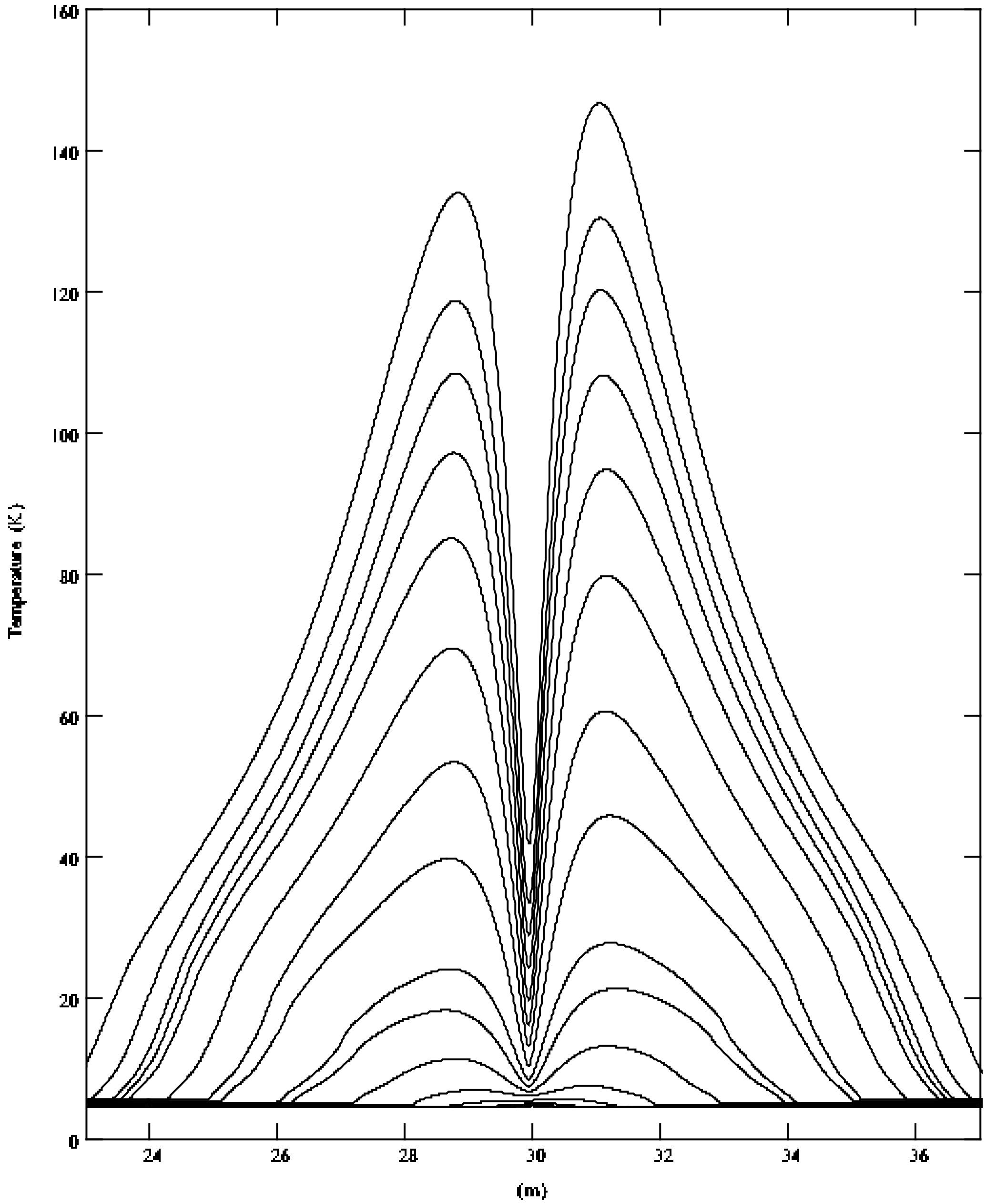

Figure 5.3.1.2 Evolution of the helium temperature inside the conductor channel during quench protection (current decay constant τ=1s, quench detection time delay t_{det}=0.125s, times: 0.125, 0.225, 0.325, 0.425, 0.525, 0.625, 0.825, 1.025, 1.225, 1.425, 1.625, 1.825, 2.025, 2.425s).

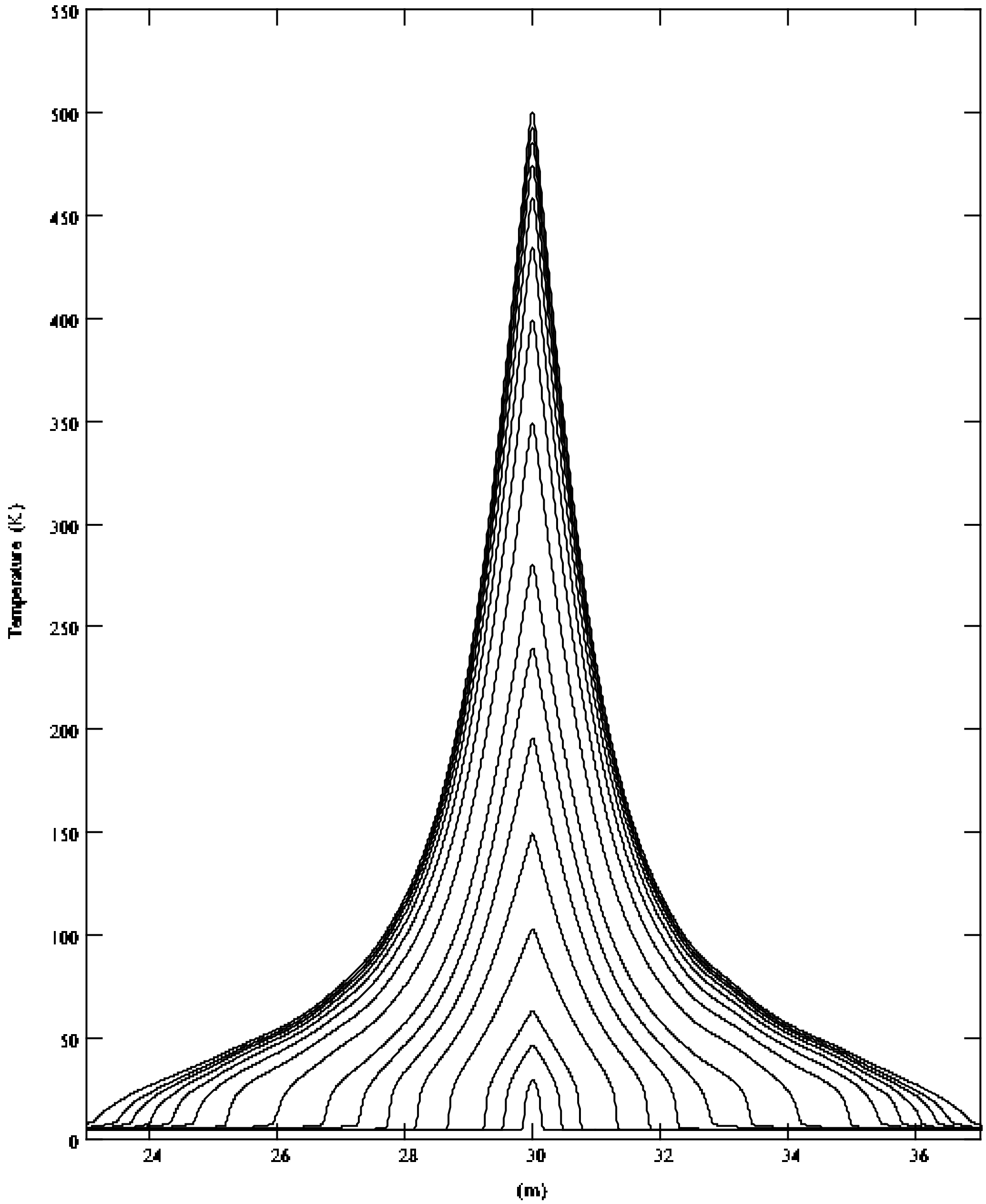

Figure 5.3.1.3 Evolution of the helium temperature inside the cable space during quench protection (current decay constant τ=1s, quench detection time delay t_{det}=0.125s, times: 0.025, 0.075, 0.125, 0.225, 0.325, 0.425, 0.525, 0.625, 0.825, 1.025, 1.225, 1.425, 1.625, 1.825, 2.025, 2.425s).

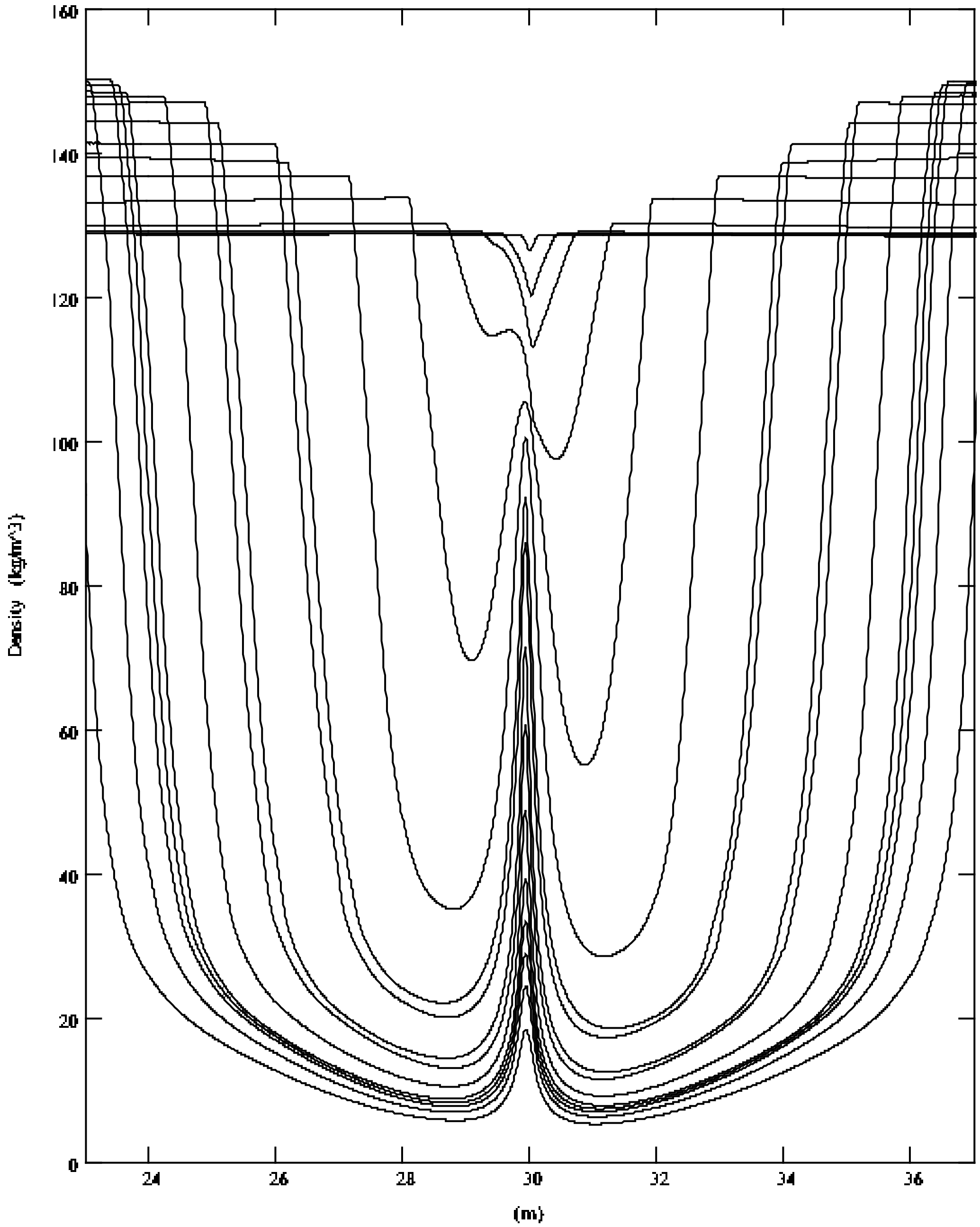

Figure 5.3.1.4 Evolution of the helium density inside the cable channel during quench protection (current decay constant τ=1s, quench detection time delay t_{det}=0.125s, times: 0.025, 0.075, 0.125, 0.225, 0.325, 0.425, 0.525, 0.625, 0.825, 1.025, 1.225, 1.425, 1.625, 1.825, 2.025, 2.425s).

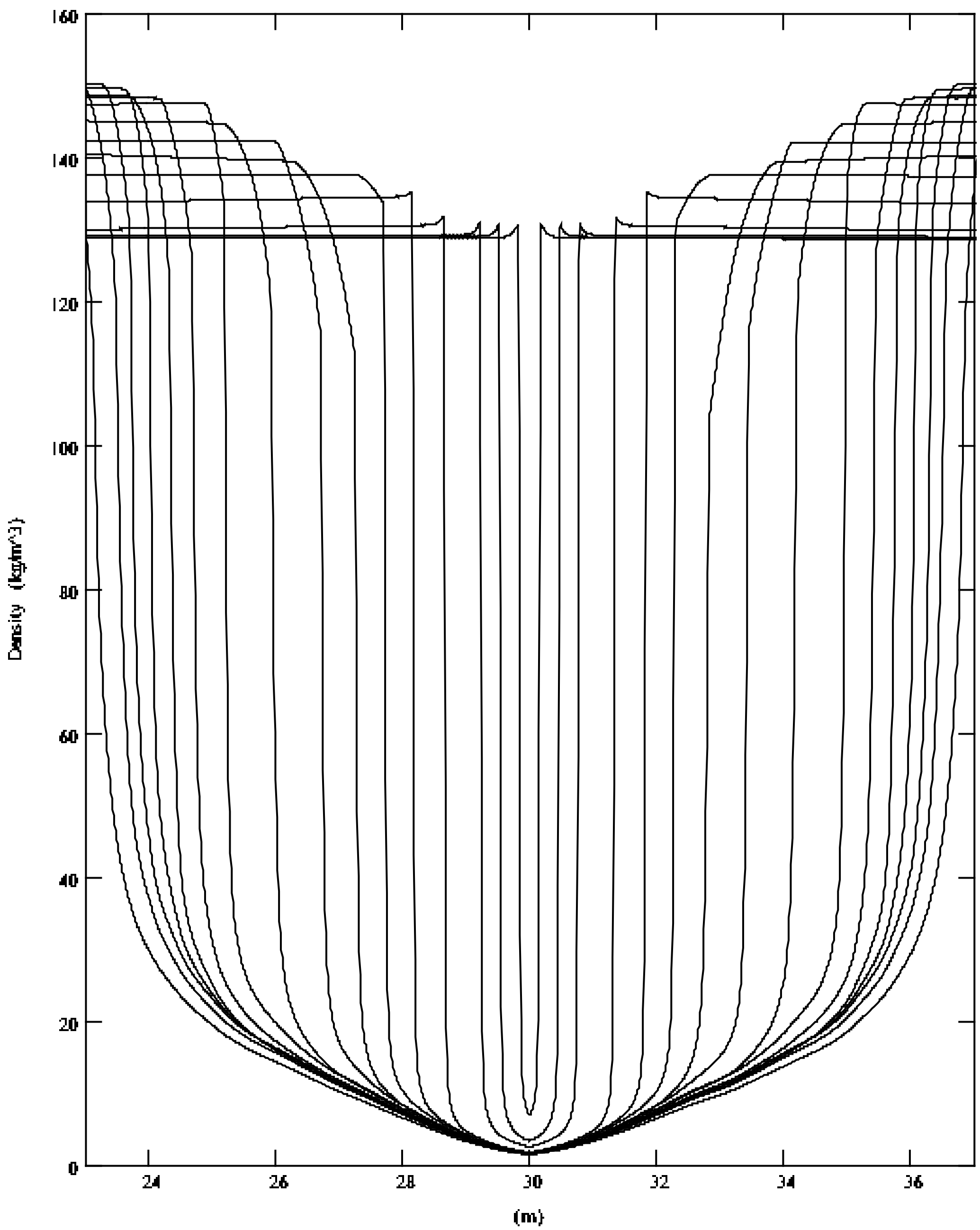

Figure 5.3.1.5 Evolution of the helium density inside the cable space during quench protection (current decay constant τ=1s, quench detection time delay t_{det}=0.125s, times: 0.025, 0.075, 0.125, 0.225, 0.325, 0.425, 0.525, 0.625, 0.825, 1.025, 1.225, 1.425, 1.625, 1.825, 2.025, 2.425s).

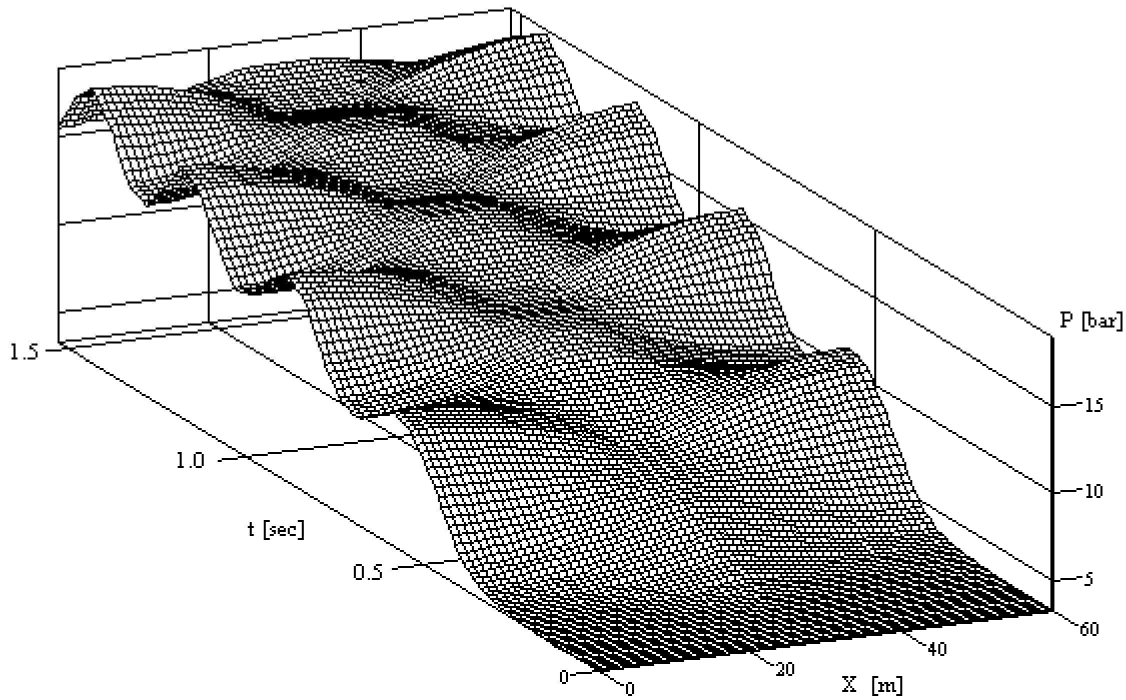

Figure 5.3.1.6 Evolution of SHe pressure inside the cable channel (0-1.525s).

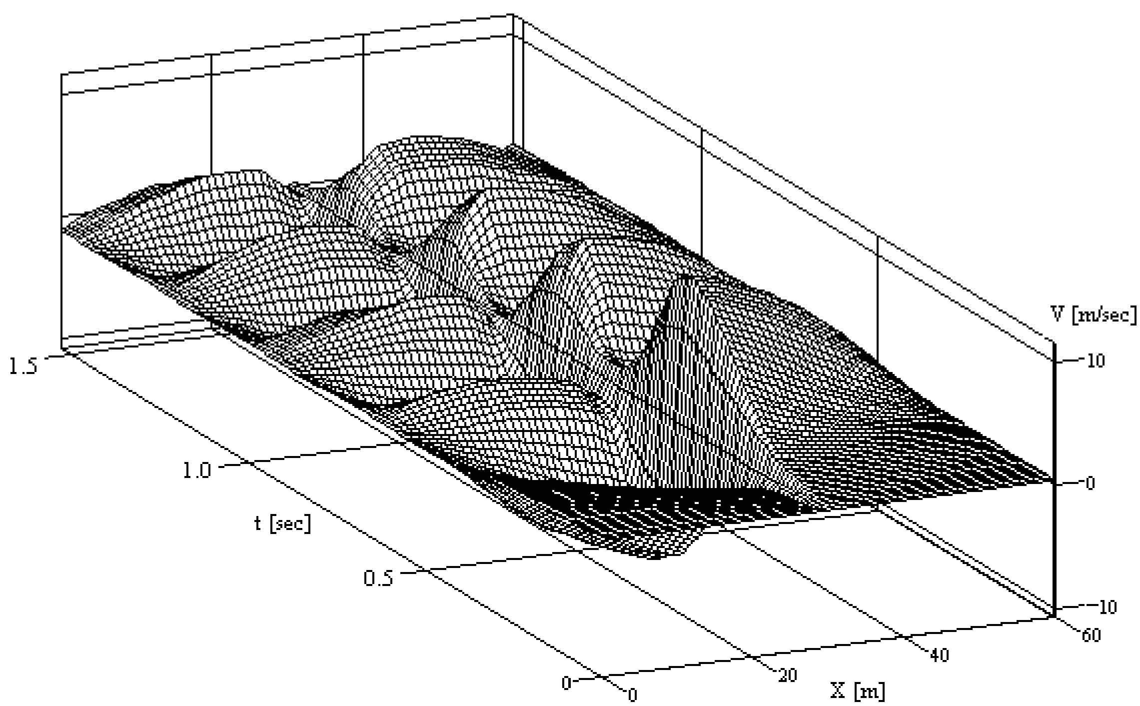

Figure 5.3.1.7 Evolution of helium velocity inside the cable channel (0-1.525s)

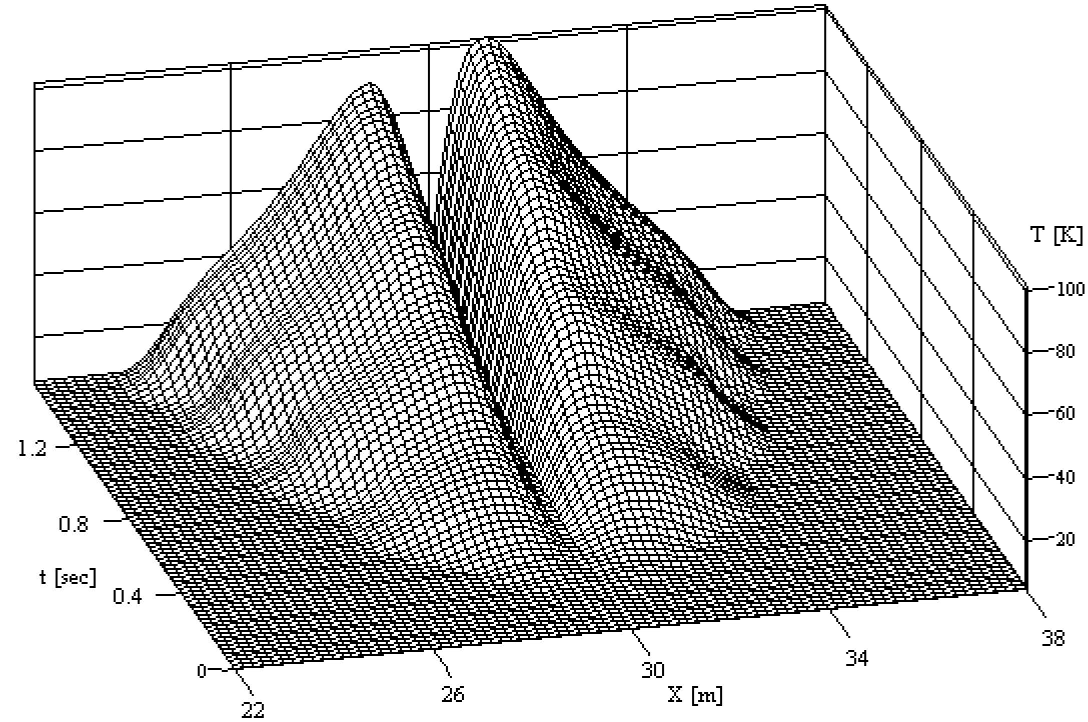

Figure 5.3.1.8 Evolution of helium temperature inside the cable channel (0-1.525s)

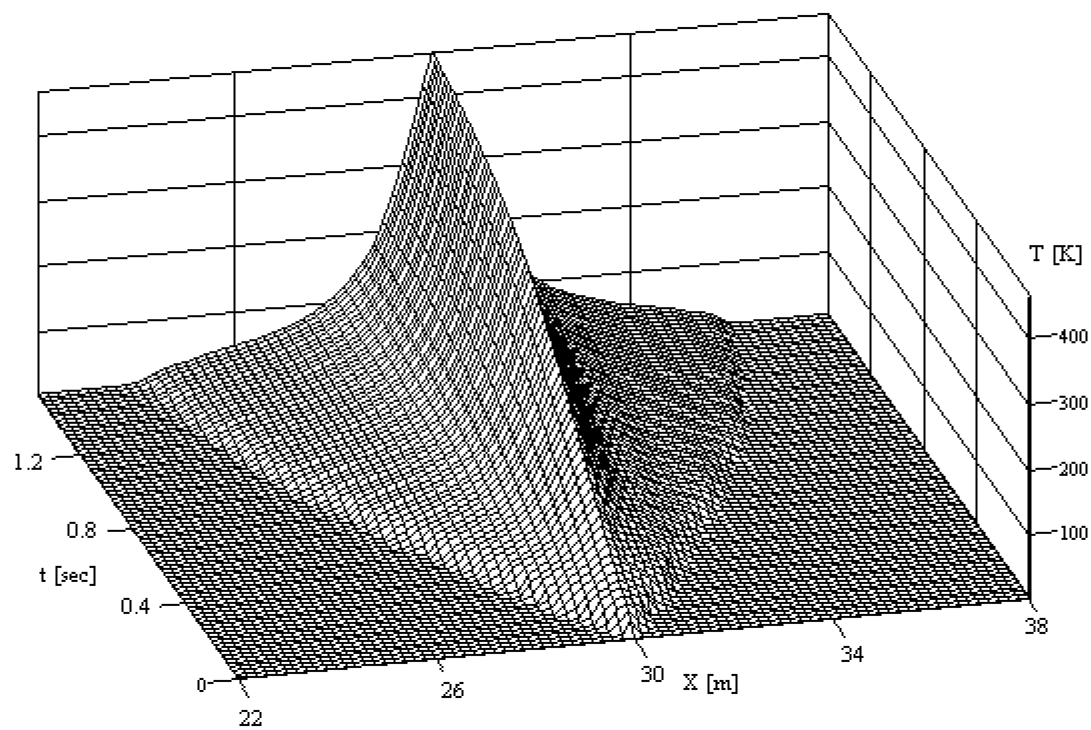

Figure 5.3.1.9 Evolution of helium temperature inside the cable space (0-1.525s)

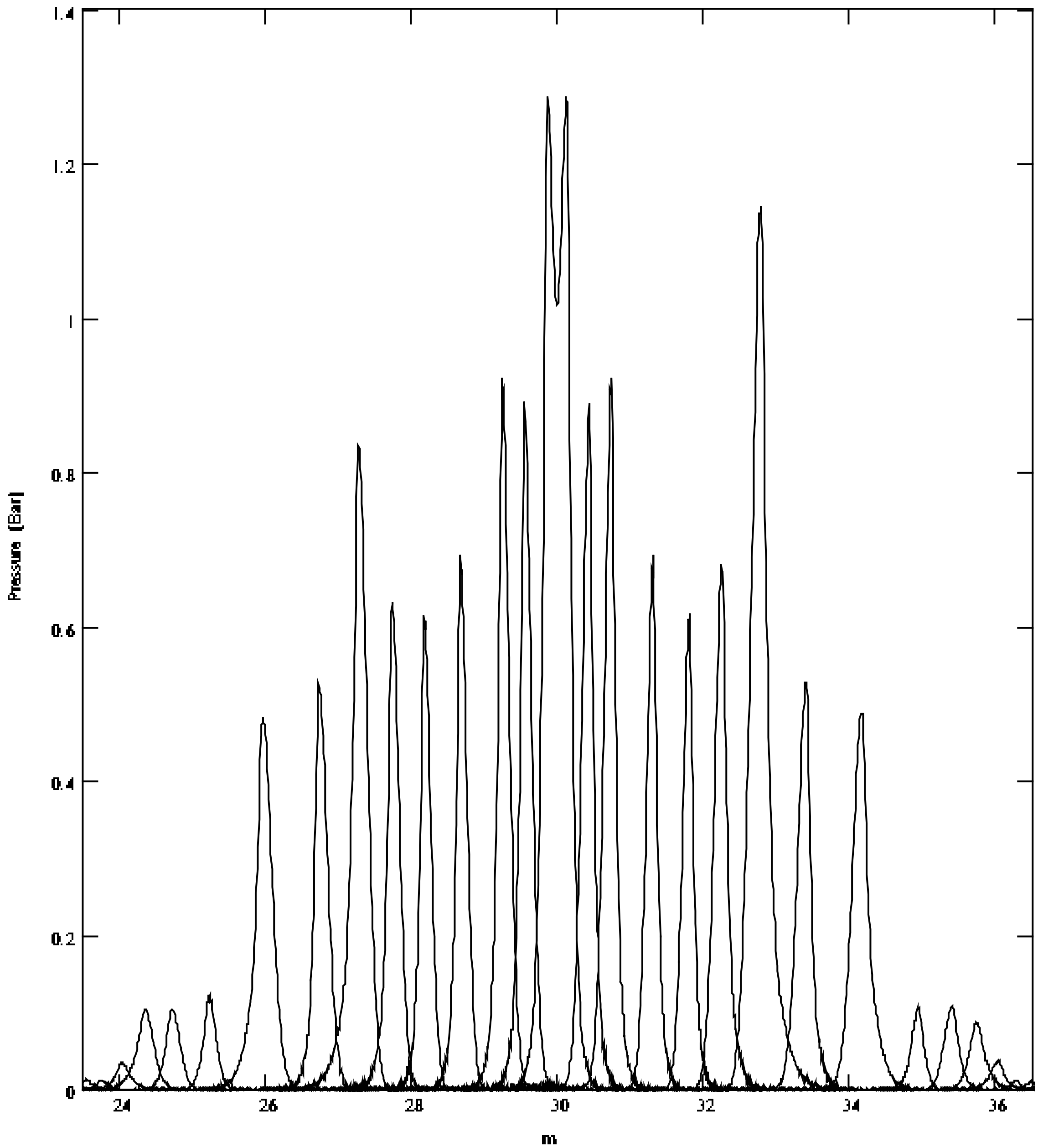

Figure 5.3.1.10 **Evolution of the He** pressure drop between the cable space and cable channel during the quench (times: 0.025, 0.075, 0.125, 0.225, 0.325, 0.425, 0.525, 0.625, 0.825, 1.025, 1.225, 1.425, 1.625, 1.825, 2.025, 2.425s).

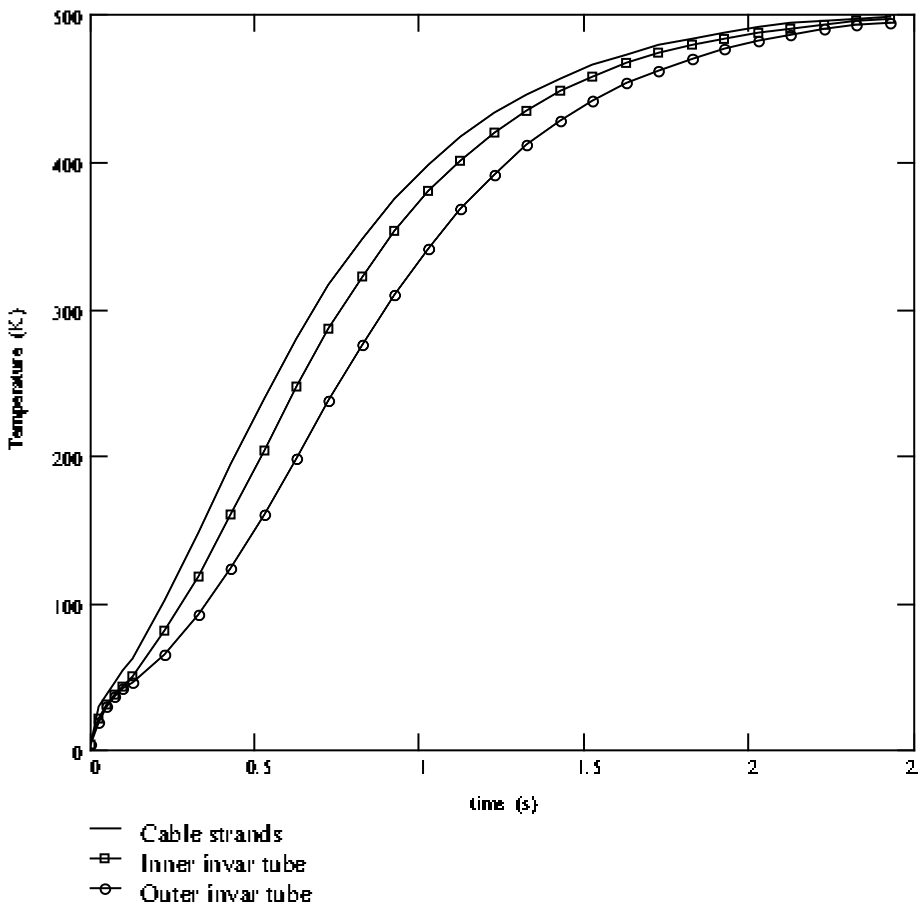

Figure 5.3.1.11 Evolution of maximal temperature (the middle of cable) for the Cable strands and external surfaces of Inner and Outer invar tubes.

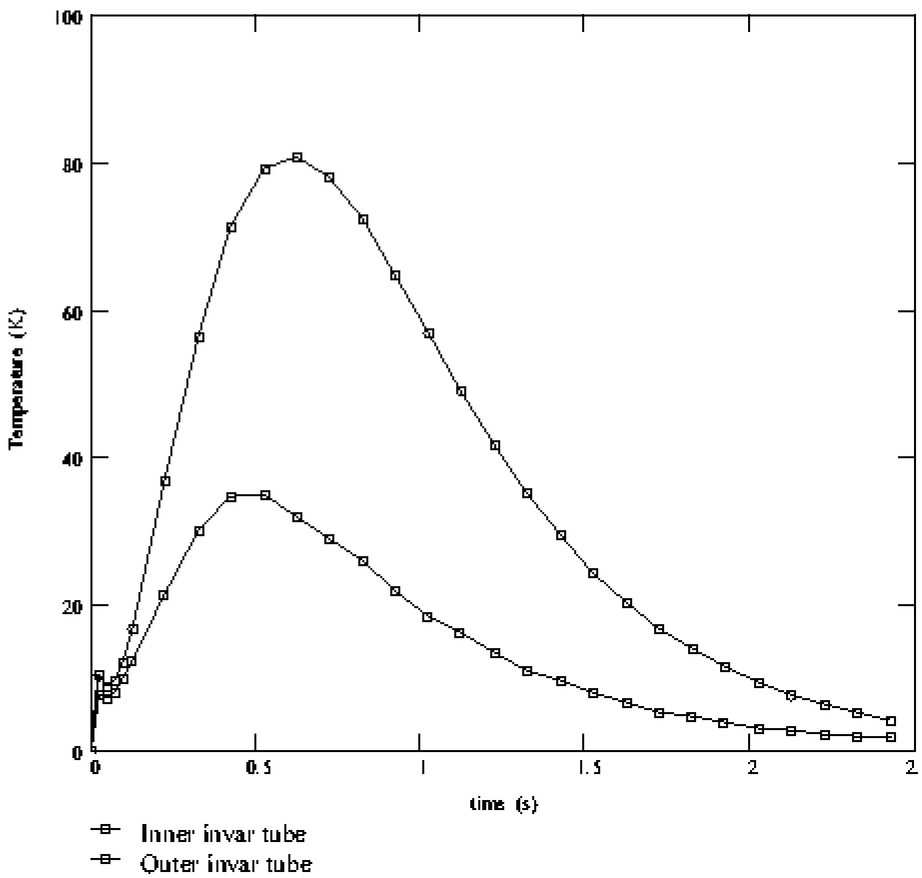

Figure 5.3.1.12 Evolution of the temperature differences across the thickness of Inner and Outer invar tubes.

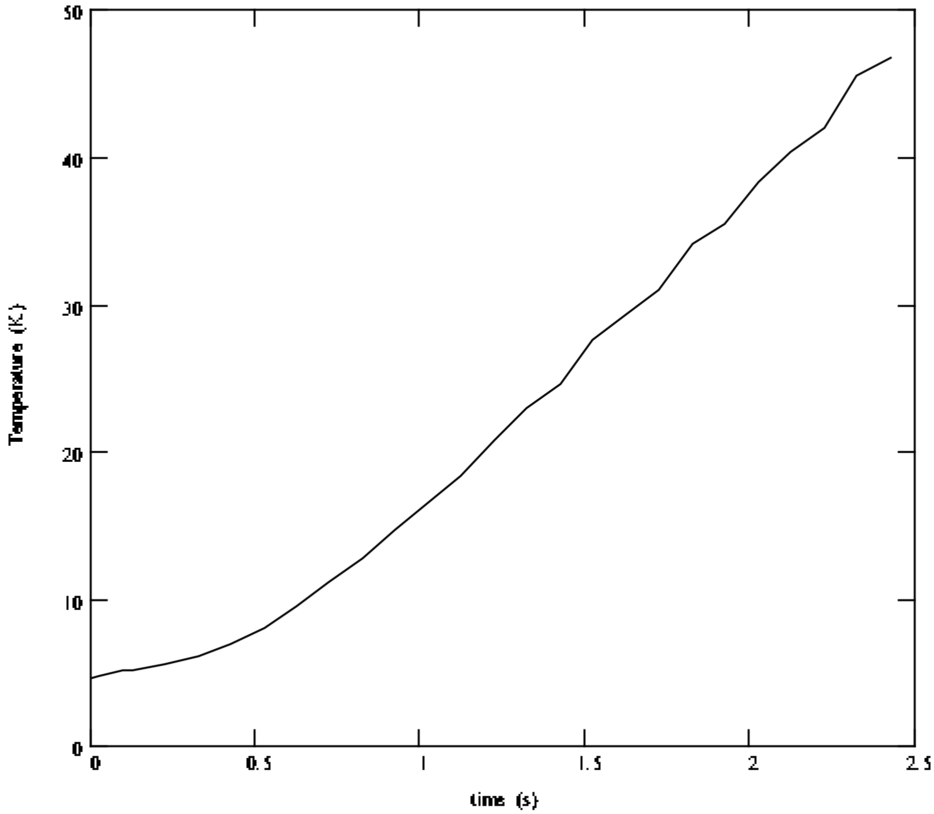

Figure 5.3.1.13 Evolution of the SHe temperature in the middle of the conductor channel during quench protection.

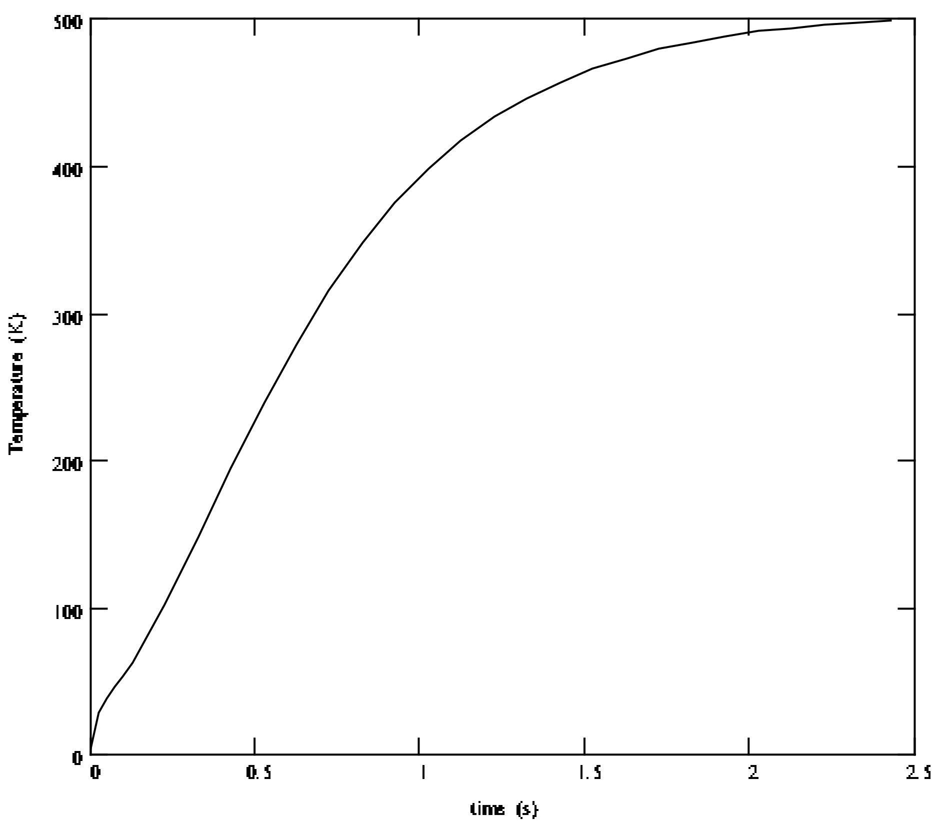

Figure 5.3.1.14 Evolution of the SHe temperature in the middle of the cable space during quench protection.

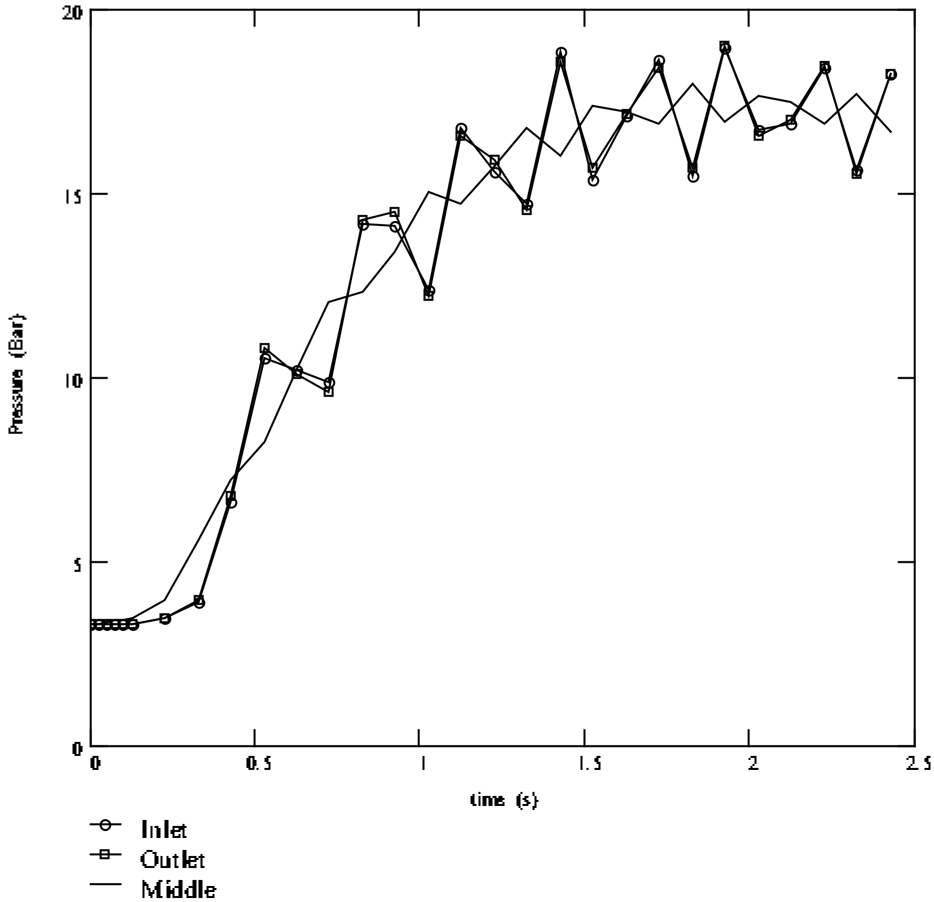

Figure 5.3.1.15 Evolution of the SHe pressure at the cable ends and center during quench protection.

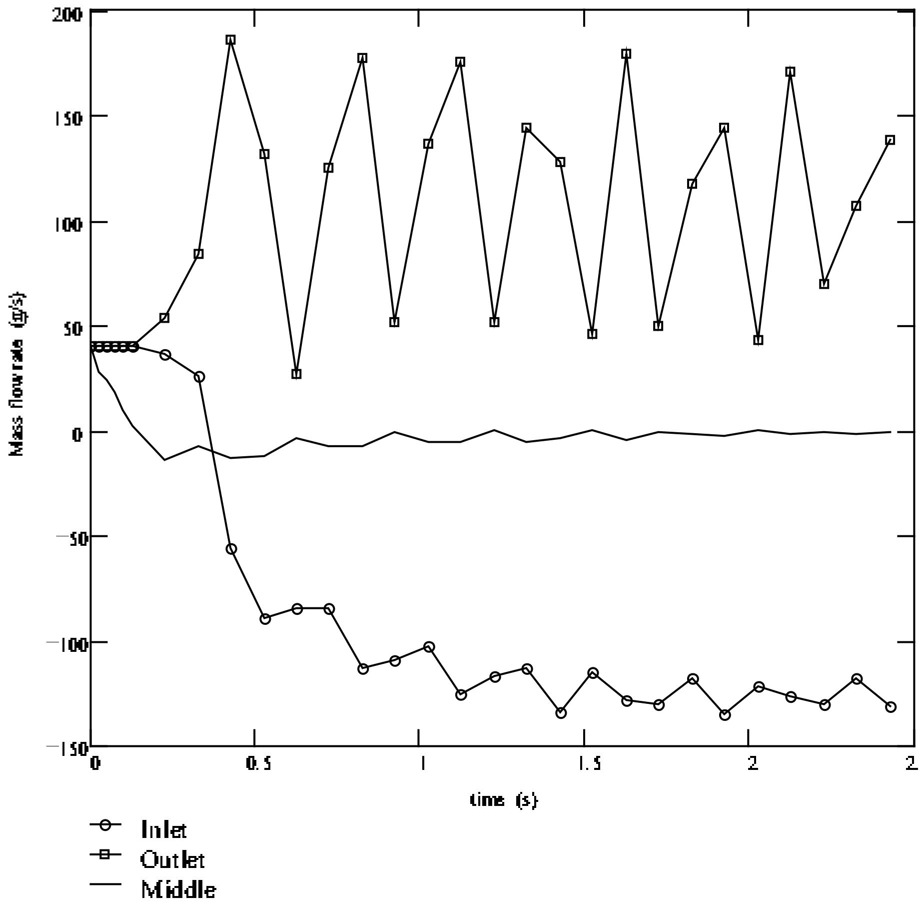

Figure 5.3.1.16 Evolution of the SHe mass flow rate at the conductor ends (inlet & outlet valves) and center during quench protection.

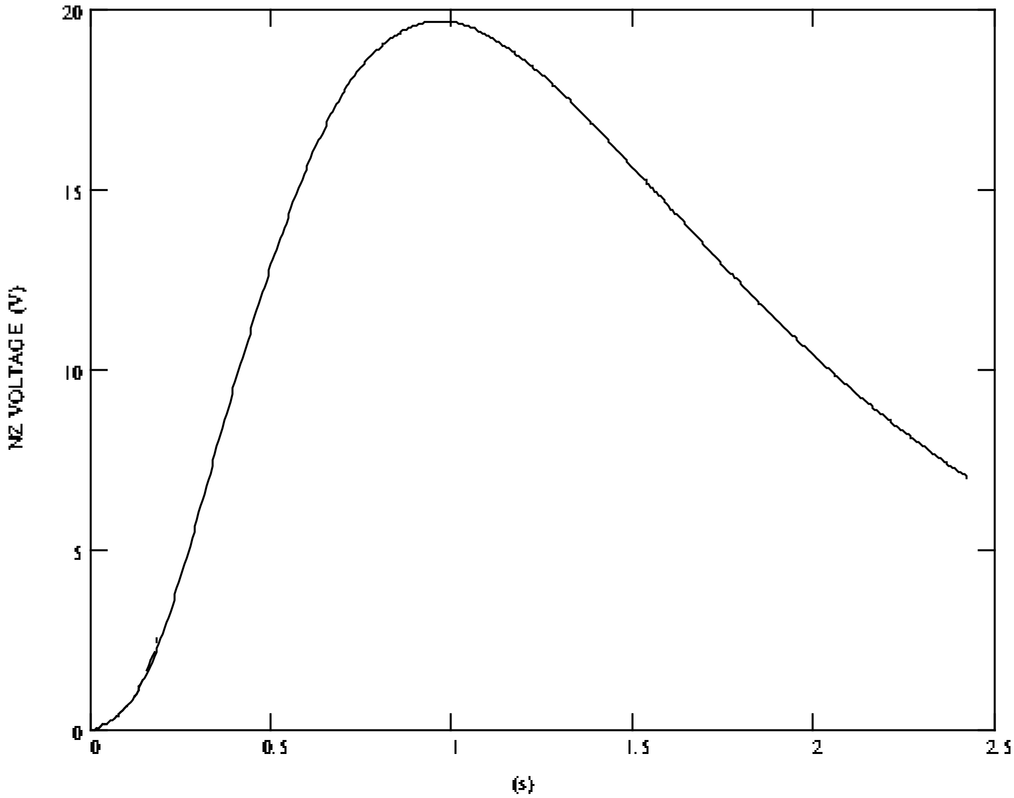

Figure 5.3.1.17 Evolution of Normal Zone voltage during quench protection.

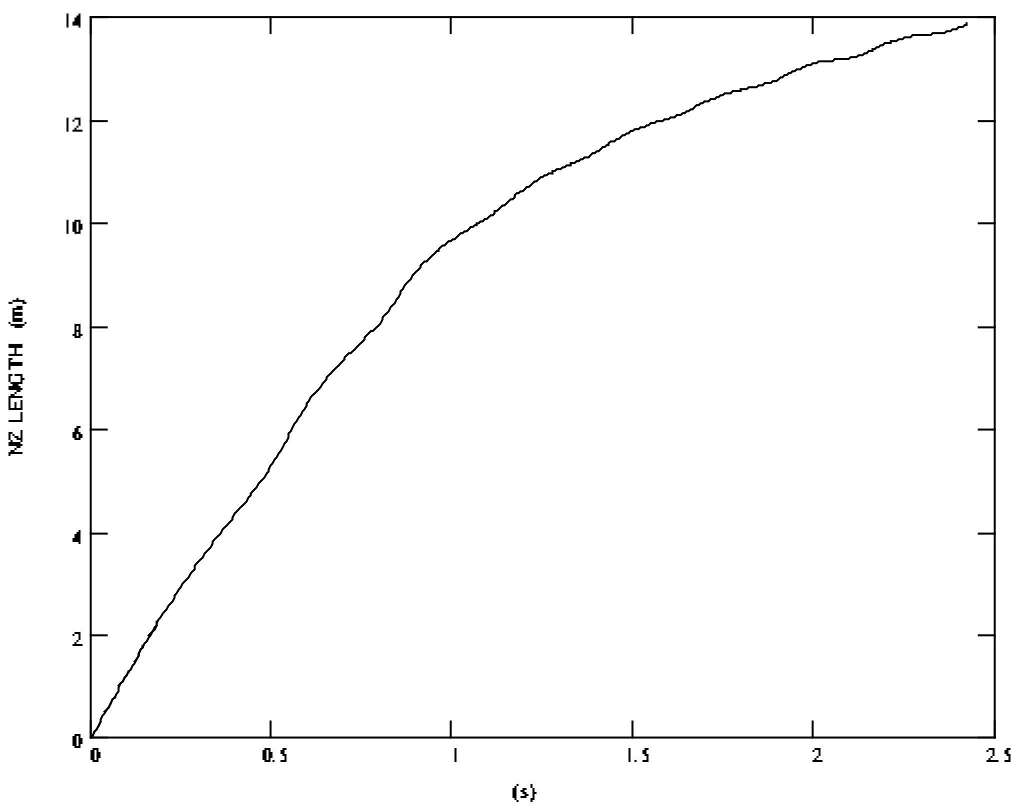

Figure 5.3.1.18 Evolution of Normal Zone length during quench protection.

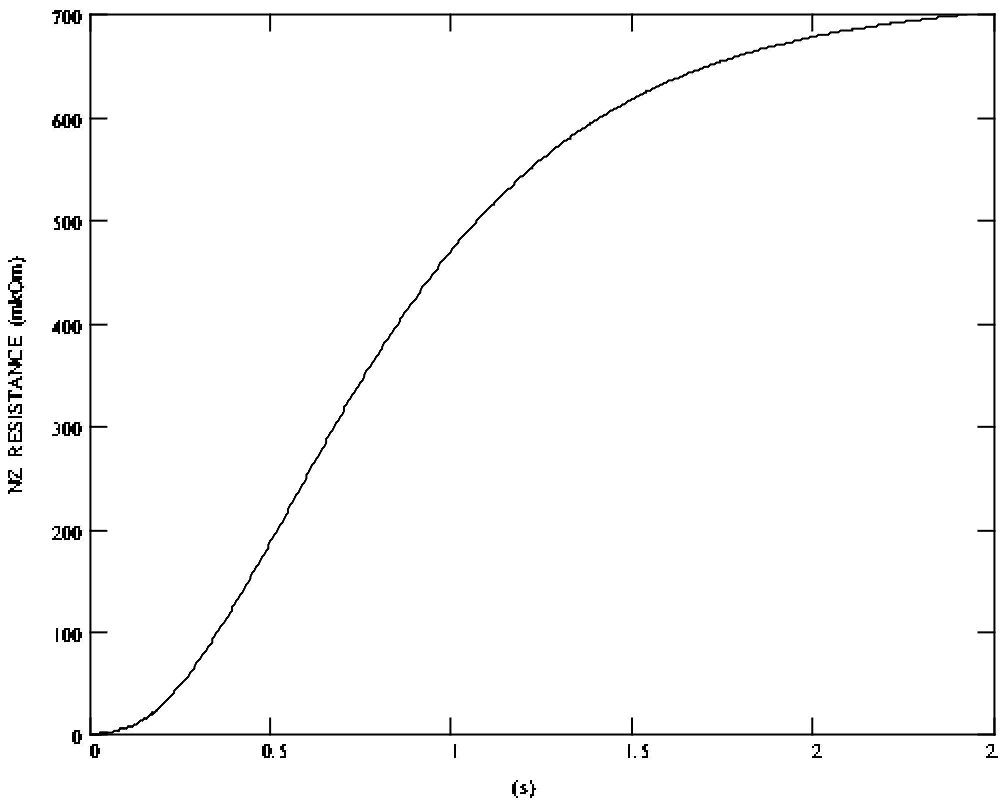

Figure 5.3.1.19 Evolution of Normal Zone resistance during quench protection.

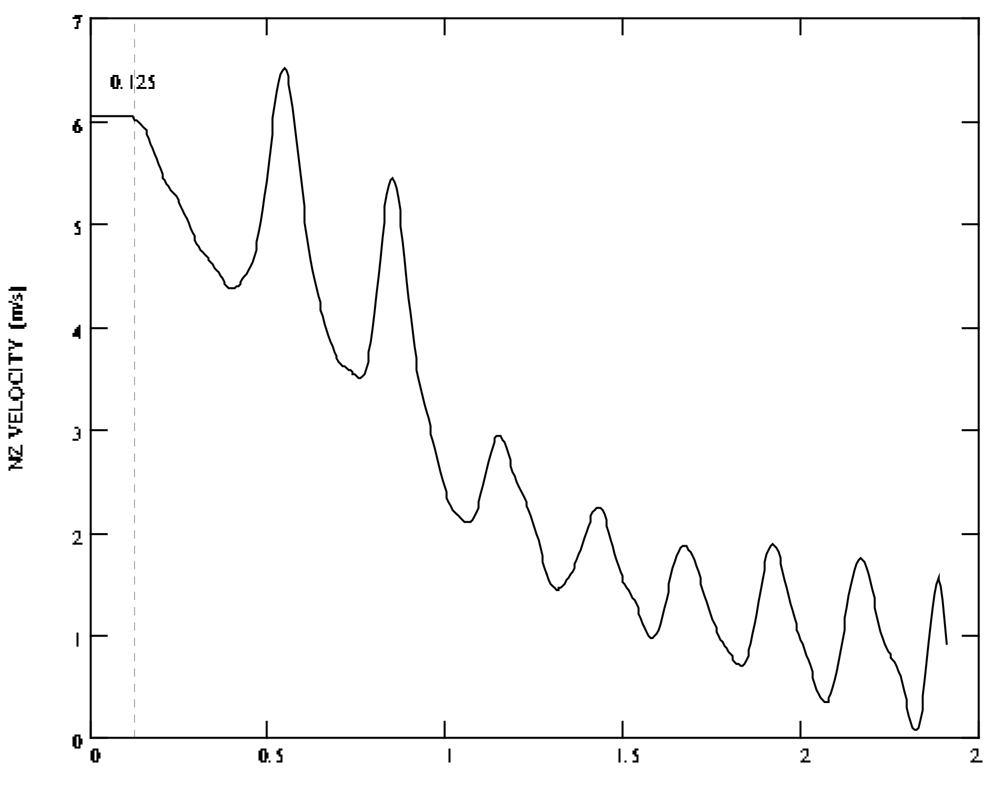

Figure 5.3.1.20 Evolution of Normal Zone velocity during quench protection.

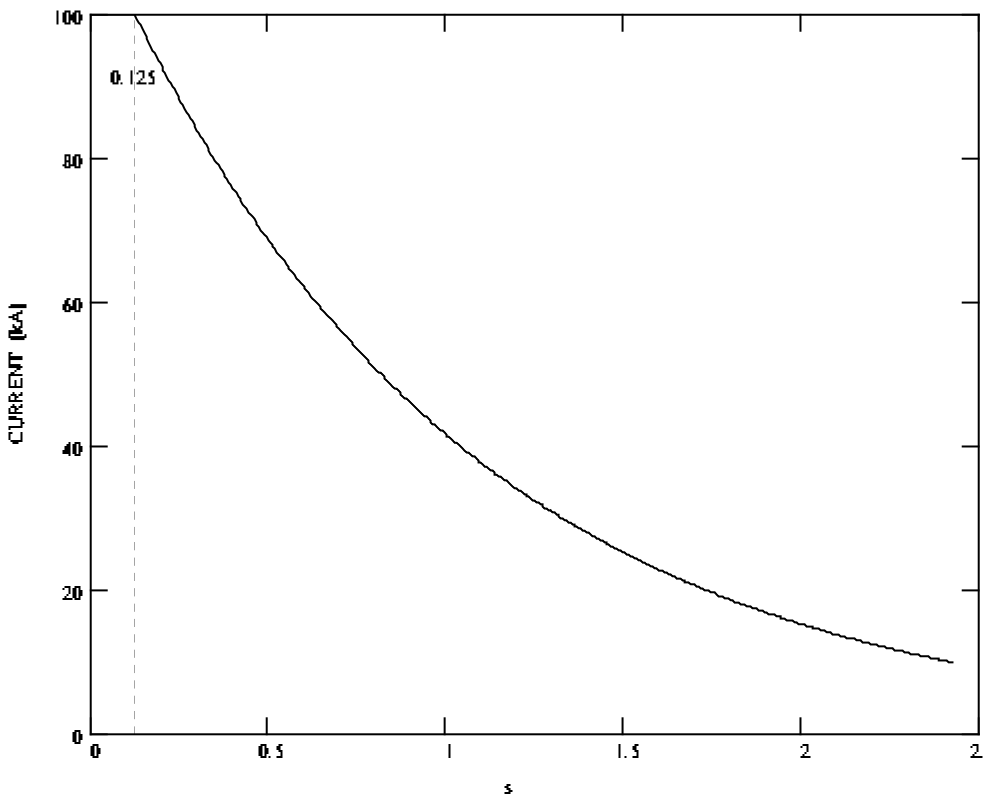

Figure 5.3.1.21 Current decay during protection (t_{det}=0.125s, τ=1s).

5.4 Impact of contact thermal resistance on hot spot temperature

Effect of thermal resistance between the current carrier (Rutherford type cable plus copper tape) and invar tubes on hot spot temperature of conductor is considered on simplified model.

Simple formula usually used for hot spot temperature calculation of a composite conductor is

$$\int_0^{\infty} I^2(t)dt = A_{Cu}\sum_n A_n \int_{T_c}^{T_{hs}} \frac{\gamma_n}{\rho_{Cu}} C_n dT \quad , (5.4.1)$$

where I the conductor current and the integrals over temperature are performed for each constituent of the conductor with A_n the cross sectional area, γ_n the density, C_n the specific heat, and ρ_{Cu} the electrical resistivity of copper.

For the transmission line drive conductor this formula should be slightly changed due to the twist of the Rutherford type composite cable along the tube. If take the same assumption for multi component conductor as for the composite one (the same temperature for components) and treat A_n as cross sectional area of component in a plane perpendicular to the tube axis formula (5.4.1) transforms to following view

$$\int_0^{\infty} I^2(t)dt = A_{Cu}\cos(\theta)^2 \sum_n A_n \int_{T_c}^{T_{hs}} \frac{\gamma_n}{\rho_{Cu}} C_n dT \quad , (5.4.2)$$

where θ is the angle of the cable twist.

In common case for the multi component conductor with current sharing between its twisted components (single temperature model) it is easy to obtain

$$\int_0^{\infty} I^2(t)dt = \int_{T_c}^{T_{hs}} \left(\sum_n A_n \gamma_n C_n \right) \left(\sum_n A_n \cos^2(\theta_n)/\rho_n \right) dT \quad . (5.4.3)$$

Consider simple two temperatures model of transmission line to define impact of thermal resistance between the current carrier (Rutherford type cable plus copper tape) and invar tubes on hot spot temperature. Let θ is effective average angle of current carrier twist (including strand transposition). It is assumed no current in components but copper during quench.

Equation of energy conservation for the current carrier:

$$\left(A_{Cu}\gamma_{Cu}C_{Cu} + A_{NbTi}\gamma_{NbTi}C_{NbTi}\right)\frac{dT_{cc}}{dt} = \frac{\rho_{Cu}I^2(t)}{A_{Cu}\cos^2(\theta)} - hp\left(T_{cc} - T_{inv}\right) \quad , (5.4.4)$$

where p the contact area between the current carrier and invar tubes per unit of tube length, h the heat transfer coefficient. Thermal resistance R is considered as magnitude inversely proportional to product hp.

Equation of energy conservation for the invar tubes:

$$A_{Inv}\gamma_{Inv}C_{Inv}\frac{dT_{inv}}{dt} = hp\left(T_{cc} - T_{inv}\right) \quad (5.4.5).$$

For illustration purpose replace h by ratio of $k_{inv}(T)$ the thermal conductivity of invar to δ_{inv} the effective thickness. Let time detection delay t_{det}=0.12sec, current decay time constant τ=1sec, initial quench current I_0=100kA, non-twisted (actual) copper cross sectional area A_{Cu} = 138.7mm^2, non-twisted NbTi cross sectional area A_{NbTi} = 62.3mm^2, total of both invar tubes cross sectional area A_{Inv} = 222 mm^2, contact perimeter p=0.2m, material properties as reported. Solving numerically the system of ordinary differential equations (5.4.4), (5.4.5) the following dependency of hot spot temperature vs. effective thickness is obtained

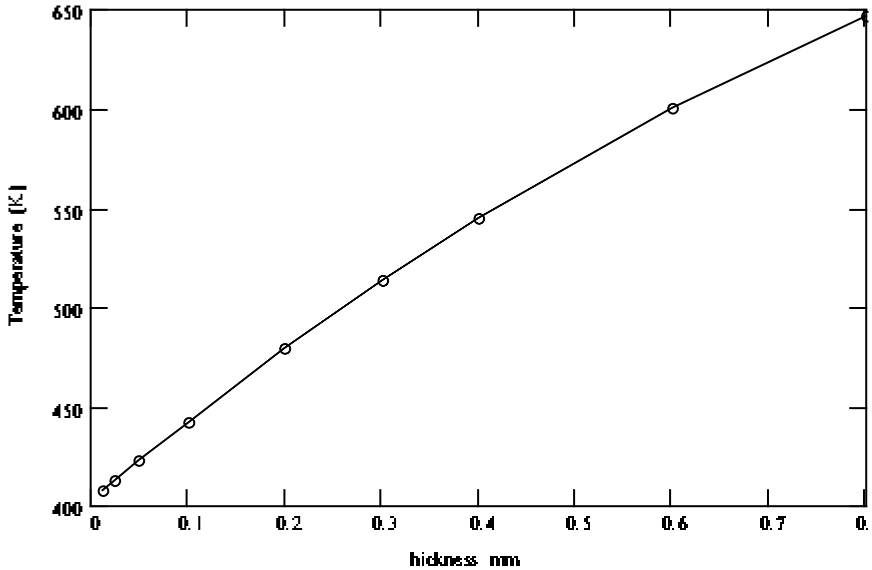

Figure 5.4.1. Dependency of hot spot temperature from effective invar thickness.

Figure 5.4.1 shows that for ideal thermal contact (δ=0) the hot-spot temperature are equal to 402K for referenced resistivity (RRR=55).

Temperature evolution of the current carrier and invar tubes for some values of effective invar thickness are shown in Figures 5.4.2 through 5.4.7.

The mostly close to reported data is variant shown in Fig. 5.4.2, 5.4.3 with δ=0.3mm. This value seems to be valid for continuous thermal contact between the cable and tubes but small for non-continuos contact. So more accurate estimation of extra thermal resistivity due to interrupted contact is needed.

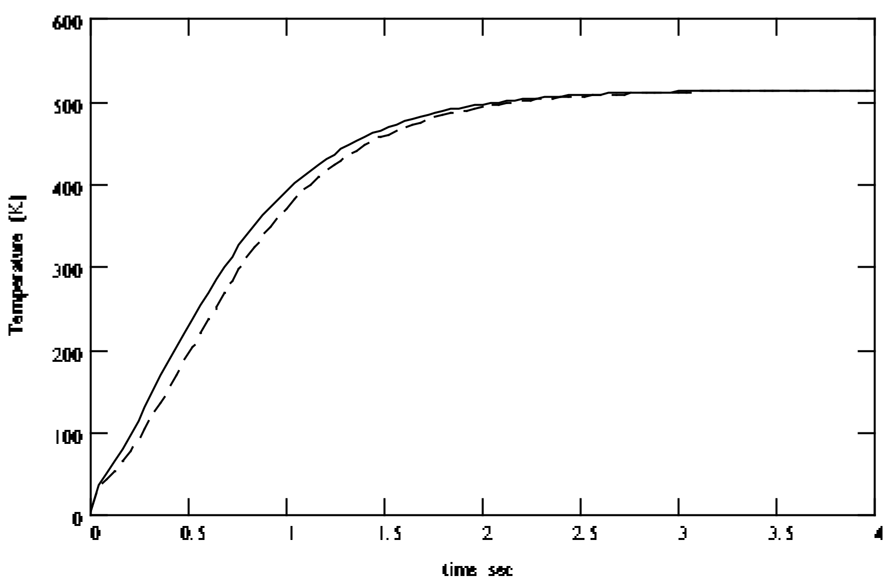

Figure 5.4.2 Temperature evolution of current carrier (solid) and invar tubes (dash). RRR=55, δ=0.3mm.

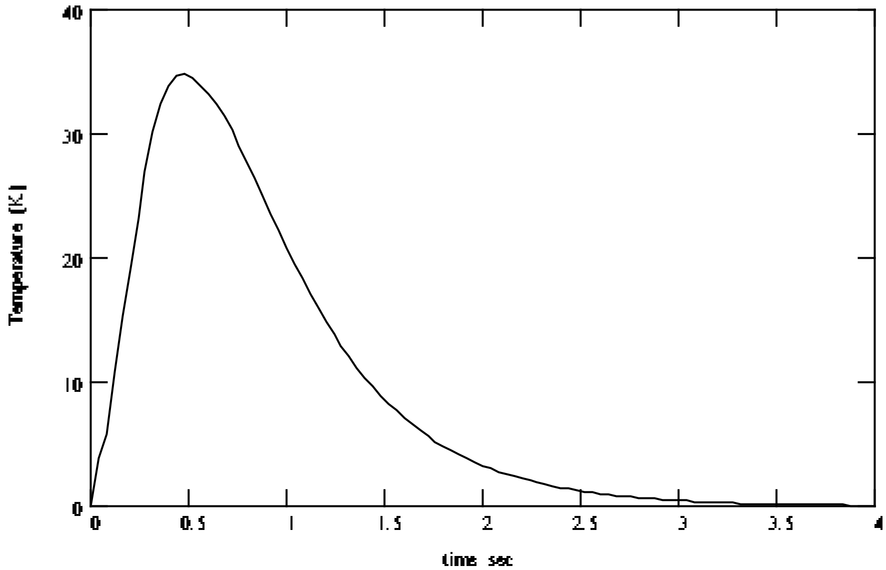

Figure 5.4.3 Evolution of temperature difference between current carrier and invar tubes. RRR=55, δ=0.3mm.

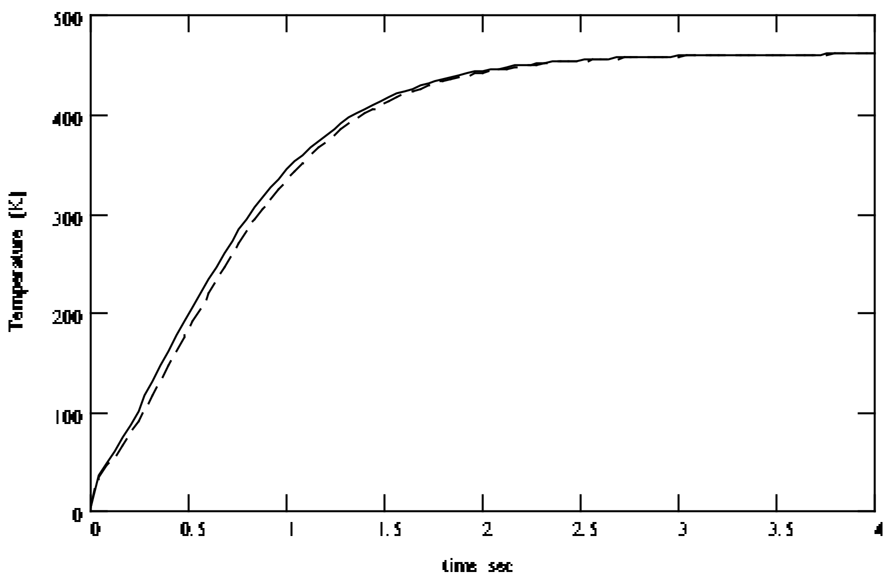

Figure 5.4.4 Temperature evolution of current carrier (solid) and invar tubes (dash). RRR=55, δ=0.15mm.

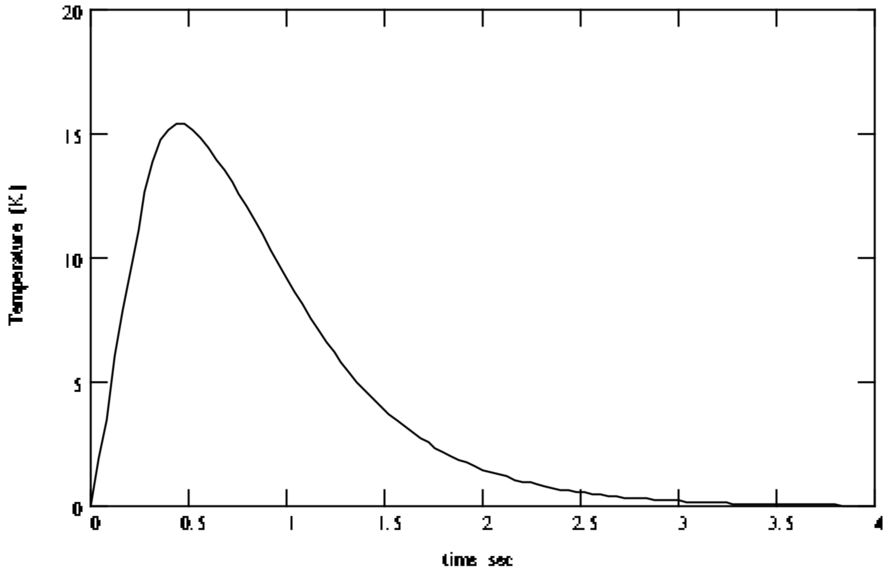

Figure 5.4.5 Evolution of temperature difference between current carrier and invar tubes. RRR=55, δ=0.15mm.

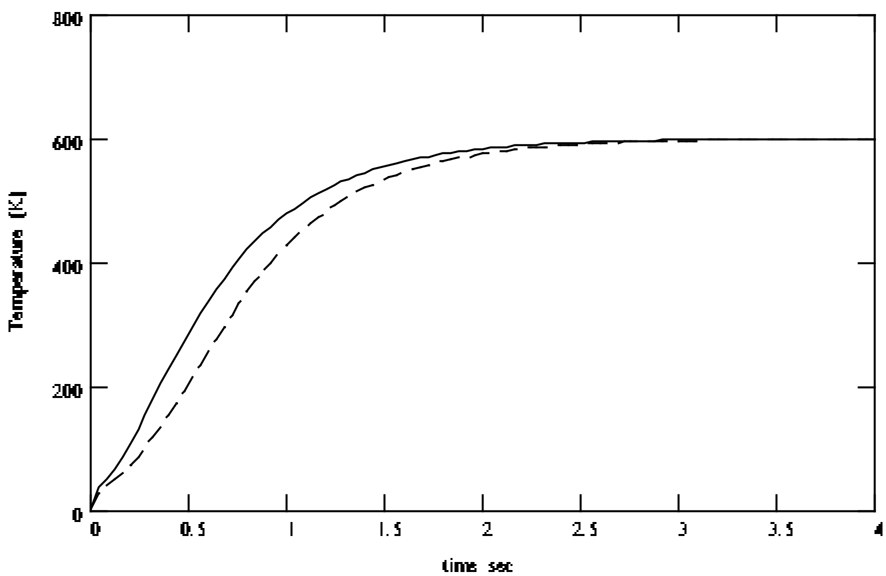

Figure 5.4.6 Temperature evolution of current carrier (solid) and invar tubes (dash). RRR=55, d=0.6mm.

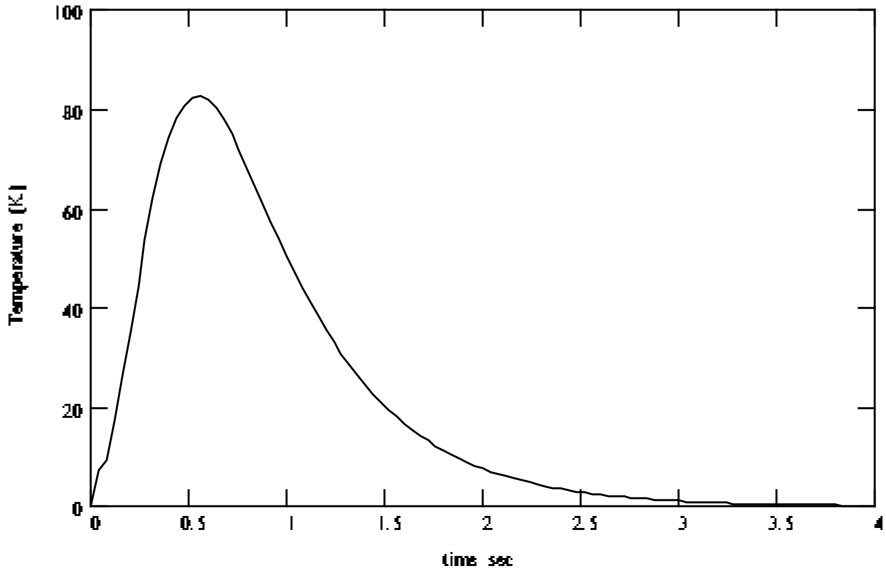

Figure 5.4.7 Evolution of temperature difference between current carrier and invar tubes. RRR=55, δ=0.6mm.

CONCLUSION

Analysis of simulated variants allows come to some conclusions

- Heat transfer to SHe in compare with "adiabatic" case does not affect significantly on the maximal (hot spot) temperature of the cable during quench protection. It seems to be clear if take into account the huge ohmic heat releases in compare with power removed by SHe from the cable strands indirectly through the invar tube wall.
- Helium in void space (less 7% of cable space) increases the stability margin and does not affect on quench evolution.
- Current carrier copper should be increased in compare with considered total Cu/nonCu value.
- The copper RRR does not has significant influence on hot spot temperature because the purer copper the greater quench detection time delay.
- For quench caused by heat pulse with longer initial the hot spot temperature is less because the shorter quench detector time delay for the same 1V quench detection threshold.
- Hot-spot temperature of cable strongly depends on the thermal resistance. So extra thermal resistance because of non-continuous contact between the Rutherford type cable and invar tube should be taken into account. Respectively the present heat model that used ideal thermal contact between the cable and coating shell should be slightly corrected to get more accurate result.

References

[1] A.Duke, V.Kokotkov, V.Kukhtin, E.Lamzin, N.Shatil, S.Sytchevsky, V.Vasiliev, M.Zhelamsky, "Coupled Electromagnetic and Themohydraulic Analysis of the Cable Joint," *ASC, 1996, Pittsburgh, USA (IEEE Transaction on Applied Superconductivity, Vol.7, No 2, June 1997)*

[2] N.Shatil, M.Zhelamskij (Efremov Institute, RF), A.Anghel, G.Vecsey (CRPP-EPFL, Switzerland), Y.Takahashi, K.Hamada (JAERI, Japan) "The first experimental observation of the He mass exchange between cable space and central channel in CICC obtained by SHF method during QUELL" *Proceedings of 20th SOFT*, Marseille, France, 1998, vol. 1, pp.715-718

[3] N.Shatil, M.Zhelamskij (Efremov Institute, RF), A.Anghel, G.Vecsey (CRPP-EPFL, Switzerland), Y.Takahashi, K.Hamada (JAERI, Japan), S.Pourrahimi (MIT, US) "An investigation of inner heat input in CICC with central channel by the Super High Frequency method" *Proceedings of ASC98*

[4] Arp V.D., "Thermodynamic of single phase one dimensional fluid flow," *Cryogenics*, vol. 15, pp.285-289, 1975

[5] Arp V.D., "New forms of state equations for helium," *Cryogenics*, vol. 14, pp.593-598, 1974

[6] Arp V.D., McCarty R.D. "Thermophysical Properties of Helium-4 From 0.8 to 1500 K With Pressures to 2000 MPa", NIST Technical Note 1334, 1989

[7] Arp V.D. "Electrical and Thermal Conductivities of Elemental Metals below 300K," Thirteenth Symposium on the Thermophysical Properties, June 22-27, 1997, Bolder Colorado, USA.

[8] A.Fevrier and D.Morize, "The effect of magnetic field on the thermal conductivity and electrical resistivity of different materials," Cryogenics, October 1973, p.p. 603-606

List of Figures